

# Gaussian Match-and-Copy

## A Minimalist Benchmark for Studying Transformer Induction

Antoine Gonon

Alexandre Cordonnier

Nicolas Boumal

Institute of Mathematics, EPFL, Switzerland

### Abstract

Match-and-copy is a core retrieval primitive used at inference time by large language models to retrieve a matching token from the context then copy its successor. Yet, understanding how this behavior emerges on natural data is challenging because retrieval and memorization are entangled. To disentangle the two, we introduce *Gaussian Match-and-Copy* (GMC), a minimalist benchmark that isolates long-range retrieval through pure second-order correlation signals. Numerical investigations show that this task retains key qualitative aspects of how Transformers develop match-and-copy circuits in practice, and separates architectures by their retrieval capabilities. We also analyze the optimization dynamics in a simplified attention setting. Although many solutions are *a priori* possible under a regression objective, including ones that do not implement retrieval, we identify an implicit-bias regime in which gradient descent drives the parameters to diverge while their direction aligns with the max-margin separator, yielding hard match selection. We prove this max-margin alignment for GD trajectories that reach vanishing empirical loss under explicit technical conditions.

## 1 Introduction

How do Transformers learn to learn in-context? A long-studied hypothesis in the literature is that *match-and-copy* is an important primitive underlying in-context learning (ICL) in large language models [6–8, 11, 14, 26, 28, 34, 36, 37]. For instance, in

“Granny Susie comes tomorrow. I love Granny \_\_\_\_”

a natural continuation is “Susie”. This prediction can arise either from memorization (a stored association “Granny” $\mapsto$ “Susie”) or from an inference-time retrieval procedure that searches the current context for a match, then copies its successor. Because the space of possible associations is vast, models that can perform match-and-copy are better equipped to adapt to the context.

In practice, Transformers of various scales have been shown to develop a two-head attention circuit that implements a match-and-copy mechanism in an abstract way (the same heads work independently of the token distribution) [14, 28]. Moreover, the formation of such heads coincides with sharp decreases in training loss, suggesting that acquiring match-and-copy is important for overall model performance. This two-head circuit is composed of a *Previous-Token Head* (PTH) that marks the predecessor of a token, and an *Induction Head* (IH) in a subsequent layer that searches for that mark to copy the continuation [7, 14, 28].

Despite these insights, it remains difficult to pinpoint *why* and *when* this circuit emerges so reliably. Analyses based on large-scale language data are expensive to run and entangle many factors, offering limited experimental control [11, 14, 22, 25, 28]. This has motivated the development of synthetic benchmarks that are cheaper to run and amenable to analysis. There is a long history of such synthetic tasks in the literature (see our review in Section 2), each with its own set of design choices. Different constructions are meant to emphasize different aspects of match-and-copy (or more generally, in-context learning) mechanisms. In this work, we focus on isolating *long-range correlation-based* match-and-copy retrieval, in an inexpensive and robust way (i.e., we want the PTH $\rightarrow$ IH circuit to emerge systematically, without shortcut solutions). This focus reflects two properties of attention-based models: their ability to model long-range dependencies—often cited as a key strength over other sequence models [3, 15, 19, 29]—and the fact that correlation provides a particularly natural signal for attention to exploit.

To this end, we introduce **Gaussian Match-and-Copy (GMC)**. GMC is a minimalist prediction task where the only signal is a single, hidden correlation between the query (the last token in the context) and an earlier context token positioned at random in an otherwise i.i.d. Gaussian context. To solve it, a model cannot memorize associations; it must learn an active search-and-retrieval algorithm.

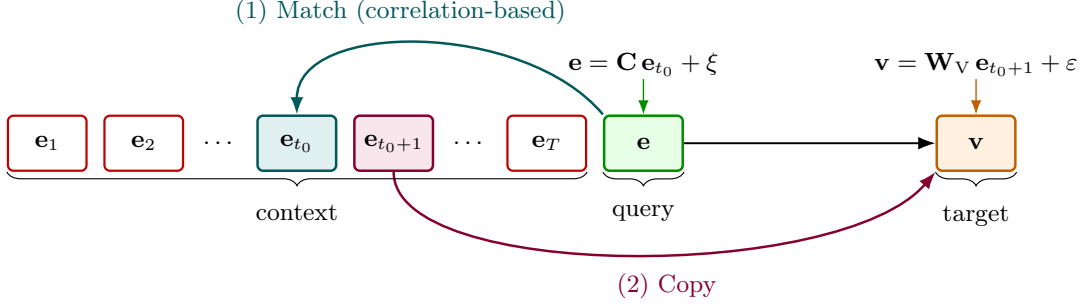


Figure 1: **Gaussian Match-and-Copy** task (Theorem 1.1). The query matches a hidden context token via correlation, and the target copies the successor of that token.

**Definition 1.1** (Gaussian Match-and-Copy). Fix dimensions  $d_{\text{in}}, d_{\text{out}}$ , noise level  $\sigma_{\text{noise}}^2$ , and token variance  $\sigma_{\text{token}}^2$ . Consider  $\mathbf{W}_V \in \mathbb{R}^{d_{\text{out}} \times d_{\text{in}}}$ ,  $\mathbf{C} \in \mathbb{R}^{d_{\text{in}} \times d_{\text{in}}}$  called value and correlation matrix, and  $\mathcal{D}_\xi$  a distribution over  $d_{\text{in}}$ -dimensional tokens. A sample  $(\mathbf{e}_1, \dots, \mathbf{e}_T, \mathbf{e}, \mathbf{v})$  is generated as follows:

1. **Context:** Draw  $T$  independent token embeddings  $\mathbf{e}_1, \dots, \mathbf{e}_T \sim \mathcal{N}(0, \frac{\sigma_{\text{token}}^2}{d_{\text{in}}} \mathbf{I}_{d_{\text{in}}})$ .
2. **Hidden Match:** Select a hidden index  $t_0$  uniformly at random from  $\{1, \dots, T-1\}$ .
3. **Query Injection:** The query  $\mathbf{e}$  is drawn such that it is correlated *only* with  $\mathbf{e}_{t_0}$ :

$$\text{Cov}(\mathbf{e}, \mathbf{e}_t) = \begin{cases} \frac{\sigma_{\text{token}}^2}{d_{\text{in}}} \mathbf{C} & \text{if } t = t_0, \\ 0 & \text{if } t \neq t_0. \end{cases}$$

Concretely, this is achieved by setting  $\mathbf{e} = \mathbf{C} \mathbf{e}_{t_0} + \xi$ , where  $\xi \sim \mathcal{D}_\xi$  is independent noise.

4. **Target:** The target is the *next* token, projected and noisy:  $\mathbf{v} = \mathbf{W}_V \mathbf{e}_{t_0+1} + \varepsilon$ , where  $\varepsilon \sim \mathcal{N}(0, \sigma_{\text{noise}}^2 \mathbf{I}_{d_{\text{out}}})$ .

The most natural strategy is clear: compare  $\mathbf{e}$  with all  $\mathbf{e}_t$  to maximize the overlap  $\mathbf{e}_t^\top \mathbf{C} \mathbf{e}$ , identify  $t_0$ , and output  $\mathbf{W}_V \mathbf{e}_{t_0+1}$ . This requires a mechanism that can (1) Match and (2) Copy, see Figure 1.

The key design choices are as follows. First, there is no fixed association rule to memorize: the matched token  $\mathbf{e}_{t_0}$  and its successor  $\mathbf{e}_{t_0+1}$  are independent random variables, so successful prediction cannot rely on stored input–output pairs. Second, all context tokens share identical marginal distributions. In particular, the matched token  $\mathbf{e}_{t_0}$  cannot be identified by any local statistic, such as its moments or a special marker. The only signal distinguishing it is its second-order correlation with the query. Third, the match index  $t_0$  can occur arbitrarily far in the context, requiring genuine long-range retrieval. Finally, the Gaussian construction admits simple geometric and concentration properties, which we later exploit to analyze the optimization dynamics theoretically.

**Contributions.** From the proposed GMC task, we extract several conclusions.

(i) **Reliable PTH→IH emergence in Transformers.** In our experiments, standard Transformers trained on GMC develop a PTH→IH circuit, and the appearance of these heads aligns with a sharp drop in the validation loss. This mirrors prior observations made on LLMs, e.g., in [14, 28] for models with sizes ranging between 13M and 13B parameters trained to predict the next token on generic web data. We find this behavior to be robust across a range of architectural and optimization choices.

(ii) **Transfer beyond the Gaussian distribution.** Freezing the attention blocks after training on GMC, then fine-tuning only input/output embeddings enables rapid adaptation to new data distributions. This provides evidence that the learned heads implement an abstract match-and-copy strategy rather than Gaussian-specific heuristics.

(iii) **Architectural separation.** Under similar training and inference budgets, Transformers solve GMC reliably, whereas structured state-space models and other non-attention sequence models perform substantially worse. This reveals a clear architectural gap in long-range, correlation-based retrieval.

(iv) **Induction via an implicit max-margin regime in simplified attention models.** Motivated by the architectural gap observed above, we study a minimal attention-only model that can implement a PTH→IH circuit. In this setting, many optimization outcomes are *a priori* plausible under square loss (MSE, a natural loss for GMC regression), including finite-norm interpolants or divergence along different

separating directions. Empirically, we observe regimes in which gradient descent attains very small training loss while the weights grow in norm and their direction aligns with the max-margin separator, driving attention toward increasingly hard match selection. On the theory side, we prove a conditional max-margin result: for GMC data conditioned on a high-probability geometric event, any gradient descent trajectory that reaches vanishing loss and satisfies explicit MSE-specific regularity conditions converges in direction to the max-margin solution and diverges at a logarithmic rate. A central ingredient is the geometric event, which rules out finite-norm MSE minimizers and forces successful runs into a diverging, increasing-margin regime. The remaining assumptions isolate MSE-specific interaction terms needed to recover the max-margin limit.

Together, these results position GMC as an inexpensive and simple diagnostic task for studying induction mechanisms in sequence models: it isolates a core inference primitive, exposes a capability gap between architectures, and opens a promising route toward theoretical understanding.

## 2 Related Work

Mechanistic studies has established *previous-token heads* (PTH) and *induction heads* (IH) as canonical circuits enabling match-and-copy behaviors in language models [14, 28], with subsequent work refining probes, metrics, and interpretations of induction-style behavior [2, 5–9, 11, 13, 14, 17, 26–28, 33, 34, 36, 37, 42, 45]. A growing set of studies now explicitly tracks or ablates induction-style heads in diverse in-context learning (ICL) settings, providing evidence that such circuits can matter beyond next-token prediction on natural text [5, 9, 11, 26, 27, 34, 37, 45].

At the same time, many influential synthetic ICL studies focus on high-level task behavior or learning dynamics without explicitly probing for PTH/IH mechanisms [1, 3, 4, 8, 12, 15, 16, 22–25, 31, 36, 44, 46]. This distinction motivates controlled benchmarks where the emergence of induction circuits can be studied directly and reproducibly, while still enabling comparisons across architectures.

**Match-and-copy benchmarks, and related ICL tasks.** To study these mechanisms, a natural data structure involves sequences of the form:

$$\underbrace{\mathbf{e}_1, \dots, \mathbf{e}_{t_0}, \mathbf{e}_{t_0+1}, \dots, \mathbf{e}_T}_{\text{context}}, \underbrace{\mathbf{e}}_{\text{query}} \rightarrow \underbrace{\mathbf{e}_{t_0+1}}_{\text{target}} \quad (1)$$

Here, the model receives a query  $\mathbf{e}$  (the final prompt token) that “matches” a context token embedding  $\mathbf{e}_{t_0}$  (placed at an unknown position  $t_0$ ) and must copy the subsequent token embedding  $\mathbf{e}_{t_0+1}$  or a function thereof. This template has a long history in associative recall and retrieval-style sequence modeling, with variants spanning discrete and continuous tokens and multiple architectural choices [3, 4, 15, 17, 31]. Match-and-copy is also related to broader ICL tasks where the model must learn a function  $f$  (new at each prompt) from  $n$  demonstrations  $(x_i, f(x_i))_{i \leq n}$  to predict  $f(x)$  for a new input  $x$ , i.e., tasks of the form:

$$(x_1, f(x_1), \dots, x_n, f(x_n), x) \mapsto f(x), \quad (2)$$

where  $f$  may be linear regression [1, 16, 22, 24, 44], a classifier [8, 11, 12, 22, 34, 36, 37], a Markov/ $n$ -gram rule [2, 6, 9, 13, 23, 27, 33, 42, 46], or a Boolean function [5]. Note that here, depending on how the  $x_i$ ’s and  $x$  are generated, there might not be an explicit “match” signal injected at data generation time between  $x$  and one of the  $x_i$ ’s: the model may need to interpolate/extrapolate based on similarity. In some regimes, however, ICL tasks can in principle be solved by a match-and-copy circuit (by retrieving the  $x_i$  closest to  $x$  and copying  $f(x_i)$  as a best guess for  $f(x)$ ).

**Design choices and shortcut solutions.** Synthetic benchmarks for match-and-copy and in-context learning (ICL) necessarily involve many design choices: discrete versus continuous tokens; exact matches (equality) versus similarity-based matches; explicit injection of match signals or not; the nature of the match signal (e.g., first- versus second-order statistics); copying a successor token versus copying a function/label; the presence of distractors; and the choice of objective, architecture, and evaluation protocol. These choices strongly affect whether the generic PTH→IH solution is required to solve the task. Instead, heuristics based on memorization or simpler retrieval mechanisms can sometimes be used. E.g., if the set of possible match token values is finite and fixed globally across samples, it can be memorized, and used to trigger, only conditionally to these values, a PTH→IH-like behavior, ending up with conditional PTH→IH circuits that are not truly general-purpose match-and-copy mechanisms [6, 15].

Simpler retrieval mechanisms can also be used when the token are distinguishable (not i.i.d.)—for instance, relying on first-order statistics when the match token has a distinct mean compared to other context tokens [24]. When such shortcuts are available, the emergence of PTH→IH circuits is not guaranteed and can be quite sensitive to other design choices: whether induction-style solutions arise robustly or only in narrow regimes can be delicate to characterize—e.g., the emergence of PTH→IH circuits can depend on structural properties of the data [5, 8], can co-exist with other mechanisms, or can be transient over training time [36]. Overall, these factors complicate the use of existing benchmarks to reliably probe specific capabilities when designing new architectures, and make theoretical analysis more challenging.

**Most closely related benchmark constructions.** Our task instantiates (1) with i.i.d. Gaussian context tokens and defines the match through a *second-order* correlation between the query and a single hidden context token, which can occur arbitrarily far in the context. The first most related task is the original associative recall (AR) from Graves et al. [17], which is essentially discrete match-and-copy with exact match and exact copy. Indeed, it instantiates (1) with i.i.d. discrete tokens sampled uniformly from a finite vocabulary, with the query equal to one of the context tokens, and the target equal to the successor token. This early work does not study PTH→IH circuits (pre-Transformer era), and the GMC task can be seen as a continuous-valued analogue that isolates more generally correlation-based retrieval. We also note that most explicit constructions of PTH→IH circuits use orthogonal embeddings of discrete tokens, and our choice of Gaussian tokens can be seen as a continuous relaxation of this idea in high dimension, so this AR task from [17] is definitely the most closely related to GMC. Since then, AR benchmarks have been revisited and now span a variety of design [3, 4, 6, 15]. These more recent AR variants are less directly related to GMC: instead they instantiate discrete ICL tasks of the form (2). In particular, the match→target mapping  $x \mapsto f(x)$  changes at each prompt, so success cannot rely on memorizing a global match→target dictionary stored in the weights; these tasks all require in-context retrieval. GMC offers a complementary design point to these AR benchmarks with two key features: (i) an architectural gap (Transformers succeed, other models like Hyena/state-space models (SSM)/RNN fail), and (ii) its amenability to theoretical analysis of PTH→IH emergence. In contrast, (i) AR benchmarks admit non-attention architectures that can solve them reliably. Indeed, Hyena/SSM have been explicitly designed to close the gap with attention models [15, 31] on these AR benchmarks. Moreover, (ii) there are no existing theoretical analyses of the optimization dynamics when training on AR benchmarks [3, 6], which we believe is mostly due to the fact that in these AR settings, the PTH→IH circuits do not always emerge reliably across optimization and architectural choices. This makes it difficult to isolate a meaningful regime for theoretical guarantees. The second most related existing task appears in Marion et al. [24]: single-location Gaussian regression. It can be interpreted as an instance of (1) with i.i.d. Gaussian tokens, but with a fixed deterministic query across samples, injected as a mean shift to the matched token. Because the matched token is not identically distributed as the other context tokens, this does not naturally promote a PTH→IH circuit, whose key operation is correlation-based retrieval, as the model can simply learn to identify the mean-shifted token via first-order statistics.

**Positioning and novelty.** Rather than proposing a “new match-and-copy task” per se or claiming superiority over existing setups, our goal is to identify a point in the design space where several desiderata are simultaneously satisfied, with the next question in mind: *What is a simple, inexpensive and theory-friendly benchmark for testing architectures on long-range correlation-based retrieval via PTH→IH-like circuits?* We come up with GMC, that we see as complementary to prior benchmarks. **GMC is a synthetic match-and-copy benchmark where (i) retrieval can only exploit long-range second-order correlations, (ii) the PTH→IH circuit emerges reliably across optimization and architectural choices, with qualitative similarities to that observed in large language models, (iii) attention and non-attention models can be compared on their ability to perform long-range correlation-based retrieval without shortcut solutions, and (iv) the setup is amenable to theoretical analysis.** Table 4 in Section H summarizes how the most closely related prior benchmarks instantiate key design choices and highlights the specific combination realized by GMC.

### 3 Empirical Properties of Gaussian Match-and-Copy

We now study how sequence models trained on GMC behave in practice. All experiments minimize the mean-squared error

$$\frac{1}{nd_{\text{out}}} \sum_{i=1}^n \|\mathbf{v}^{(i)} - \text{model}(x^{(i)}; W)\|_2^2 \quad (3)$$

over a training set of  $n$  samples, where  $x^{(i)} = (\mathbf{e}_1^{(i)}, \dots, \mathbf{e}_T^{(i)}, \mathbf{e}^{(i)})$  and  $\mathbf{v}^{(i)}$  form the  $i$ -th GMC sample and  $\text{model}(\cdot; W)$  is a model with trainable weights  $W$ . For experiments, we normalize by  $nd_{\text{out}}$  to make the loss comparable across different settings.

Our experiments address three questions: (i) Do Transformers trained on GMC reproduce the qualitative behavior seen in large scale LLMs, i.e., do previous-token and induction-head circuits emerge, and does this coincide with a sharp change in training dynamics? (ii) Do the learned mechanisms transfer beyond the Gaussian training distribution? (iii) Do competing sequence models perform as well as Transformers on GMC when given equal resources?

#### 3.1 Transformers solve GMC via PTH → IH circuits

In the settings we tested, Transformers reliably learn the GMC task, and when trained long enough they approach the irreducible noise floor induced by the observation noise. Crucially, we observe the characteristic loss drop documented in LLMs trained on large-scale web data [28], together with the spontaneous emergence of PTH and IH circuits:

1. **Loss Drop:** The loss follows a plateau-drop-plateau pattern (Figure 2).
2. **Coincidental PTH → IH Formation:** The **PTH Score** and **IH Scores** (defined below) follow the same plateau-drop-plateau pattern. During the initial plateau, scores remain close to random baselines. Coinciding exactly with the loss drop, they rise sharply to values close to 1 (perfect PTH and IH behavior) and remain stable thereafter.

Layer-wise analysis confirms the expected circuit topology: PTHs always appear in an earlier layer than IHs (e.g., in our 2-layer default: Layer 0 specializes as PTH and Layer 1 as IH), adhering to the composition mechanism originally described in Elhage et al. [14], Olsson et al. [28]. In Section A.5, we provide a more detailed per-head analysis to confirm that the identified heads indeed look similar in function and structure to the ones documented in LLMs. Overall, GMC-trained Transformers thus reproduce key qualitative aspects of induction head formation seen in LLMs trained on natural language data, despite the drastic difference in scale and data distribution.

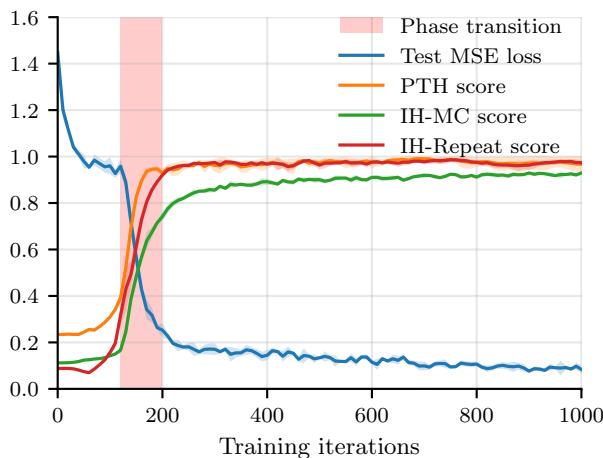


Figure 2: **Co-occurrence of Loss Drop and Circuit Emergence.** The sudden drop in test loss aligns perfectly with the saturation of PTH and IH attention scores. Here: 2-layer Llama 3 trained on GMC with  $T = 8$ ,  $d_{\text{in}} = 16$ ,  $\mathbf{C} = \frac{1}{(1.2)^2} \mathbf{I}$ , and hyperparameters from Table 1 in the appendix. See Section A.4 for other settings (varying depth,  $T$ ,  $d_{\text{in}}$ , and  $\mathbf{C}$ ), all showing the same behavior.

**Cost and robustness of PTH → IH emergence.** A central motivation for GMC is to provide inexpensive setups where induction-style circuits can be studied in a controlled and reproducible way. To keep the benchmark accessible, we therefore focus on small-dimensional regimes that already exhibit a clear loss-drop together with PTH and IH scores. We also ran additional sweeps over Llama 3 and GPT-2 architectures across various depths ( $n_{\text{layer}} \in \{2, 4, 8, 16, 32\}$ ), context length (up to  $T = 1024$ ), data dimension (up to  $d_{\text{in}} = 1024$ ), correlation strength and optimization hyperparameters (reported in Section A.4). While suboptimal choices can affect the *timing* and *sharpness* of the transition (or lead to non-convergence), when a model solves the task in our experiments, it does so with high PTH/IH scores that rise concurrently with the loss drop.

**Head scores definition.** Following the seminal work by Olsson et al. [28], we probe attention heads using scores computed from attention coefficients  $a_{t,s}$  (from query position  $t$  to key position  $s$ ). A *previous-token head* concentrates its attention to the immediately preceding position: the *PTH score* of a head is  $a_{t,t-1}$  averaged over query positions  $t$ . We report the maximum PTH score over all heads. An *induction head* links a query token to the successor of a matched position. We use the *IH-MC score*, tailored to GMC, which measures attention from the query to the successor of the hidden match ( $a_{\text{last,match}+1}$ ), and the *IH-Repeat* score [28], which measures attention on duplicated sequences. All scores are in  $[0, 1]$ ; precise definitions and random baselines are provided in Section A.3.

### 3.2 Transfer beyond Gaussian data

Does GMC teach a general match-and-copy mechanism or just Gaussian statistics? We take a Llama 3 model pretrained *only* on GMC, freeze its internals (hence the induction circuit), replace the linear input/output embeddings by new ones with compatible dimensions with the Omniglot dataset [21], which is a standard ICL benchmark [8, 22, 36, 37], and fine-tune only these embeddings on this new task. Details of the setup are in Section B. **Result in Figure 3:** The GMC-pretrained model rapidly learns to solve Omniglot just by adapting the input/output embeddings, suggesting the match-and-copy mechanism learned on GMC is abstract and transferable to other data distributions beyond Gaussians. Compared to a baseline where we train the full model from scratch on Omniglot, the GMC-pretrained model reaches 0.9 accuracy with at least  $3\times$  fewer FLOPs, demonstrating that the learned induction circuit also helps efficiency of downstream learning.

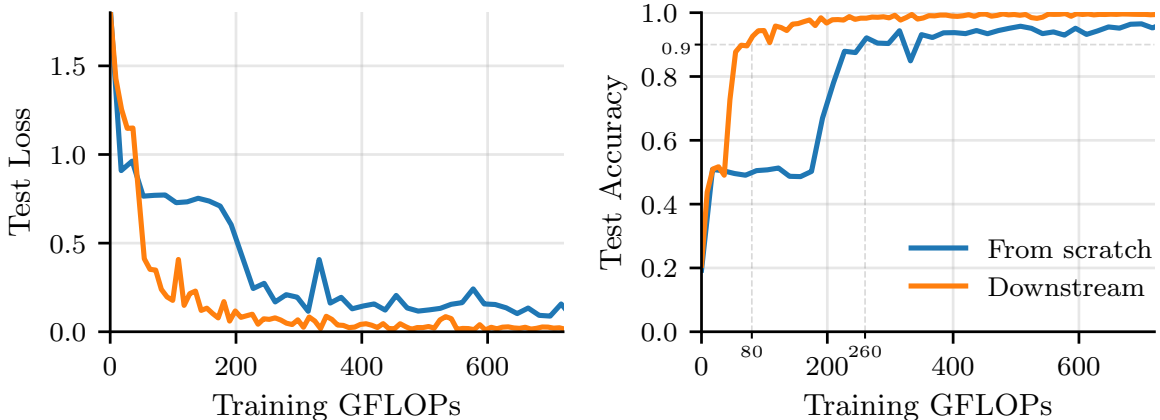


Figure 3: **Transfer Learning.** A model pretrained on GMC can reuse its attention layers to solve Omniglot few-shot classification via lightweight embedding adaptation.

### 3.3 GMC separates attention from non-attention sequence models

Finally, we compare Transformers against Gated RNNs (GRU) and State-Space Models (S4, H3, Hyena), at matched parameter counts ( $\approx 2.5 - 3M$ ), inference GFLOPS ( $\approx 24$ ), and training FLOPs (see Section C for details). **Result in Figure 4:** While Transformers hit the noise floor, all non-attention baselines—including RNNs and SSM-based or convolutional sequence models—plateau at significantly higher loss,

even when granted  $30\times$  more training steps (Section C), or when exploring different compute-equivalent hyperparameter trade-offs (e.g., depth versus width).

Note that H3 and Hyena have both been designed to perform well on associative recall tasks [15, 31], yet Figure 4 shows they still struggle on GMC. This suggests that small differences in the task structure (as highlighted in Section 2) can matter, and that long-range correlation-based retrieval is still a regime where attention-based architectures have a clear advantage. This could serve as a useful diagnostic for future architecture design.

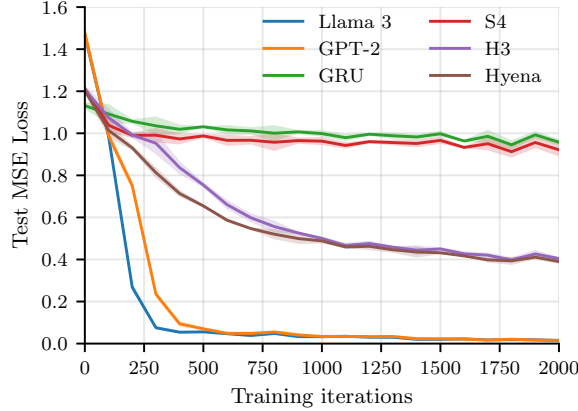


Figure 4: **Architecture Gap.** Transformers solve GMC; alternatives struggle.

## 4 Implicit Bias in a Minimal PTH→IH Attention Model

### 4.1 Overview and main result

We zoom in on a simplified setting where a minimal attention model can realize a PTH→IH circuit on GMC. In this regime, the task trained with MSE (3) can *a priori* be solved in many different ways: there may exist finite-norm global minimizers, and even when there are none, there is typically a cone of separating directions along which the parameters can diverge while the loss vanishes. Empirically, in a range of regimes we observe that gradient descent exhibits a beneficial implicit bias: the parameters diverge while aligning with a *max-margin* separator, which drives attention toward hard match selection and yields margins that keep increasing over training. We confirm this behavior theoretically in a specific setting under explicit assumptions. The proof is deferred to Section D.

**Theorem 4.1** (Max-margin implicit bias for MSE in the minimal model). *Under the technical assumptions collected in Section 4.4, for GMC data conditioned on the event of Section 4.3 (which holds with high probability), the following holds. Consider gradient descent on the empirical MSE loss for the minimal model of Section 4.2. If along the iterates  $(\mathbf{W}_{\text{KQ}}(\tau))_{\tau \geq 0}$  we have*

$$\text{MSE}(\mathbf{W}_{\text{KQ}}(\tau)) \rightarrow 0 \text{ and } \sum_{\tau=0}^{\infty} \|\nabla \text{MSE}(\mathbf{W}_{\text{KQ}}(\tau))\|_F^2 < \infty, \quad (4)$$

then:

$$\frac{\mathbf{W}_{\text{KQ}}(\tau)}{\|\mathbf{W}_{\text{KQ}}(\tau)\|_F} \rightarrow \frac{\hat{\mathbf{W}}_{\text{KQ}}}{\|\hat{\mathbf{W}}_{\text{KQ}}\|_F}, \quad (5)$$

where  $\hat{\mathbf{W}}_{\text{KQ}}$  is the max-margin solution defined in Section 4.2. Moreover,  $\|\mathbf{W}_{\text{KQ}}(\tau)\|_F$  diverges at a rate  $\frac{\|\hat{\mathbf{W}}_{\text{KQ}}\|_F}{2} \log(\tau)$ , and the induced margins increase accordingly (hence attention becomes asymptotically hard on the true match).

The conclusion is conditional: it applies to trajectories that both succeed in driving the MSE to zero and satisfy the regularity conditions in Section 4.4. In Section G.3 we provide an empirical sanity check for these conditions on a representative successful run.

The remainder of this section is devoted to (i) specifying the minimal setting and the empirical phenomena we aim to explain, (ii) stating the event and justifying it holds whp for GMC data, and

(iii) isolating the remaining MSE-specific technical assumptions and explaining how they differ from the standard max-margin theory for monotone margin losses [20, 38–40, 43]. This organization is meant to clarify which parts of the conclusion are driven by typical GMC geometry (point (ii)), and which parts rely on additional MSE-specific asymptotic regularity conditions once optimization succeeds (point (iii)).

## 4.2 Simplified setting and empirical observations

**Simplified task: exact match, exact copy.** To isolate the core retrieval mechanism, we strip away the stochastic noise in GMC and work with the noiseless match-and-copy template:

$$\mathbf{e}^{(i)} = \mathbf{e}_{t_0^{(i)}}^{(i)} \quad \text{and} \quad \mathbf{v}^{(i)} = \mathbf{e}_{t_0^{(i)}+1}^{(i)}, \quad (6)$$

for  $n$  training sequences  $x^{(i)} = (\mathbf{e}_1^{(i)}, \dots, \mathbf{e}_T^{(i)}, \mathbf{e}^{(i)})$ .

**Minimal model: two-layer attention-only, with a frozen PTH.** The smallest architecture that can implement a PTH→IH circuit is a 2-layer attention-only model with one head per layer. We freeze the first layer to implement an exact previous-token head (PTH). This is equivalent to shifting the keys of the second layer by one position; hence, we work directly with the standard *shifted-key* parametrization [37, 45]. We fix  $\mathbf{W}_V$  to the ground-truth value map used by GMC (and in the present simplified exact-copy setup,  $\mathbf{W}_V = \mathbf{I}$ ). This isolates the non-convex match-selection mechanism in  $\mathbf{W}_{KQ}$ .

Fixing  $\mathbf{W}_V$  is justified because the problem is *strictly convex* with respect to  $\mathbf{W}_V$ , and it does not interact with the match selection mechanism. In principle,  $\mathbf{W}_V$  could be recovered optimally in a first optimization stage. Prior works typically do optimization in stages [9, 27, 45]. Here we directly focus on the second stage, optimizing over the merged key-query matrix

$$\mathbf{W}_{KQ} := \mathbf{W}_K^\top \mathbf{W}_Q \in \mathbb{R}^{d_{in} \times d_{in}}. \quad (7)$$

This isolates the *non-convex* part of the model, responsible for selecting the match position.

Concretely, for context  $\mathbf{E} = (\mathbf{e}_1, \dots, \mathbf{e}_T)$  and query  $\mathbf{e}$ , the model output is

$$\begin{aligned} \text{model}(\mathbf{W}_{KQ}; \mathbf{E}, \mathbf{e}) = \\ \underbrace{\sum_{t=2}^T \text{softmax} \left( (\mathbf{e}_s^\top \mathbf{W}_{KQ} \mathbf{e})_{s=1}^{T-1} \right)_{t-1}}_{=:a_t(\mathbf{W}_{KQ}; \mathbf{E}, \mathbf{e})} \mathbf{W}_V \mathbf{e}_t. \end{aligned} \quad (8)$$

This is exactly the computation performed by an IH that reads a PTH mark: it scores predecessors via  $\mathbf{e}_s^\top \mathbf{W}_{KQ} \mathbf{e}$  and copies the successor token through the one-step shift [37, 45].

**Objective: empirical MSE.** We train with the empirical MSE loss, which is the objective used throughout the empirical study in Section 3:

$$\text{MSE}(\mathbf{W}_{KQ}) := \sum_{i=1}^n \left\| \mathbf{v}^{(i)} - \text{model}(\mathbf{W}_{KQ}; \mathbf{E}^{(i)}, \mathbf{e}^{(i)}) \right\|_2^2. \quad (9)$$

We focus on MSE (rather than a cross-entropy over the match position  $\text{CE}(\mathbf{W}_{KQ}) = -\sum_i \log a_{t_0^{(i)}+1}(\mathbf{W}_{KQ}; \mathbf{E}^{(i)}, \mathbf{e}^{(i)})$ ) because our benchmark is a regression task so it is the natural objective. And more importantly, because there is no architecture-agnostic analogue of such a cross-entropy for non-attention models (no attention weights to interpret as match probabilities), so MSE is the meaningful objective for the architecture comparisons in Section 3.3.

**Margins and the associated max-margin problem.** For each sample  $i$  and distractor position  $t \neq t_0^{(i)}$ , define the match margin

$$\text{margin}_{i,t}(\mathbf{W}_{KQ}) := (\mathbf{e}_{t_0^{(i)}}^{(i)} - \mathbf{e}_t^{(i)})^\top \mathbf{W}_{KQ} \mathbf{e}^{(i)}. \quad (10)$$

Large positive margins imply  $a_{t_0^{(i)}+1}(\mathbf{W}_{KQ}; \mathbf{E}^{(i)}, \mathbf{e}^{(i)}) \approx 1$  and thus  $\text{model}(\mathbf{W}_{KQ}; \mathbf{E}^{(i)}, \mathbf{e}^{(i)}) \approx \mathbf{W}_V \mathbf{e}_{t_0^{(i)}+1}^{(i)} = \mathbf{v}^{(i)}$ .

We define the max-margin separator by the SVM problem:

$$\begin{aligned} \hat{\mathbf{W}}_{\text{KQ}} &= \operatorname{argmin}_{\mathbf{W}_{\text{KQ}}} \frac{1}{2} \|\mathbf{W}_{\text{KQ}}\|_F^2 \\ \text{s.t. } \text{margin}_{i,t}(\mathbf{W}_{\text{KQ}}) &\geq 1 \quad \forall i \in [n], \quad \forall t \neq t_0^{(i)}. \end{aligned} \quad (11)$$

**Empirical observations.** When we train (9) by gradient descent in this minimal setting, we observe the following behavior in regimes where training attains very small loss and alignment is visible within our iteration budget:

1.  $\text{MSE}(\mathbf{W}_{\text{KQ}}(\tau))$  decreases to a small value and the cumulative squared gradient norm remains bounded, matching the success condition (4);
2.  $\|\mathbf{W}_{\text{KQ}}(\tau)\|_F$  grows over training;
3. the normalized direction  $\mathbf{W}_{\text{KQ}}(\tau)/\|\mathbf{W}_{\text{KQ}}(\tau)\|_F$  becomes increasingly aligned with  $\hat{\mathbf{W}}_{\text{KQ}}/\|\hat{\mathbf{W}}_{\text{KQ}}\|_F$ ;
4. the margins  $\min_{i,t \neq t_0^{(i)}} \text{margin}_{i,t}(\mathbf{W}_{\text{KQ}}(\tau))$  increase, and attention becomes hard on the correct match.

An example is given in Section G.3. In other configurations, the cosine similarity between  $\mathbf{W}_{\text{KQ}}(\tau)/\|\mathbf{W}_{\text{KQ}}(\tau)\|_F$  and  $\hat{\mathbf{W}}_{\text{KQ}}/\|\hat{\mathbf{W}}_{\text{KQ}}\|_F$  does not reach 1 within the iteration budget. While it reaches the range [0.8, 0.95] in general, it is unclear if it reflects slow convergence or if it converged toward a different asymptotic direction, hence settled that way.

Recent work on implicit bias in attention models with monotone margin losses shows that some regimes can converge to *locally optimal* max-margin directions rather than the globally optimal one, depending on data geometry and parameterization [39]. Whether analogous phenomena occur under MSE remains open. In this work, we focus on identifying and explaining regimes where clear global max-margin alignment is observed within a finite horizon, and on characterizing the properties of trajectories that lead to this behavior.

### 4.3 A geometric event on GMC data

A key difference between MSE and the usual monotone margin losses for max-margin implicit bias results [20, 38–40, 43] (e.g., logistic or exponential losses in binary classification, discussed in Section D.3) is that MSE can admit finite-norm minimizers. Even when it does not, the margins need not keep increasing *monotonically* along the trajectory, as MSE gradients contain interaction terms absent in monotone margin losses. Here we identify a *geometric event* on the training set under which: (i) there is *no* finite-norm minimizer for (9), and (ii) any successful optimization trajectory must enter a regime where margins keep increasing *monotonically*.

**The event.** We define an explicit event  $\mathcal{E}_{\text{GMC}}$  on the  $n$  sampled GMC sequences. It is purely geometric, as it can be expressed as a set of inequalities involving the token Gram matrices and the difference vectors  $\{\mathbf{e}_{t_0^{(i)}}^{(i)} - \mathbf{e}_t^{(i)}\}_{i,t \neq t_0^{(i)}}$ . We defer its full statement to Section D and only summarize its role here: it rules out the existence of a finite-norm zero-loss interpolant (Section G.2), and it enforces a favorable geometry under which the leading terms in the dynamics promote increasing margins *monotonically* in the successful regime (see the discussion above Theorem F.3).

**High-probability guarantee on GMC.** We prove that  $\mathcal{E}_{\text{GMC}}$  holds with high probability under the GMC sampling model (stated for the exact-match/exact-copy specialization considered here). A precise statement and proof are given in Section G.1. The probability improves as the geometry becomes more overparameterized in the sense relevant to match selection (informally: larger  $d_{\text{in}}$  relative to the effective number of distractors). It justifies why GMC instances *typically* land in a regime where divergence and margin growth are unavoidable, even though alternative behaviors are conceivable in other data geometries.

#### 4.4 MSE-specific technical assumptions

With  $\mathcal{E}_{\text{geom}}$  in place, the remaining obstacles are not about GMC geometry but about the optimization dynamics induced by (9). For margin-based classification losses (like logistic/exponential) [20, 38–40, 43], the gradient is a positive combination of separating directions, with *fixed* coefficients multiplied by a monotone function of the margins. For MSE, the gradient is also a positive combination of separating directions (thanks to  $\mathcal{E}_{\text{geom}}$ ), keeping margins growing, but the coefficients depend on the  $\ell^2$  residuals, and includes cross-terms induced by the square (this comparison is discussed in details in Theorem F.2). To recover a max-margin limit, this motivates the next assumption. We defer the precise statement to Section D.

**Assumption 4.2** (Asymptotic stabilization of MSE/softmax interactions). Asymptotically along the trajectory, (i) the gradient coefficients that are not monotone functions of the margins stabilize asymptotically so that the dynamics become effectively margin-driven, and (ii) the cross-terms become negligible relative to the main margin terms so that the gradient becomes dominated by a stable set of support constraints.

Theorem 4.2 is the main MSE-specific hypothesis. It replaces automatic simplifications enjoyed by monotone margin losses: it rules out interference from MSE-specific cross-terms and enforces a support-dominated asymptotic regime in which max-margin arguments can be adapted. In Section G.3 we provide an empirical sanity check of these conditions on a representative run where strong alignment is observed within the training budget.

## 5 Conclusion

GMC provides a simple and theory-friendly benchmark in which retrieval circuits emerge reliably, separate architectures by their retrieval capabilities, and admit analytical study. In a minimal attention setting, we show that despite many *a priori* possible regression solutions, there exists a regime in which successful training is accompanied by a max-margin implicit bias that drives attention toward hard match selection.

Open questions include how this bias changes when optimizing the unmerged key-query parameterization (e.g., toward a nuclear-norm max-margin solution [39]), whether the analysis extends beyond the minimal setting, and what additional ingredients are required to explain the sharp loss-drop dynamics observed in deeper Transformers.

## Acknowledgements

We thank Pierre Marion for insightful discussions. This work was supported in part by the Swiss State Secretariat for Education, Research and Innovation (SERI) under contract number MB22.00027.

## References

- [1] Ekin Akyürek, Dale Schuurmans, Jacob Andreas, Tengyu Ma, and Denny Zhou. What learning algorithm is in-context learning? investigations with linear models. In *The Eleventh International Conference on Learning Representations, ICLR 2023, Kigali, Rwanda, May 1-5, 2023*. OpenReview.net, 2023. URL <https://openreview.net/forum?id=0g0X4H8yN4I>.
- [2] Ekin Akyürek, Bailin Wang, Yoon Kim, and Jacob Andreas. In-context language learning: Architectures and algorithms. In *Forty-first International Conference on Machine Learning, ICML 2024, Vienna, Austria, July 21-27, 2024*. OpenReview.net, 2024. URL <https://openreview.net/forum?id=3Z9CRr5srL>.
- [3] Simran Arora, Sabri Eyuboglu, Aman Timalsina, Isys Johnson, Michael Poli, James Zou, Atri Rudra, and Christopher Ré. Zoology: Measuring and improving recall in efficient language models. In *The Twelfth International Conference on Learning Representations, ICLR 2024, Vienna, Austria, May 7-11, 2024*. OpenReview.net, 2024. URL <https://openreview.net/forum?id=LY3ukUANko>.
- [4] Jimmy Ba, Geoffrey E. Hinton, Volodymyr Mnih, Joel Z. Leibo, and Catalin Ionescu. Using fast weights to attend to the recent past. In Daniel D. Lee, Masashi Sugiyama, Ulrike von Luxburg, Isabelle Guyon, and Roman Garnett, editors, *Advances in Neural Information Processing Systems*

29: Annual Conference on Neural Information Processing Systems 2016, December 5-10, 2016, Barcelona, Spain, pages 4331–4339, 2016. URL <https://proceedings.neurips.cc/paper/2016/hash/9f44e956e3a2b7b5598c625fcc802c36-Abstract.html>.

[5] Satwik Bhattacharya, Arkil Patel, Phil Blunsom, and Varun Kanade. Understanding in-context learning in transformers and llms by learning to learn discrete functions. In *The Twelfth International Conference on Learning Representations, ICLR 2024, Vienna, Austria, May 7-11, 2024*. OpenReview.net, 2024. URL <https://openreview.net/forum?id=ekeyCgeRfC>.

[6] Alberto Bietti, Vivien Cabannes, Diane Bouchacourt, Hervé Jégou, and Léon Bottou. Birth of a transformer: A memory viewpoint. In Alice Oh, Tristan Naumann, Amir Globerson, Kate Saenko, Moritz Hardt, and Sergey Levine, editors, *Advances in Neural Information Processing Systems 36: Annual Conference on Neural Information Processing Systems 2023, NeurIPS 2023, New Orleans, LA, USA, December 10 - 16, 2023*, 2023.

[7] Callum McDougall. Induction heads illustrated, 2023. URL <https://www.lesswrong.com/posts/TvrfY4c9eaGLeyDkE/induction-heads-illustrated>. Accessed: 2026-01-15.

[8] Stephanie C. Y. Chan, Adam Santoro, Andrew K. Lampinen, Jane X. Wang, Aaditya K. Singh, Pierre H. Richemond, James L. McClelland, and Felix Hill. Data distributional properties drive emergent in-context learning in transformers. In Sanmi Koyejo, S. Mohamed, A. Agarwal, Danielle Belgrave, K. Cho, and A. Oh, editors, *Advances in Neural Information Processing Systems 35: Annual Conference on Neural Information Processing Systems 2022, NeurIPS 2022, New Orleans, LA, USA, November 28 - December 9, 2022*, 2022.

[9] Siyu Chen, Heejune Sheen, Tianhao Wang, and Zhuoran Yang. Unveiling induction heads: Provable training dynamics and feature learning in transformers. In Amir Globersons, Lester Mackey, Danielle Belgrave, Angela Fan, Ulrich Paquet, Jakub M. Tomczak, and Cheng Zhang, editors, *Advances in Neural Information Processing Systems 38: Annual Conference on Neural Information Processing Systems 2024, NeurIPS 2024, Vancouver, BC, Canada, December 10 - 15, 2024*, 2024.

[10] Kyunghyun Cho, Bart van Merriënboer, Çağlar Gülcehre, Dzmitry Bahdanau, Fethi Bougares, Holger Schwenk, and Yoshua Bengio. Learning phrase representations using RNN encoder-decoder for statistical machine translation. In Alessandro Moschitti, Bo Pang, and Walter Daelemans, editors, *Proceedings of the 2014 Conference on Empirical Methods in Natural Language Processing, EMNLP 2014, October 25-29, 2014, Doha, Qatar, A meeting of SIGDAT, a Special Interest Group of the ACL*, pages 1724–1734. ACL, 2014. doi: 10.3115/V1/D14-1179. URL <https://doi.org/10.3115/v1/d14-1179>.

[11] Joy Crosbie and Ekaterina Shutova. Induction heads as an essential mechanism for pattern matching in in-context learning. *CoRR*, abs/2407.07011, 2024. doi: 10.48550/ARXIV.2407.07011. URL <https://doi.org/10.48550/arXiv.2407.07011>.

[12] Damai Dai, Yutao Sun, Li Dong, Yaru Hao, Shuming Ma, Zhifang Sui, and Furu Wei. Why can GPT learn in-context? language models secretly perform gradient descent as meta-optimizers. In Anna Rogers, Jordan L. Boyd-Graber, and Naoaki Okazaki, editors, *Findings of the Association for Computational Linguistics: ACL 2023, Toronto, Canada, July 9-14, 2023*, pages 4005–4019. Association for Computational Linguistics, 2023. doi: 10.18653/V1/2023.FINDINGS-ACL.247. URL <https://doi.org/10.18653/v1/2023.findings-acl.247>.

[13] Ezra Edelman, Nikolaos Tsilivis, Benjamin L. Edelman, Eran Malach, and Surbhi Goel. The evolution of statistical induction heads: In-context learning markov chains. In Amir Globersons, Lester Mackey, Danielle Belgrave, Angela Fan, Ulrich Paquet, Jakub M. Tomczak, and Cheng Zhang, editors, *Advances in Neural Information Processing Systems 38: Annual Conference on Neural Information Processing Systems 2024, NeurIPS 2024, Vancouver, BC, Canada, December 10 - 15, 2024*, 2024.

[14] Nelson Elhage, Neel Nanda, Catherine Olsson, Tom Henighan, Nicholas Joseph, Ben Mann, Amanda Askell, Yuntao Bai, Anna Chen, Tom Conerly, Nova DasSarma, Dawn Drain, Deep Ganguli, Zac Hatfield-Dodds, Danny Hernandez, Andy Jones, Jackson Kernion, Liane Lovitt, Kamal Ndousse, Dario Amodei, Tom Brown, Jack Clark, Jared Kaplan, Sam McCandlish, and Chris Olah. A mathematical framework for transformer circuits. *Transformer Circuits Thread*, 2021. URL <https://transformer-circuits.pub/2021/framework/index.html>.

[15] Daniel Y. Fu, Tri Dao, Khaled Kamal Saab, Armin W. Thomas, Atri Rudra, and Christopher Ré. Hungry hungry hippos: Towards language modeling with state space models. In *The Eleventh International Conference on Learning Representations, ICLR 2023, Kigali, Rwanda, May 1-5, 2023*. OpenReview.net, 2023. URL <https://openreview.net/forum?id=COZDy0WYGg>.

[16] Shivam Garg, Dimitris Tsipras, Percy Liang, and Gregory Valiant. What can transformers learn in-context? A case study of simple function classes. In Sanmi Koyejo, S. Mohamed, A. Agarwal, Danielle Belgrave, K. Cho, and A. Oh, editors, *Advances in Neural Information Processing Systems 35: Annual Conference on Neural Information Processing Systems 2022, NeurIPS 2022, New Orleans, LA, USA, November 28 - December 9, 2022*, 2022.

[17] Alex Graves, Greg Wayne, and Ivo Danihelka. Neural turing machines. *CoRR*, abs/1410.5401, 2014. URL <http://arxiv.org/abs/1410.5401>.

[18] Albert Gu, Karan Goel, and Christopher Ré. Efficiently modeling long sequences with structured state spaces. In *The Tenth International Conference on Learning Representations, ICLR 2022, Virtual Event, April 25-29, 2022*. OpenReview.net, 2022. URL <https://openreview.net/forum?id=uYLFozivlAC>.

[19] Samy Jelassi, David Brandfonbrener, Sham M. Kakade, and Eran Malach. Repeat after me: Transformers are better than state space models at copying. In *Forty-first International Conference on Machine Learning, ICML 2024, Vienna, Austria, July 21-27, 2024*. OpenReview.net, 2024. URL <https://openreview.net/forum?id=duRRoGeoQT>.

[20] Ziwei Ji and Matus Telgarsky. The implicit bias of gradient descent on nonseparable data. In Alina Beygelzimer and Daniel Hsu, editors, *Conference on Learning Theory, COLT 2019, 25-28 June 2019, Phoenix, AZ, USA*, volume 99 of *Proceedings of Machine Learning Research*, pages 1772–1798. PMLR, 2019. URL <http://proceedings.mlr.press/v99/ji19a.html>.

[21] Brenden M. Lake, Ruslan Salakhutdinov, and Joshua B. Tenenbaum. Human-level concept learning through probabilistic program induction. *Science*, 350(6266):1332–1338, 2015. doi: 10.1126/science.aab3050. URL <https://www.science.org/doi/abs/10.1126/science.aab3050>.

[22] Ivan Lee, Nan Jiang, and Taylor Berg-Kirkpatrick. Is attention required for icl? exploring the relationship between model architecture and in-context learning ability. In *The Twelfth International Conference on Learning Representations, ICLR 2024, Vienna, Austria, May 7-11, 2024*. OpenReview.net, 2024. URL <https://openreview.net/forum?id=Qwq4cpLtoX>.

[23] Ashok Vardhan Makkuvu, Marco Bondaschi, Adway Girish, Alliot Nagle, Martin Jaggi, Hyeji Kim, and Michael Gastpar. Attention with markov: A curious case of single-layer transformers. In *The Thirteenth International Conference on Learning Representations, ICLR 2025, Singapore, April 24-28, 2025*. OpenReview.net, 2025. URL <https://openreview.net/forum?id=SqZOKY4qBD>.

[24] Pierre Marion, Raphaël Berthier, Gérard Biau, and Claire Boyer. Attention layers provably solve single-location regression. In *The Thirteenth International Conference on Learning Representations, ICLR 2025, Singapore, April 24-28, 2025*. OpenReview.net, 2025. URL <https://openreview.net/forum?id=DV1Pp7Jd7P>.

[25] Sewon Min, Xinxi Lyu, Ari Holtzman, Mikel Artetxe, Mike Lewis, Hannaneh Hajishirzi, and Luke Zettlemoyer. Rethinking the role of demonstrations: What makes in-context learning work? In Yoav Goldberg, Zornitsa Kozareva, and Yue Zhang, editors, *Proceedings of the 2022 Conference on Empirical Methods in Natural Language Processing, EMNLP 2022, Abu Dhabi, United Arab Emirates, December 7-11, 2022*, pages 11048–11064. Association for Computational Linguistics, 2022. doi: 10.18653/V1/2022.EMNLP-MAIN.759. URL <https://doi.org/10.18653/v1/2022.emnlp-main.759>.

[26] Tiberiu Musat, Tiago Pimentel, Lorenzo Noci, Alessandro Stolfo, Mrinmaya Sachan, and Thomas Hofmann. On the emergence of induction heads for in-context learning. *CoRR*, abs/2511.01033, 2025. doi: 10.48550/ARXIV.2511.01033. URL <https://doi.org/10.48550/arXiv.2511.01033>.

[27] Eshaan Nichani, Alex Damian, and Jason D. Lee. How transformers learn causal structure with gradient descent. In *Forty-first International Conference on Machine Learning, ICML 2024, Vienna, Austria, July 21-27, 2024*. OpenReview.net, 2024. URL <https://openreview.net/forum?id=jNM4im1HZv>.

[28] Catherine Olsson, Nelson Elhage, Neel Nanda, Nicholas Joseph, Nova DasSarma, Tom Henighan, Ben Mann, Amanda Askell, Yuntao Bai, Anna Chen, Tom Conerly, Dawn Drain, Deep Ganguli, Zac Hatfield-Dodds, Danny Hernandez, Scott Johnston, Andy Jones, Jackson Kernion, Liane Lovitt, Kamal Ndousse, Dario Amodei, Tom Brown, Jack Clark, Jared Kaplan, Sam McCandlish, and Chris Olah. In-context learning and induction heads. *CoRR*, abs/2209.11895, 2022. doi: 10.48550/ARXIV.2209.11895. URL <https://doi.org/10.48550/arXiv.2209.11895>.

[29] Badri Narayana Patro and Vijay Srinivas Agneeswaran. Mamba-360: Survey of state space models as transformer alternative for long sequence modelling: Methods, applications, and challenges. *CoRR*, abs/2404.16112, 2024. doi: 10.48550/ARXIV.2404.16112. URL <https://doi.org/10.48550/arXiv.2404.16112>.

[30] Mary Phuong and Marcus Hutter. Formal algorithms for transformers. *CoRR*, abs/2207.09238, 2022. doi: 10.48550/ARXIV.2207.09238. URL <https://doi.org/10.48550/arXiv.2207.09238>.

[31] Michael Poli, Stefano Massaroli, Eric Nguyen, Daniel Y. Fu, Tri Dao, Stephen Baccus, Yoshua Bengio, Stefano Ermon, and Christopher Ré. Hyena hierarchy: Towards larger convolutional language models. In Andreas Krause, Emma Brunskill, Kyunghyun Cho, Barbara Engelhardt, Sivan Sabato, and Jonathan Scarlett, editors, *International Conference on Machine Learning, ICML 2023, 23-29 July 2023, Honolulu, Hawaii, USA*, volume 202 of *Proceedings of Machine Learning Research*, pages 28043–28078. PMLR, 2023. URL <https://proceedings.mlr.press/v202/poli23a.html>.

[32] Alec Radford, Jeff Wu, Rewon Child, David Luan, Dario Amodei, and Ilya Sutskever. Language models are unsupervised multitask learners. *OpenAI Blog*, 2019. URL [https://cdn.openai.com/better-language-models/language\\_models\\_are\\_unsupervised\\_multitask\\_learners.pdf](https://cdn.openai.com/better-language-models/language_models_are_unsupervised_multitask_learners.pdf).

[33] Nived Rajaraman, Marco Bondaschi, Ashok Vardhan Makkula, Kannan Ramchandran, and Michael Gastpar. Transformers on markov data: Constant depth suffices. In Amir Globersons, Lester Mackey, Danielle Belgrave, Angela Fan, Ulrich Paquet, Jakub M. Tomczak, and Cheng Zhang, editors, *Advances in Neural Information Processing Systems 38: Annual Conference on Neural Information Processing Systems 2024, NeurIPS 2024, Vancouver, BC, Canada, December 10 - 15, 2024*, 2024.

[34] Gautam Reddy. The mechanistic basis of data dependence and abrupt learning in an in-context classification task. In *The Twelfth International Conference on Learning Representations, ICLR 2024, Vienna, Austria, May 7-11, 2024*. OpenReview.net, 2024. URL <https://openreview.net/forum?id=aN4Jf6Cx69>.

[35] Clayton Sanford, Daniel Hsu, and Matus Telgarsky. One-layer transformers fail to solve the induction heads task. *CoRR*, abs/2408.14332, 2024. doi: 10.48550/ARXIV.2408.14332. URL <https://doi.org/10.48550/arXiv.2408.14332>.

[36] Aaditya K. Singh, Stephanie C. Y. Chan, Ted Moskovitz, Erin Grant, Andrew M. Saxe, and Felix Hill. The transient nature of emergent in-context learning in transformers. In Alice Oh, Tristan Naumann, Amir Globerson, Kate Saenko, Moritz Hardt, and Sergey Levine, editors, *Advances in Neural Information Processing Systems 36: Annual Conference on Neural Information Processing Systems 2023, NeurIPS 2023, New Orleans, LA, USA, December 10 - 16, 2023*, 2023.

[37] Aaditya K. Singh, Ted Moskovitz, Felix Hill, Stephanie C. Y. Chan, and Andrew M. Saxe. What needs to go right for an induction head? A mechanistic study of in-context learning circuits and their formation. In *Forty-first International Conference on Machine Learning, ICML 2024, Vienna, Austria, July 21-27, 2024*. OpenReview.net, 2024. URL <https://openreview.net/forum?id=08rrXl71D5>.

[38] Daniel Soudry, Elad Hoffer, Mor Shpigel Nacson, Suriya Gunasekar, and Nathan Srebro. The implicit bias of gradient descent on separable data. *J. Mach. Learn. Res.*, 19:70:1–70:57, 2018. URL <https://jmlr.org/papers/v19/18-188.html>.

[39] Davoud Ataee Tarzanagh, Yingcong Li, Christos Thrampoulidis, and Samet Oymak. Transformers as support vector machines. *CoRR*, abs/2308.16898, 2023. doi: 10.48550/ARXIV.2308.16898. URL <https://doi.org/10.48550/arXiv.2308.16898>.

[40] Davoud Ataee Tarzanagh, Yingcong Li, Xuechen Zhang, and Samet Oymak. Max-margin token selection in attention mechanism. In Alice Oh, Tristan Naumann, Amir Globerson, Kate Saenko,

Moritz Hardt, and Sergey Levine, editors, *Advances in Neural Information Processing Systems 36: Annual Conference on Neural Information Processing Systems 2023, NeurIPS 2023, New Orleans, LA, USA, December 10 - 16, 2023*, 2023.

- [41] Llama Team. The llama 3 herd of models. *CoRR*, abs/2407.21783, 2024. doi: 10.48550/ARXIV.2407.21783. URL <https://doi.org/10.48550/arXiv.2407.21783>.
- [42] Aditya Varre, Gizem Yüce, and Nicolas Flammarion. Learning in-context n-grams with transformers: Sub-n-grams are near-stationary points. In *Forty-second International Conference on Machine Learning, ICML 2025, Vancouver, BC, Canada, July 13-19, 2025*. OpenReview.net, 2025. URL <https://openreview.net/forum?id=0MwdvGDeHL>.
- [43] Bhavya Vasudeva, Punceesh Deora, and Christos Thrampoulidis. Implicit bias and fast convergence rates for self-attention. *Trans. Mach. Learn. Res.*, 2025, 2025. URL <https://openreview.net/forum?id=pKilnjQsb0>.
- [44] Johannes von Oswald, Eyvind Niklasson, Ettore Randazzo, João Sacramento, Alexander Mordvintsev, Andrey Zhmoginov, and Max Vladymyrov. Transformers learn in-context by gradient descent. In Andreas Krause, Emma Brunskill, Kyunghyun Cho, Barbara Engelhardt, Sivan Sabato, and Jonathan Scarlett, editors, *International Conference on Machine Learning, ICML 2023, 23-29 July 2023, Honolulu, Hawaii, USA*, volume 202 of *Proceedings of Machine Learning Research*, pages 35151–35174. PMLR, 2023. URL <https://proceedings.mlr.press/v202/von-oswald23a.html>.
- [45] Mingze Wang, Ruoxi Yu, Weinan E, and Lei Wu. How transformers get rich: Approximation and dynamics analysis. *arXiv preprint arXiv:2410.11474*, 2025.
- [46] Sang Michael Xie, Aditi Raghunathan, Percy Liang, and Tengyu Ma. An explanation of in-context learning as implicit bayesian inference. In *The Tenth International Conference on Learning Representations, ICLR 2022, Virtual Event, April 25-29, 2022*. OpenReview.net, 2022. URL <https://openreview.net/forum?id=RdJVFCHjUMI>.

## A Experimental Details for Gaussian Match-and-Copy

This section provides the implementation details, hyperparameters, and additional results for the GMC experiments discussed in Section 3.

### A.1 Computational Resources

All experiments were conducted on a single NVIDIA RTX 4050 GPU (Ubuntu 24.04, CUDA 12.4) using PyTorch 2.6.0 and HuggingFace Transformers 4.49.0. We deliberately selected hyperparameters to enable rapid experimentation—a 1000-step run on the average dimensions tested completes in approximately one minute—while preserving qualitative behaviors of interest that are known to emerge at larger scales. This design allows us to replicate core properties of the PTH→IH circuit in a simpler environment (e.g., Gaussian data rather than natural language), while ensuring that the benchmark remains computationally accessible.

### A.2 Task and Model Configurations

Table 1 summarizes all task and model configurations used by default in Section 3, unless stated otherwise. We now discuss *how* each choice was made.

**Data Generation (Table 1).** The GMC task parameters (Theorem 1.1) are chosen to balance difficulty and computational efficiency.

- **Dimensions:** We set  $d_{\text{in}} = d_{\text{out}}$  for simplicity. We report results for  $d_{\text{in}} \in \{16, 32\}$  and sequence lengths  $T \in \{8, 16\}$ . We verified that results hold for larger dimensions (tested up to  $d_{\text{in}} = 1024, T = 1024$ ), but we adhere to the small-dimensionality regime to highlight a minimal setting where the task retains key properties of larger models while allowing for rapid iteration.
- **Token and Value Generation:** Context tokens are sampled as  $\mathbf{e}_t \sim \mathcal{N}(0, \frac{\sigma_{\text{token}}^2}{d_{\text{in}}} \mathbf{I}_{d_{\text{in}}})$  with  $\sigma_{\text{token}} = 1$ . This scaling ensures that the token norm  $\|\mathbf{e}_t\|_2$  remains roughly constant regardless of the dimension  $d_{\text{in}}$ . We also experimented with  $\mathbf{e}_t, \mathbf{e} \sim \mathcal{N}(0, \mathbf{I}_{d_{\text{in}}})$ , which produced similar results but led to sharper loss drops at the emergence of the PTH and IH, likely because the larger token norms increased the correlation between the hidden match and the query, making it easier to detect. We stick to the former scaling for consistency across dimensions. The value matrix  $\mathbf{W}_V$  is fixed for a given task instance, with entries drawn i.i.d. from  $\mathcal{N}(0, 1)$ . Finally, the noise distribution  $\mathcal{D}_\xi$  in Theorem 1.1 is chosen such that  $\mathbf{e} \sim \mathcal{N}(0, \frac{\sigma_{\text{token}}^2}{d_{\text{in}}} \mathbf{I}_{d_{\text{in}}})$ , i.e., the same marginal distribution as the other tokens. Concretely, we set  $\mathbf{e} = \mathbf{C}\mathbf{e}_{t_0} + S\xi$ , where  $\xi \sim \mathcal{N}(0, \frac{\sigma_{\text{noise}}^2}{d_{\text{in}}} \mathbf{I}_{d_{\text{in}}})$  is independent noise and  $S$  satisfies  $SS^\top = \mathbf{I}_{d_{\text{in}}} - \mathbf{C}\mathbf{C}^\top$ .
- **Signal-to-Noise Ratio (SNR):** The target is defined as  $\mathbf{v} = \mathbf{W}_V \mathbf{e}_{t_0+1} + \varepsilon$ , where  $\varepsilon \sim \mathcal{N}(0, \sigma_{\text{noise}}^2 \mathbf{I}_{d_{\text{out}}})$  with  $\sigma_{\text{noise}} = 0.1$ . Given the definitions above, the signal component  $\mathbf{W}_V \mathbf{e}_{t_0+1}$  has coordinate-wise variance  $d_{\text{in}} \cdot 1 \cdot (\sigma_{\text{token}}^2 / d_{\text{in}}) = \sigma_{\text{token}}^2 = 1$ . The noise component has variance  $\sigma_{\text{noise}}^2 = 0.01$ . This yields a signal-to-noise variance ratio of roughly 100.
- **Correlations:** The covariance matrix is chosen isotropic  $\mathbf{C} = \frac{1}{c^2} \mathbf{I}_{d_{\text{in}}}$  for simplicity. Since  $\text{Cov}(\mathbf{e}, \mathbf{e}_{t_0}) \propto \mathbf{C}$ , the parameter  $c$  controls difficulty; higher  $c$  reduces the correlation between the query and the match. We use  $c \in \{1.1, 1.2, 1.3\}$  to span different difficulty levels. Indeed, for the dimensions we used, we found that  $c = 1.1$  and  $c = 1.3$  were good choices to ensure that (1) all considered models were able to learn the task, and (2) the training curves differed enough for these two values of  $c$  to consider them as different difficulty levels. Note however that the task difficulty is not only controlled by  $c$  but also by the sequence length  $T$  and the noise level  $\sigma_\varepsilon$ , as can be seen from Figure 5 where larger  $T$  and  $c$  slows down the learning process.
- **Test Set:** We evaluate models on a fixed test set of 128 fresh GMC sequences. These are generated using the same parameters  $(d_{\text{in}}, d_{\text{out}}, T, \mathbf{W}_V, \mathbf{C}, \sigma_{\text{token}}, \sigma_{\text{noise}})$  as the training set, but with different random seeds for the tokens, hidden match indices, and noise.

**Transformer Architectures (Table 1).** We train GPT-2 [32] and Llama 3 [41] architectures initialized with the default HuggingFace scheme (weights  $\sim \mathcal{N}(0, 0.02^2)$ ). Unless stated otherwise, we use 2-layer models, as this is the minimal depth required to implement a full induction circuit (PTH in layer 0, IH in layer 1) [14, 28, 35]. Hidden and head sizes are adapted from Lee et al. [22], as summarized in Table 1.

**Optimization and Robustness (Table 1).** We use AdamW ( $\beta_1 = 0.9, \beta_2 = 0.95$ ) with a batch size of 512 and a learning rate of  $10^{-3}$  (with 200 steps warmup and cosine decay). We selected these hyperparameters after performing sweeps over:

- **Learning rates:** Range  $10^{-1}$  to  $10^{-5}$ . Larger rates caused instability; smaller rates shifted the loss drop later without changing the qualitative outcome.
- **Batch sizes:** Range 32 to 1024. 512 offered the best tradeoff between training speed and curve smoothness.
- **Optimizers:** AdamW consistently outperformed SGD and standard Adam in preliminary tests.

We found the emergence of the PTH→IH circuit to be robust to these optimization choices: suboptimal hyperparameters typically led to non-convergence, but whenever the model solved the task, it did so via the same phase-transition mechanism described in Section 3.

Table 1: Hyperparameters for standard GMC experiments in Section 3.

Parameter	Value
<i>GMC Task</i>	
Context length ( $T$ )	$\{8, 16\}$
Dimension ( $d_{\text{in}} = d_{\text{out}}$ )	$\{16, 32\}$
Covariance ( $\mathbf{C}$ )	$\frac{1}{c^2} \mathbf{I}_{d_{\text{in}}}$
Inverse correlation strength ( $c$ )	$\{1.1, 1.2, 1.3\}$
Token standard deviation ( $\sigma_{\text{token}}$ )	1
Noise standard deviation ( $\sigma_{\text{noise}}$ )	0.1
<i>Model Architecture</i>	
Type	{Llama 3, GPT-2}
Hidden dimension ( $d_{\text{model}}$ )	288
Head dimension ( $d_{\text{head}}$ )	32
Number of heads	9
FFN dimension	$4 \times d_{\text{model}} = 1152$
Layers ( $n_{\text{layer}}$ )	$\{2, 4, 8, 16, 32\}$ (default: 2)
<i>Optimization</i>	
Optimizer	AdamW ( $\beta_1 = 0.9, \beta_2 = 0.95$ )
Learning rate	$10^{-3}$
Scheduler	Linear warmup (200 steps) + Cosine decay
Batch size	512
Training steps	1000

### A.3 Head Detection Metrics

To track the emergence of mechanistic circuits, we compute three attention-pattern scores for every head in the model. Unless specified otherwise, we report the **maximum** score across all heads in a given model (e.g., Figure 2 or Figure 5), as the emergence of a single specialized head is sufficient to implement the mechanism.

For a head with attention weights  $a_{t,s}$  (query position  $t$  attending to key position  $s$ ), we define:

1. **PTH Score:** Measures attention to the immediate predecessor [14].

$$\text{PTH} = \frac{1}{T} \sum_{t=2}^{T+1} a_{t,t-1} \in [0, 1].$$

2. **IH-MC Score:** A metric tailored to GMC (Theorem 1.1) that measures attention from the query to the token *following* the hidden match  $t_0$ .

$$\text{IH-MC} = a_{\text{query}, t_0+1} \in [0, 1].$$

3. **IH-Repeat Score:** A standard metric [28] using a duplicated sequence  $(\mathbf{e}_1, \dots, \mathbf{e}_K, \mathbf{e}_1, \dots, \mathbf{e}_K)$ . Unless stated otherwise, we use  $K = T$ . It measures attention from the second occurrence of a token to the successor of its first occurrence.

$$\text{IH-Repeat} = \frac{1}{K} \sum_{t=1}^K a_{K+t, t+1} \in [0, 1].$$

**Typical score values at initialization.** With Gaussian-initialized projection matrices the attention weights are almost uniform at initialization. Hence  $a_{t,s} \approx \frac{1}{t-1}$  for  $s < t$  (causal attention) and  $a_{t,s} \approx 0$  for  $s \geq t$ . Denote by  $H_t = \sum_{k=1}^t \frac{1}{k} \approx \ln t + O(1)$  the  $t$ -th harmonic number. We deduce that the expected scores at initialization for each head are:

- $\mathbb{E}[\text{PTH}] \approx \frac{1}{T} \sum_{t=2}^{T+1} \frac{1}{t-1} = \frac{H_T}{T} \approx \frac{\ln T}{T}$ ,
- $\mathbb{E}[\text{IH-MC}] \approx \frac{1}{T}$ ,
- $\mathbb{E}[\text{IH-Repeat}] \approx \frac{1}{K} \sum_{t=1}^K \frac{1}{K+t-1} = \frac{1}{K} \sum_{j=K}^{2K-1} \frac{1}{j} = \frac{H_{2K-1} - H_{K-1}}{K} \approx \frac{\ln 2}{K}$ .

All our experiments roughly confirm these values at step 0 (e.g. Figure 2).

#### A.4 Robustness of Emergence

Besides the robustness to optimization choices discussed in Section A.2, we verified that the emergence of induction circuits is robust across different GMC configurations.

**Robustness to GMC Parameters.** As noted in Section 3.1, we found that across GMC settings where the task is successfully solved, the model consistently develops PTH and IH circuits coinciding with a sharp drop in loss. The only difference lies in the timing and speed of this transition: harder tasks (higher  $c$  and ratio  $T/d_{\text{in}}$ ) lead to later and more gradual transitions. Figure 5 shows examples of that for different correlation strengths ( $1/c^2$ ), dimensions ( $d_{\text{in}}$ ) context lengths ( $T$ ), and Llama 3 and GPT-2 architectures.

**Robustness to Depth.** We ran experiments for  $n_{\text{layer}} \in \{2, 4, 8, 16, 32\}$  (see Figure 5 and Figure 6). All configurations with  $n_{\text{layer}} \geq 2$  led to similar behavior: an induction circuit emerges coinciding with a drop in loss. We also observe that single-layer models ( $n_{\text{layer}} = 1$ ) never solve the task, even though they attempt to develop primitive PTHs or IHs (see Figure 6). This aligns with the mechanistic understanding that PTHs and IHs must reside in *consecutive* layers to interact effectively (composition of heads), thus requiring at least two layers for the full circuit implementing match-and-copy.

#### A.5 Mechanistic Validation of the PTH→IH Circuit

We confirm that the induction circuits learned by the model strictly adhere to the PTH→IH compositional structure found in practice in large language models [14, 28]: IHs must come in a layer *after* PTHs, since it is the composition of these two head types that implements the match-and-copy mechanism. We also analyze more closely the attention patterns (instead of printing scores only) to confirm that the heads implement the functional definitions of PTH and IH (attend to previous token, and attend to the match’s successor). Below, we report these analyses for the specific 2-layer Llama 3 run ( $T = 8, c = 1.2, d_{\text{in}} = 16$ ) shown in Figure 2.

**Head-wise Scores: Confirms Compositional Structure.** Figure 7 tracks the evolution of attention scores for every head in the model. Prior to the loss drop (left, step 120), all heads exhibit negligible scores. Coinciding with the drop in loss (right, step 200), we observe a clean separation of roles: heads in Layer 0 specialize as Previous Token Heads (high PTH score), while heads in Layer 1 specialize as Induction Heads (high IH-MC and IH-Repeat scores). This simultaneous emergence confirms that the model solves the task precisely when it unlocks the composition of these two head types. See also Figure 6 where single-layer models fail to solve the task, lacking the necessary compositional structure [35].

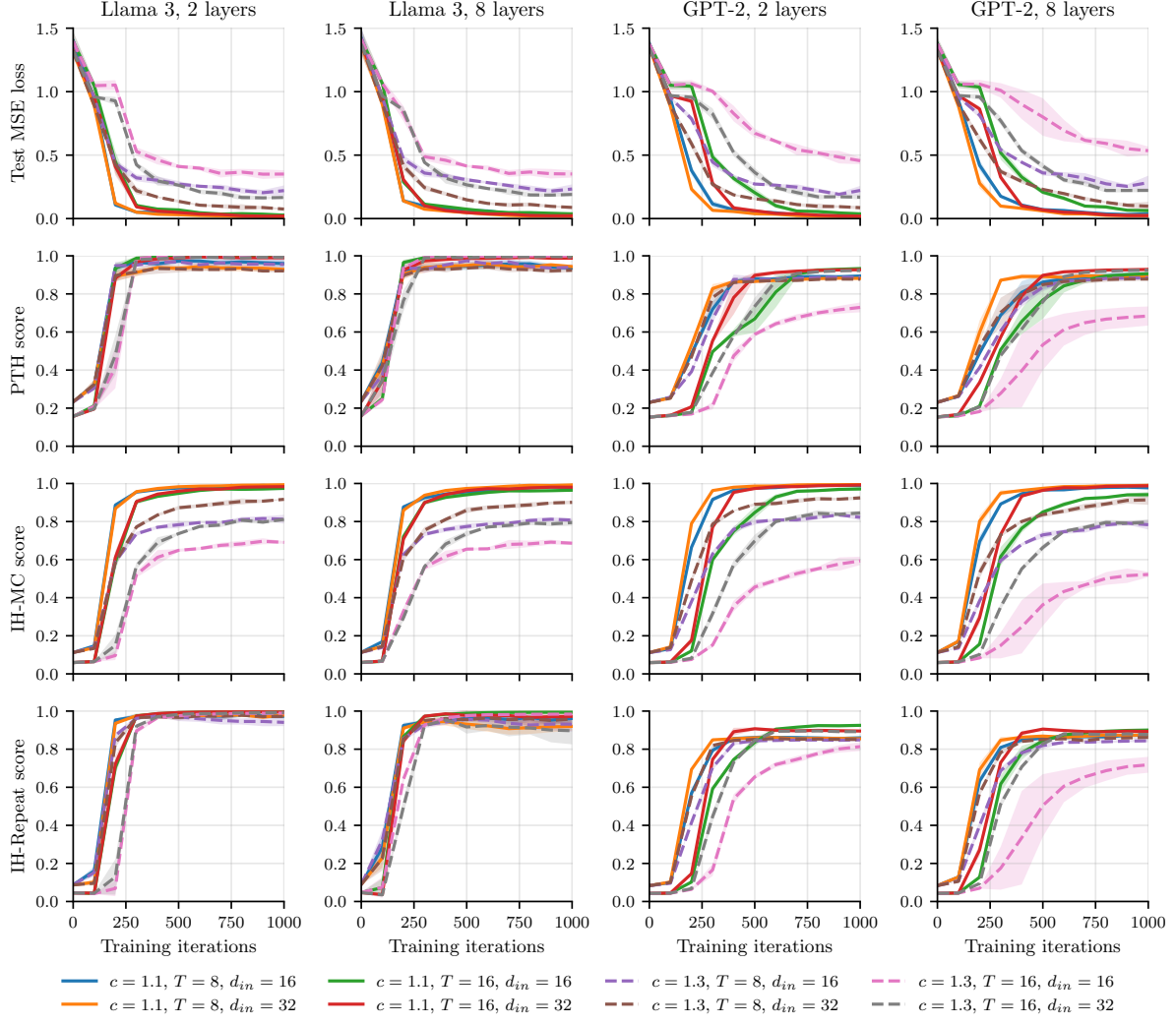


Figure 5: **Robustness of Emergence.** The alignment between the loss drop (top row) and the saturation of PTH/IH scores (bottom rows) across different architectures (Llama 3, GPT-2) and GMC configurations (varying  $c$ ,  $d_{in}$ ,  $T$ ).

**Attention Patterns: Confirms Functional Definition of PTH and IH.** We validate the functional definition of these heads using the IH-Repeat sequence format  $(\mathbf{e}_1, \dots, \mathbf{e}_K, \mathbf{e}_1, \dots, \mathbf{e}_K)$  described in Section A.3. Figure 8 visualizes the attention weights averaged over all 9 heads per layer and a batch of 32 sequences of length  $2K = 16$ .

- **Layer 0 (PTHs):** The attention mass concentrates on the first subdiagonal (Figure 8a), confirming that these heads consistently attend to the immediate predecessor token.
- **Layer 1 (IHs):** The attention mass concentrates on the  $(K - 1)$ -th subdiagonal during the second half of the sequence (Figure 8b). This offset indicates that for a repeated token  $\mathbf{e}_{K+t}$ , the head attends to the token *following* its first occurrence  $\mathbf{e}_{t+1}$ .

## B Transfer Beyond Gaussian Data: ICL Classification on Omnipiglot

To test if the learned induction mechanisms are abstract (transferable) or specific to Gaussian data, we transfer a GMC-trained model to the Omnipiglot few-shot classification task [21].

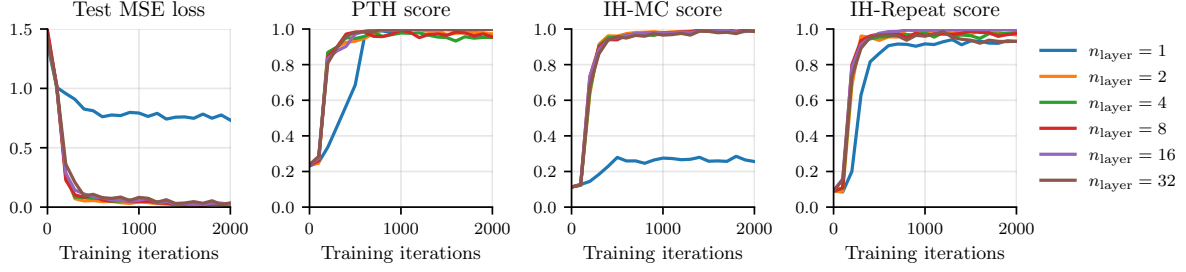


Figure 6: **Robustness to Depth.** Evolution of loss and detection scores for Llama 3 models with varying layer counts ( $n_{\text{layer}}$ ). While all models with  $n_{\text{layer}} \geq 2$  exhibit the characteristic loss drop and emergence of PTH/IH circuits, the single-layer model ( $n_{\text{layer}} = 1$ ) attempts to increase head scores but fails to solve the task. This confirms that the solution requires the composition of heads across at least two layers.

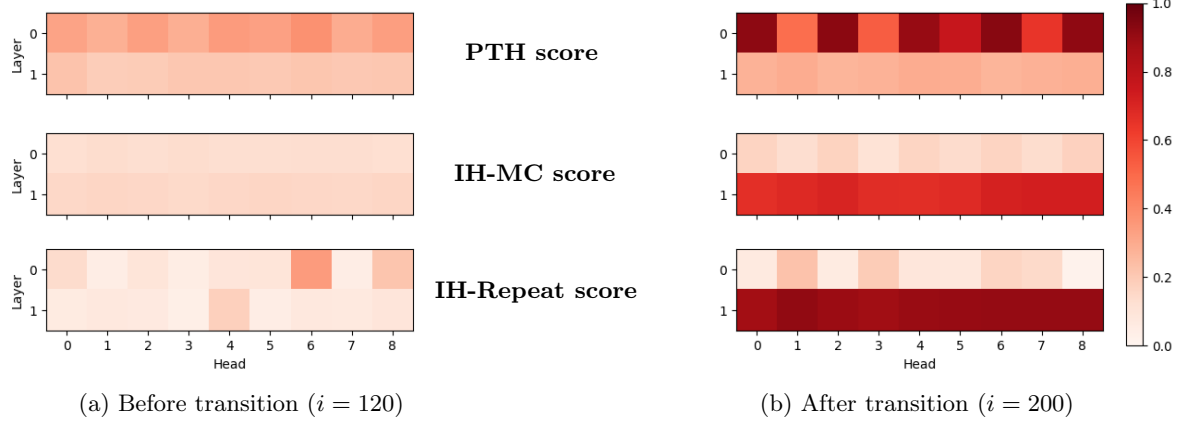


Figure 7: **Compositional Structure Confirmed by Head-wise Scores.** Per-head attention scores for the 2-layer Llama 3 model ( $T = 8, c = 1.2, d_{\text{in}} = 16$ ) from Figure 2. (a) Before the loss drop, scores are noise. (b) Immediately after, Layer 0 heads (top markers) maximize PTH scores, and Layer 1 heads (bottom markers) maximize IH scores.

**Dataset and Protocol.** We use the setup from Singh et al. [37]. Sequences consist of interleaved images and labels:

$$(x_1, y_1, x_2, y_2, x_q) \rightarrow y_q$$

where  $x_i$  are embeddings<sup>1</sup> of handwritten characters and  $y_i \in \{1, \dots, 5\}$  are labels. In each sequence,  $x_q$  is a copy of either  $x_1$  or  $x_2$ , and the target  $y_q$  is the corresponding label. This is a match-and-copy task requiring visual feature matching rather than Gaussian correlation matching.

In particular, just as in Singh et al. [37], the data is a restriction of the original Omniglot dataset [21] ( $C = 1623$  classes of characters with  $N = 20$  examples each) to single exemplars ( $E = 1$ ) drawn from disjoint  $C_{\text{train}} = 50$  classes for training and  $C_{\text{test}} = 100$  classes for testing. Sequences are constructed by sampling uniformly two distinct characters ( $x_1, x_2$ ) and assigning them uniformly random distinct labels  $y \in \{1, \dots, L\}$  with  $L = 5$  (hence the same image  $x$  can have different associated labels across sequences). The query  $x_q$  is set to either  $x_1$  or  $x_2$  with equal probability, and the target  $y_q$  is the corresponding label. The label randomization across sequences (same  $x$  with different  $y$ ) forces the model to perform in-context learning rather than memorizing fixed image-label associations. The total number of unique training sequences is:

$$\underbrace{C_{\text{train}}(C_{\text{train}} - 1)}_{\text{pairs } (x_1, x_2)} \cdot \underbrace{L(L - 1)}_{\text{pairs } (y_1, y_2)} \cdot \underbrace{2}_{\text{query } x_q} = 50 \cdot 49 \cdot 5 \cdot 4 \cdot 2 = 98,000$$

Unlike Singh et al. [37], which reserves 20% of training data to test "relabeling" performance for a separate purpose, we train on the full set of 98,000 sequences and we evaluate exclusively on the disjoint  $C_{\text{test}}$  classes.

<sup>1</sup>We utilize the 512-dimensional ResNet-18 embeddings of Omniglot characters provided by [37] at [https://github.com/aadityasingh/icl-dynamics/blob/main/omniglot\\_resnet18\\_randomized\\_order\\_s0.h5](https://github.com/aadityasingh/icl-dynamics/blob/main/omniglot_resnet18_randomized_order_s0.h5).

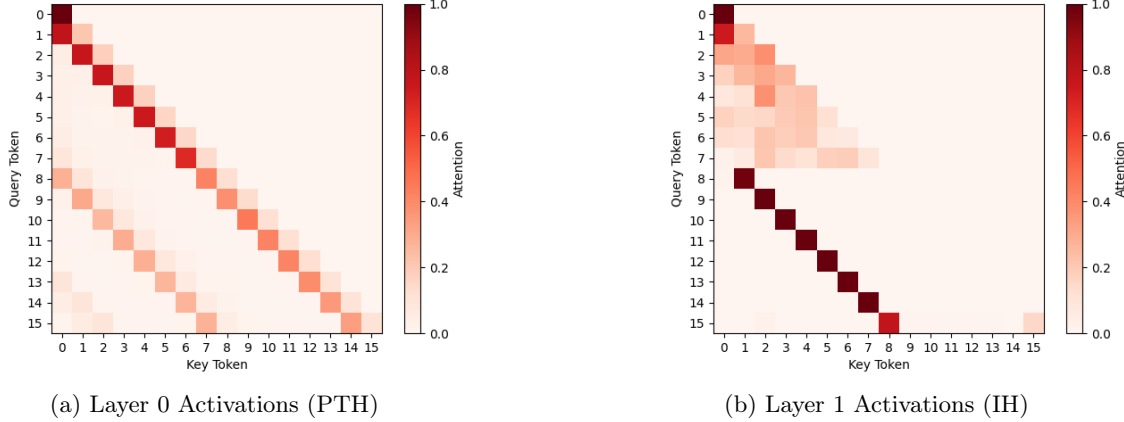


Figure 8: **Functional Definition Confirmed by Attention Maps.** Average attention weights at step  $i = 1000$  on IH-Repeat samples ( $K = 8$ ). (a) Layer 0 attends to the previous token (subdiagonal). (b) Layer 1 attends to the token following the previous occurrence of the current query (shifted subdiagonal).

Table 2: Specifications of the experiments on Omniglot.

Architecture	Omniglot Training Parameters (fine-tuning and from scratch)
Model: Llama 3	Training steps: 4000
Layers ( $n_{\text{layer}}$ ): 2	Batch size: 32
Hidden dimension ( $d_{\text{model}}$ ): 128	Optimizer: AdamW
Head dimension ( $d_{\text{head}}$ ): 32	Learning rate: $10^{-3}$
Heads per layer: $d_{\text{model}}/d_{\text{head}} : 4$	Linear warmup: 100 steps
FFN dimension: $4 \times d_{\text{model}} = 512$	Scheduler: cosine decay

**Transfer Method.** We pretrain a Llama 3 model on GMC and transfer it to Omniglot by freezing the backbone and fine-tuning only the input and output projections. The Llama 3 model is chosen to ensure sufficient capacity while remaining computationally efficient (see Table 2). The transfer learning procedure consists of three steps:

1. **GMC Pretraining:** The model is first trained to convergence on an “easy” GMC configuration ( $T = 8, c = 1.1, d_{\text{in}} = 16, \sigma = 0.1$ , “easy” in the sense that the model quickly reaches the noise floor for these parameters as shown in Figure 5). We use the procedure from Section A.2, but with 2000 training steps and 400 warmup steps (instead of 1000 and 200).
2. **Embeddings Adaptation:** We freeze the entire backbone (self-attention and FFNs). We replace the GMC input/output linear projections with new layers suited for Omniglot: the input embedding maps the concatenated image vectors and one-hot labels (dimension  $512 + L$ ) to  $d_{\text{model}}$ , and the unembedding maps  $d_{\text{model}}$  to  $L = 5$  class logits.
3. **Fine-tuning:** We train *only* the new embedding and unembedding layers to minimize cross-entropy loss, using the hyperparameters in Table 2.

**Main Result: Successful Transfer.** As shown in Figure 3 (main text), the model successfully learns Omniglot despite having its entire inference mechanism (attention + FFN) frozen from the Gaussian task. This indicates that the GMC-trained heads implement a distribution-agnostic “match-and-copy” operation, regardless of whether the input data is Gaussian or character embeddings.

**Additional Result: Efficiency of Transfer.** For comparison, we also train the same Llama 3 model from scratch using the same optimization hyperparameters listed in Table 2.<sup>2</sup> Note that these optimization hyperparameters were originally tuned for this from-scratch training, not for fine-tuning, so the comparison is biased in favor of training from scratch. The GMC-pretrained model achieves 90% test accuracy using

<sup>2</sup>For which we obtain a loss curve similar to that reported in Singh et al. [37], where they used an attention-only architecture trained from scratch on the same Omniglot setup.

Table 3: Model specifications for architecture comparison. All models operate with  $d_{\text{model}} \approx 192\text{--}320$  and maintain comparable compute budgets.

Model	Architecture	Parameter count	Inference GFLOPs
GPT-2 [32]	2 layers, 10 heads, $d_{\text{head}} = 32$	2.47M	22.8
Llama 3 [41]	2 layers, 9 heads, $d_{\text{head}} = 32$	2.66M	24.6
GRU [10]	10 layers, $d_{\text{model}} = 208$	2.60M	24.0
S4 [18]	8 layers, $d_{\text{model}} = 192$ , $d_{\text{state}} = 64$	2.77M	24.5
H3 [15]	6 layers, $d_{\text{model}} = 192$ , $d_{\text{state}} = 64$	3.04M	24.6
Hyena [31]	5 layers, $d_{\text{model}} = 192$ , order 5	3.10M	25.6

3 $\times$  fewer training FLOPs than the model trained from scratch. Furthermore, the model trained from scratch does not reach the 99% test accuracy achieved by the pretrained model within the allotted budget (Figure 3). This shows that the match-and-copy mechanism learned during GMC pretraining not only transfers to Omniglot, but also confers a significant optimization advantage.

## C Comparison with Non-Attention Architectures

This section details the comparison between Transformers and non-attention sequence models presented in Section 3.3.

**Model Configurations.** To ensure a fair comparison, we match all models on inference FLOPs. FLOPs are directly measured with PyTorch (`torch.profiler`) on a training batch (same batch size for all models: 512, and task parameters as detailed below). We test Gated Recurrent Units (GRU) [10], two State-Space Model (SSM) variants—S4 [18] and H3 [15]—and the Hyena architecture [31], a hierarchical long-convolution sequence model.

Table 3 reports the configurations used for each architecture. A few details on the choices made:

- **Transformers (Llama 3, GPT-2).** We reuse the settings of Table 1 with two changes:
  - depth fixed to  $n_{\text{layer}} = 2$ ;
  - GPT-2 heads increased to  $H = 10$  so that  $d_{\text{model}} = H \times d_{\text{head}} = 320$ , matching the FLOPs of the Llama 3 run.

As usual the feed-forward width is  $4d_{\text{model}}$ .

- **SSMs (S4, H3), Hyena, and GRU.** For these non-attention baselines, we explored deeper (up to 15 layers) and wider (up to  $d_{\text{model}} = 512$ ) configurations; none closed the gap to Transformers. We therefore retain the mid-range settings listed in Table 3.

Parameter counts in the table *exclude* the input and output projection layers ( $d_{\text{model}} \times d_{\text{in}}$  and  $d_{\text{out}} \times d_{\text{model}}$ , respectively), whereas FLOPs *include* them.

**GMC Configuration.** All models are trained on the same “easy” GMC configuration (it is among the easiest instances in our sweep according to Figure 5):

$$T = 8, \quad d_{\text{in}} = d_{\text{out}} = 16, \quad \mathbf{C} = \frac{1}{(1.1)^2} \mathbf{I}.$$

All other parameters follow Section A.2 ( $\sigma_{\text{noise}} = 0.1$ ,  $\sigma_{\text{token}} = 1$ , i.i.d.  $\mathbf{W}_V \sim \mathcal{N}(0, 1)$ , AdamW, etc.). Short sequences (small  $T$ ) and a strong query-match correlation (small  $c$ ) maximize the chance that non-attention architectures succeed, while Transformers remain robust on much harder settings (Figure 5).

**Optimization.** Training follows the protocol of Section A.2 with one modification: we run 2000 gradient steps (five times the iterations needed for Transformers to reach near noise floor) to give slower-converging non-attention architectures a fair shot. All other hyper-parameters—AdamW with learning rate  $10^{-3}$ , batch size 512, cosine decay with 400-step linear warm-up—are kept identical across architectures.

**Loss and Noise Floor.** The irreducible contribution of the noise to the population MSE is  $\frac{1}{d_{\text{out}}} \mathbb{E} \|\varepsilon\|_2^2 = \sigma_{\text{noise}}^2 = 0.01$ . Indeed, the population version of the MSE loss (3) we optimize is:

$$\frac{1}{d_{\text{out}}} \mathbb{E} \|\text{model} - \mathbf{v}\|_2^2 = \frac{1}{d_{\text{out}}} \mathbb{E} \|\text{model} - \mathbf{W}_V \mathbf{e}_{t_0+1}\|_2^2 + \frac{1}{d_{\text{out}}} \mathbb{E} \|\varepsilon\|_2^2$$

because  $\mathbf{v} = \mathbf{W}_V \mathbf{e}_{t_0+1} + \varepsilon$  with independent  $\varepsilon \sim \mathcal{N}(0, \sigma_{\text{noise}}^2 \mathbf{I}_{d_{\text{out}}})$ . We therefore say that a model reaches the *noise floor* when its test MSE is on the order of  $\sigma_{\text{noise}}^2 = 0.01$ .

**Extended Training.** Transformers solve the task (reaching the noise floor) within 2,000 steps (Figure 4). To rule out slow convergence as a factor for the baselines, we extended their training to 20,000 steps<sup>3</sup> (10 $\times$  the Transformer budget).

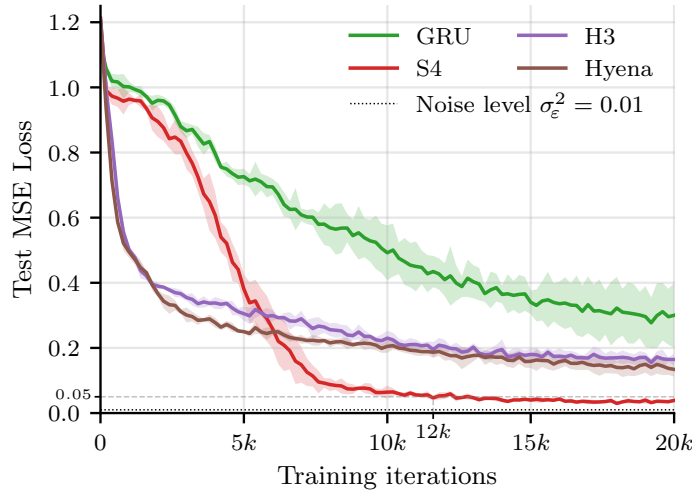


Figure 9: **Extended Training for Non-Attention Models.** Even with 20,000 training steps, SSMs (S4, H3), the Hyena architecture, and GRU fail to reach the noise floor ( $\sigma_{\text{noise}}^2 = 0.01$ ) that Transformers achieve in under 1,000 steps.

As shown in Figure 9, even with extended training, SSMs fail to solve the task. For example, S4 plateaus near MSE 0.05 ( $5 \times$  the noise floor) and it takes over 12,000 steps to reach this level, which is 30 $\times$  slower than Llama 3 (Figure 4 shows that Llama 3 reaches MSE 0.05 in under 400 steps, GPT-2 in under 600 steps, and both eventually hit the noise floor under 2,000 steps). The other baselines perform worse: Hyena and H3 plateau above 0.1, and GRU settles in 0.2 – 0.4 depending on the run. These findings reinforce a broader pattern in the literature suggesting that copying is fundamentally difficult for state-space models [3, 19, 29]. Even architectures like H3 [15] or Hyena [31] struggle to perform the precise, content-based retrieval required for GMC. This can be surprising since H3 explicitly shifts hidden states to mimic previous-token access, and both H3 and Hyena have been designed to perform well on tasks that are similar in spirit to GMC (associative retrieval, see Section 2). This shows that although GMC is similar to these tasks, it remains a distinct challenge that SSMs struggle to solve.

## D Formalization of Theorem 4.1

In this appendix, we provide the formal setup underlying Theorem 4.1. Its proof is given in Section E. The theorem is stated under explicit assumptions on the data geometry and on the optimization trajectory. These assumptions are not claimed to hold universally; rather, they delineate a regime in which a max-margin implicit bias for MSE can be rigorously established. A representative empirical sanity check illustrating this regime is given in Section G.3.

This section is organized as follows:

<sup>3</sup>Same 400-step warm-up, but with cosine decay stretched to 20,000 steps. This alters the learning rate profile (and thus the loss curve) during the first 2,000 steps, so the the first 2,000 steps of this extended run are not directly comparable to the original 2,000-step curves in Figure 4. What is comparable, however, are the *final losses* at the end of each run, corresponding to their performance for a fixed training budget.

- Section D.1 defines the data and model setup.
- Section D.2 re-expresses the model in vectorized notation to ease comparison with prior work on implicit bias.
- Section D.3 makes a small detour to discuss a case already covered in prior work: the Cross-Entropy (CE) loss.
- Section D.4 states the main theorem.

## D.1 Notation and Setup

Consider  $n$  training samples with the GMC format (Theorem 1.1)

$$\underbrace{\mathbf{e}_1, \dots, \mathbf{e}_{t_0}, \mathbf{e}_{t_0+1}, \dots, \mathbf{e}_T}_{\text{context}}, \underbrace{\mathbf{e}}_{\text{query}} \rightarrow \underbrace{\mathbf{v}}_{\text{target}}$$

with exact match  $\mathbf{e} = \mathbf{e}_{t_0}$  and exact copy  $\mathbf{v} = \mathbf{e}_{t_0+1}$ . For each sample  $i \in \{1, \dots, n\}$ , the notation is follows:

- **Data:** A context matrix  $\mathbf{E}^{(i)} = [\mathbf{e}_1^{(i)}, \dots, \mathbf{e}_T^{(i)}] \in \mathbb{R}^{d_{\text{in}} \times T}$  and a query  $\mathbf{e}^{(i)} \in \mathbb{R}^{d_{\text{in}}}$ .
- **Task:** The correct match position is  $y_i = t_0^{(i)} \in \{1, \dots, T-1\}$ , such that the target is  $\mathbf{v}^{(i)} = \mathbf{e}_{y_i+1}^{(i)}$  (exact copy) and the query satisfies  $\mathbf{e}^{(i)} = \mathbf{e}_{y_i}^{(i)}$  (exact match).

**Simplified model: shifted-key single query attention head.** The model follows the standard single-query attention head with parameters  $(\mathbf{W}_Q, \mathbf{W}_K, \mathbf{W}_V)$  [30, Algorithm 3], but with three modifications:

1. **Shifted-keys (Frozen PTH).** The token at position  $t$  is copied according to attention weights computed from keys at position  $t-1$  (i.e., shifted by one position, highlighted in magenta below):

$$\sum_{t=1}^{T-1} \text{softmax}(\mathbf{E}_{1:T-1}^{\top} \mathbf{W}_K^{\top} \mathbf{W}_Q \mathbf{e})_t \mathbf{W}_V \mathbf{e}_{t+1}.$$

This is exactly the computation needed for match-and-copy: match the query against a previous occurrence, then *copy the successor* (thanks to the shifted key positions). Shifting the keys can be understood as adding a previous layer that would implement an exact PTH [37, Sec 4.1][45, Eq 4].

2. **Merged key-query.** We set  $\mathbf{W}_{KQ} = \mathbf{W}_K^{\top} \mathbf{W}_Q \in \mathbb{R}^{d_{\text{in}} \times d_{\text{in}}}$  and optimize  $\mathbf{W}_{KQ}$  directly.
3. **Fixed value.** We *freeze* the value matrix  $\mathbf{W}_V$  to the ground truth one used in GMC data generation (namely,  $\mathbf{W}_V = \mathbf{I}$ ) and optimize only  $\mathbf{W}_{KQ}$ . This has two motivations. (i) Freezing  $\mathbf{W}_V$  allows us to isolate the non-convex dynamics induced by the softmax. In contrast, the (empirical and population) MSE loss is *strictly convex* in  $\mathbf{W}_V$  since it appears linearly in the model output. Thus,  $\mathbf{W}_V$  is not the main source of the optimization difficulty and, in principle, can be solved optimally at each step. In fact, already at initialization, starting from  $\mathbf{W}_{KQ} = 0$  and solving first for  $\mathbf{W}_V$  yields an unbiased estimator of the true  $\mathbf{W}_V$ , which converges to the exact solution in the infinite-data limit. This observation echoes multi-stage training procedures proposed in prior work [9, 27, 45]; we do not pursue this here. (ii)  $\mathbf{W}_V$  does not affect *which position is attended to*, and hence does not directly influence the directional implicit bias studied here.

For a context  $\mathbf{E} = (\mathbf{e}_1, \dots, \mathbf{e}_T)$  and query  $\mathbf{e}$ , the model output from (8) is:

$$\text{model}(\mathbf{W}_{KQ}; \mathbf{E}, \mathbf{e}) = \sum_{t=2}^T \underbrace{\text{softmax}((\mathbf{e}_s^{\top} \mathbf{W}_{KQ} \mathbf{e})_{s=1}^{T-1})_{t-1}}_{=:a_t(\mathbf{W}_{KQ}; \mathbf{E}, \mathbf{e})} \mathbf{W}_V \mathbf{e}_t. \quad (12)$$

The implicit bias we prove is not specific to this key-shift: if instead of a target  $\mathbf{v} = \mathbf{e}_{t_0+1}$  we had  $\mathbf{v} = \mathbf{e}_{\sigma(t_0)}$  for a given injective map  $\sigma$  fixed across all samples (i.e., the target was copied from a fixed pairing  $t_0 \mapsto \sigma(t_0)$ ), the results would hold verbatim with notational changes, e.g., replacing  $t_0+1$  by  $\sigma(t_0)$ , and the shifted-keys by a model with keys shifted according to  $\sigma$ :  $\sum_{t \in \sigma^{-1}(\{1, \dots, T\})} \text{softmax}(\mathbf{E}_{\sigma^{-1}(\{1, \dots, T\})}^{\top} \mathbf{W}_{KQ} \mathbf{e})_{\sigma^{-1}(t)} \mathbf{e}_t$ .

## D.2 Vectorized Notation to Ease Comparison with [38]

For readers who are familiar with max-margin bias results, we first reformulate the model using vectorized notation. This facilitates comparison with the seminal work of Soudry et al. [38] which characterizes the implicit bias of logistic regression (linear model with CE loss). This highlights how the MSE gradients diverge from the standard CE gradients and motivates the specific assumptions used to bridge the gap.

Denote the vectorized form of  $\mathbf{W}_{\text{KQ}} \in \mathbb{R}^{d_{\text{in}} \times d_{\text{in}}}$  by

$$w = \text{flatten}(\mathbf{W}_{\text{KQ}}) \in \mathbb{R}^{d_{\text{in}}^2}.$$

We introduce the feature vector for sample  $i$  and position  $t$ :

$$x_{i,t} := \text{flatten}(\mathbf{e}_t^{(i)} \mathbf{e}^{(i)\top}) \in \mathbb{R}^{d_{\text{in}}^2}. \quad (13)$$

Using the identity  $\mathbf{e}_t^\top \mathbf{W}_{\text{KQ}} \mathbf{e} = \langle \mathbf{W}_{\text{KQ}}, \mathbf{e}_t \mathbf{e}^\top \rangle_F = w^\top \text{flatten}(\mathbf{e}_t \mathbf{e}^\top)$ , the model's attention weights in (12) can be expressed as:

$$a_1^{(i)}(w) = 0, \quad a_{t+1}^{(i)}(w) = \text{softmax}(\{w^\top x_{i,s}\}_{s=1}^{T-1})_t, \quad \text{for } t \in \{1, \dots, T-1\}.$$

Introducing the *difference vectors* relative to the correct match position  $y_i$ :

$$\tilde{x}_{i,t} := x_{i,y_i} - x_{i,t}, \quad \text{for } t \neq y_i, \quad (14)$$

we can rewrite the attention coefficients in terms of these difference vectors, as in [38]:

$$S_i(w) := \sum_{\substack{s=2, \dots, T \\ s \neq y_i}} \exp(-w^\top \tilde{x}_{i,s}), \quad \text{and} \quad a_{t+1}^{(i)}(w) = \frac{\exp(-w^\top \tilde{x}_{i,t})}{1 + S_i(w)}, \quad \text{for } t \neq y_i, \quad a_{y_i+1}^{(i)}(w) = \frac{1}{1 + S_i(w)}. \quad (15)$$

The margins in (10) can also be expressed in terms of these difference vectors:

$$m_{i,t}(w) := w^\top \tilde{x}_{i,t}, \quad \text{for } t \neq y_i. \quad (16)$$

As before, diverging margins ( $m_{i,t}(w) \rightarrow \infty$ ) imply that the attention mass concentrates on the correct index  $y_i$ , i.e.,  $a_{y_i+1}^{(i)} \rightarrow 1$ .

## D.3 The CE (Convex) Case: Covered by Existing Literature

This section connects Theorem 4.1 to prior work on implicit bias, by discussing the case of Cross-Entropy (CE) loss, which is already covered in Soudry et al. [38]. This serves to highlight the differences between the CE and MSE cases, and motivates the additional assumptions needed to handle MSE.

The implicit bias of gradient descent is well understood for binary classification tasks  $(x_i, y_i)_{i \leq n}$  with  $y_i \in \{\pm 1\}$ , provided the loss is strictly decreasing in a “score/margin”  $y_i f(x_i; w)$ . A canonical example is the linear model  $f(x; w) = w^\top x$ . In this regime, gradient descent converges toward the max-margin solution. This includes linear models trained with cross-entropy,

$$L(w) = \log(1 + \exp(-yw^\top x)) = \ell(yw^\top x),$$

where  $\ell$  is the logistic monotone decreasing loss [20, 38].

More recently, these results have been extended to a case of particular interest here: one-layer attention models trained with losses that are monotone in the margin (for binary classification,  $y \in \{\pm 1\}$ ). For instance, consider

$$L(w) = \ell(y v^\top X \text{softmax}(X^\top \mathbf{W}_K^\top \mathbf{W}_Q X)),$$

where  $v$  is fixed (a fixed linear decoder) and  $\ell$  is monotone decreasing (e.g., logistic  $\ell(m) = \log(1 + e^{-m})$ , exponential  $\ell(m) = e^{-m}$ , or correlation  $\ell(m) = -m$  losses) [39, 40, 43].

In particular, the existing literature already covers the multi-class CE loss defined in our setting by:

$$\text{CE}(w) := -\frac{1}{n} \sum_{i=1}^n \log a_{y_i+1}^{(i)}(w) = \frac{1}{n} \sum_{i=1}^n \log \left( 1 + \sum_{\substack{t=1 \\ t \neq y_i}}^{T-1} \exp(-m_{i,t}(w)) \right). \quad (17)$$

Indeed, the proof of Theorem 7 in Soudry et al. [38] applies with only a minor adaptation: unlike multi-class linear classification where one has a separate vector parameter  $w_t$  per class  $t$ , here *all positions share the same parameter  $w$* . This shared-parameter constraint does not fundamentally alter the core argument, and the standard proof can be adapted with minor modifications. We obtain the next implicit bias:  $w(\tau)/\|w(\tau)\|_F \rightarrow \hat{w}/\|\hat{w}\|_F$  and  $\|w(\tau)\|_F \sim \|\hat{w}\|_F \log(\tau)$  where  $\hat{w}$  is the max-margin solution:

$$\hat{w} := \operatorname{argmax}_w \frac{1}{2} \|w\|_2^2 \quad \text{s.t.} \quad \min_{i \leq n} \min_{t \neq y_i} m_{i,t}(w) \geq 1. \quad (18)$$

In terms of the original matrix  $\mathbf{W}_{\text{KQ}}$  (recall  $w = \text{flatten}(\mathbf{W}_{\text{KQ}})$ ), we get the following result, to compare with Theorem 4.1.

**Theorem D.1** (Implicit bias of CE, adapted from Soudry et al. [38]). *Consider  $\mathbf{W}_{\text{KQ}}(\tau + 1) = \mathbf{W}_{\text{KQ}}(\tau) - \eta \nabla \text{CE}(\mathbf{W}_{\text{KQ}}(\tau))$  on the CE loss (17). Assume: (i) the max-margin problem in (18) is feasible, (ii) a standard ‘‘correction vector’’ existence condition as in Soudry et al. [38], and (iii)  $\eta$  is sufficiently small (below a smoothness-based bound). Then  $\mathbf{W}_{\text{KQ}}(\tau)/\|\mathbf{W}_{\text{KQ}}(\tau)\|_F \rightarrow \hat{\mathbf{W}}_{\text{KQ}}/\|\hat{\mathbf{W}}_{\text{KQ}}\|_F$  and  $\|\mathbf{W}_{\text{KQ}}(\tau)\|_F \sim \|\hat{\mathbf{W}}_{\text{KQ}}\|_F \log \tau$ .*

In contrast, our GMC objective is MSE regression, which differs<sup>4</sup> in important ways from the classification losses above: it is not monotone in the margins (it is not of the form  $\sum_{i,t} \ell(m_{i,t})$  with  $\ell$  decreasing and  $m_{i,t}$  the margins defined in (16)), it admits finite-norm interpolants under non-identifiability, and its gradient contains quadratic interaction terms that do not need to keep increasing the margins (see Theorem F.2 for more details). These differences will motivate additional geometric and trajectory-stability structural assumptions to recover a max-margin bias. Besides these different assumptions, Theorem 4.1 provides a different growth rate for the weight norm: for MSE, we have  $\|\mathbf{W}_{\text{KQ}}(\tau)\|_F \sim \|\hat{\mathbf{W}}_{\text{KQ}}\|_F^{\frac{1}{2}} \log \tau$ , whereas for CE (Theorem D.1) it is  $\|\mathbf{W}_{\text{KQ}}(\tau)\|_F \sim \|\hat{\mathbf{W}}_{\text{KQ}}\|_F \log \tau$ . Here, the extra factor  $\frac{1}{2}$  (relative to the CE scaling of 1) is due to the different structure of the MSE gradients. Indeed, we will see in the proof that the function  $f(\tau)$  governing the norm growth by  $\|w(\tau)\| \approx f(\tau)$  solves  $f'(\tau) \approx \|\nabla \text{MSE}(w(\tau))\|$ , and the MSE gradients evolve differently from CE gradients due to the quadratic terms in the MSE gradients (discussed in more detail above (24) in Section E).

## D.4 Main Theorem

We now formally state the implicit bias result. The assumptions are grouped into three categories: *Data Geometry* (properties of the tokens and query), *Successful Optimization* (convergence of the loss), and *Admissible Trajectory* (technical controls on the softmax dynamics that ensure asymptotic stability).

**Theorem D.2** (Implicit Bias of MSE). *Consider the dataset and model defined above. We train the model’s weight vector  $w \in \mathbb{R}^{d_{\text{in}}^2}$  via GD  $w(\tau + 1) = w(\tau) - \eta \nabla \text{MSE}(w(\tau))$  with a fixed step size  $\eta > 0$  on the MSE loss:*

$$\text{MSE}(w) = \sum_{i=1}^n \frac{1}{2} \left\| \sum_{t=1}^T a_t^{(i)}(w) \mathbf{e}_t^{(i)} - \mathbf{e}_{y_i+1}^{(i)} \right\|^2. \quad (19)$$

For any sample  $i$  and token position  $t \neq y_i$ , let  $d_{i,t} := \mathbf{e}_{t+1}^{(i)} - \mathbf{e}_{y_i+1}^{(i)}$  denote the error directions in token space. Assume the following conditions hold:

### I. Formalization of the Event in Section 4.3 (data geometry).

**(A1) Separability.** The hard-margin SVM problem is feasible, i.e., the constraints in the following optimization problem are satisfiable. As a consequence, there is a unique max-margin separator  $\hat{w}$  defined by:

$$\hat{w} = \operatorname{argmin}_{w \in \mathbb{R}^{d_{\text{in}}^2}} \frac{1}{2} \|w\|^2 \quad \text{s.t.} \quad w^\top \tilde{x}_{i,t} \geq 1, \quad \forall i, \forall t \neq y_i. \quad (20)$$

Uniqueness of  $\hat{w}$  follows from the strict convexity of the problem. We denote by  $\mathcal{I}_{\text{SV}} := \{(i, t) : \hat{w}^\top \tilde{x}_{i,t} = 1\}$  the set of support vectors (active constraints) for the max-margin solution  $\hat{w}$ .

**(A2) Linear Independence.** The support vectors  $\{\tilde{x}_{i,t} : (i, t) \in \mathcal{I}_{\text{SV}}\}$  are linearly independent.

<sup>4</sup>MSE is also nonconvex, which creates additional challenges compared to the logistic regression case [38], but nonconvexity is a feature shared with prior attention implicit-bias results [39, 40, 43] so this is not a new difficulty specific to MSE.

(A3) **Identifiability.** For all  $i$ , the target  $\mathbf{e}_{y_i+1}^{(i)}$  does not lie in the convex hull of the distractor tokens  $\{\mathbf{e}_{t+1}^{(i)} : t \neq y_i\}$ .

(A4) **Half-space.** For all  $i$ , the error directions lie in a common half-space:  $\langle d_{i,t}, d_{i,s} \rangle > 0$  for all  $t, s \neq y_i$ .

## II. Assuming Successful Optimization (successful run).

(A5) **Loss Convergence.** The loss converges to zero:  $\text{MSE}(w(\tau)) \rightarrow 0$  as  $\tau \rightarrow \infty$ .

(A6) **Summable Gradients.** The gradients are square-summable:  $\sum_{\tau=0}^{\infty} \|\nabla \text{MSE}(w(\tau))\|^2 < \infty$ .

## III. Formalization of the Assumptions in Section 4.4 (Theorem 4.2) (stable trajectory).

Let  $h_{i,t}(w) := \sum_{s \neq y_i} \langle d_{i,t}, d_{i,s} \rangle \frac{a_{s+1}^{(i)}(w)}{1 - a_{i,y_i+1}(w)}$  be a renormalization of the projection of the residual onto the error direction  $d_{i,t}$ .

(A7) **Convergence of Pre-factors.** For all  $(i, t)$ , the limit  $h_{i,t}^{\infty} := \lim_{\tau \rightarrow \infty} h_{i,t}(w(\tau))$  exists, and the convergence is sufficiently fast such that  $\sum_{\tau=1}^{\infty} \tau^{-1} |h_{i,t}(w(\tau)) - h_{i,t}^{\infty}| < \infty$ .

(A8) **Alignment of Off-Diagonal Drift.** The interactions between support vectors via the softmax Jacobian satisfy the alignment condition detailed in Theorem E.2 (ensuring the drift does not destabilize the max-margin direction).

(A9) **Support Domination.** The softmax tail is dominated by the support vectors. Specifically, there exists a function  $g : \mathbb{N} \rightarrow \mathbb{R}$  with  $\sum_{\tau} g(\tau) \tau^{-1} < \infty$  such that for all  $i$ , letting  $\mathcal{I}_{\text{SV}}(i) := \{s : (i, s) \in \mathcal{I}_{\text{SV}}\}$ ,

$$\sum_{s \notin \mathcal{I}_{\text{SV}}(i)} \exp(-w(\tau)^T \tilde{x}_{i,s}) \leq g(\tau) \sum_{s \in \mathcal{I}_{\text{SV}}(i)} \exp(-w(\tau)^T \tilde{x}_{i,s}).$$

**Conclusion.** Under these assumptions, the parameter vector  $w(\tau)$  diverges in norm and aligns with the max-margin separator  $\hat{w}$ :

$$\|w(\tau)\| \sim \frac{\|\hat{w}\|}{2} \log(\tau) \quad \text{and} \quad \frac{w(\tau)}{\|w(\tau)\|} \rightarrow \frac{\hat{w}}{\|\hat{w}\|}.$$

**Interpretation.** Theorem D.2 is a *conditional* asymptotic result. It does not assert that gradient descent on MSE always converges to a max-margin direction, nor that the listed assumptions are automatically satisfied. Instead, it states that, conditioned on the right data geometry, if a trajectory achieves vanishing loss and enters a stabilized asymptotic regime described by (A6)–(A9), then its direction converges to the max-margin separator at a logarithmic rate. The size and prevalence of this regime are left open; nevertheless, our experiments indicate that such stabilized trajectories are observed in practice, and the next remark clarifies which assumptions are structural and which are primarily optimization-related.

*Remark D.3* (On the scope of the assumptions). The assumptions of Theorem D.2 serve different roles and should not be interpreted uniformly.

1. **Geometric assumptions (A1–A4).** These concern separability, identifiability, and correlation structure of GMC data. For Gaussian match-and-copy, we show in Section G.1 that these conditions hold with high probability as the embedding dimension  $d_{\text{in}}$  grows relative to  $(T, n)$ . Assumption A3 (identifiability) prevents the existence of finite-norm interpolants (Section G.2). Without it, the loss could reach zero with finite weights, and the margins would not need to diverge. Assumption A4 (half-space) ensures that the gradient will eventually point in a direction that increases all margins simultaneously as the loss vanishes (see the discussion before Theorem F.3).
2. **Successful optimization (A5–A6).** These assumptions condition on gradient descent reaching a low-loss regime with square-summable gradients. We do not attempt to characterize when this occurs; instead, we ask what happens *if* it does motivated by the empirical observation that this is typical.
3. **Trajectory stability (A7–A9).** These assumptions formalize an asymptotic stabilization regime of the MSE dynamics in which support vectors dominate and cross-terms remain controlled. They are not claimed to hold for all runs. In Section G.3, we exhibit a representative trajectory of the runs where we found this regime to hold empirically.

## E Proof of Theorem D.2

We prove Theorem D.2 in this section, which is the formal version of Theorem 4.1 in the main text.

At a high level, the proof adapts the classical implicit-bias machinery for separable losses [20, 38] to our setting, with additional assumptions and work to handle the challenges specific to MSE.

For a fixed  $\tilde{w}$  (chosen later), consider the target trajectory

$$w^*(\tau) := f(\tau)\hat{w} + \tilde{w}, \quad f(\tau) = \frac{1}{2} \log(\tau). \quad (21)$$

It is enough to show that the residual  $r(\tau) = w(\tau) - w^*(\tau)$  remains bounded as  $\tau \rightarrow \infty$ . Since  $\sup_{\tau} \|r(\tau)\|^2 = \sup_{\tau} \sum_{s=1}^{\tau} (\|r(s+1)\|^2 - \|r(s)\|^2)$  and each increment can be decomposed as:

$$\|r(\tau+1)\|^2 - \|r(\tau)\|^2 = \underbrace{\|r(\tau+1) - r(\tau)\|^2}_{\mathcal{E}(\tau): \text{energy increment}} + 2 \underbrace{\langle r(\tau+1) - r(\tau), r(\tau) \rangle}_{\mathcal{D}(\tau): \text{instantaneous drift}}, \quad (22)$$

it suffices to show that both series  $\mathcal{E}(\tau)$  and  $\mathcal{D}(\tau)$  are bounded from above by summable sequences.

Introduce the shorthand  $v(\tau) := f(\tau+1) - f(\tau)$ . The increment of the residual is given by:

$$r(\tau+1) - r(\tau) = \underbrace{-\eta \nabla \mathcal{L}(w(\tau))}_{\text{GD step}} - \underbrace{v(\tau)\hat{w}}_{\text{target drift}}.$$

In particular,  $\mathcal{E}(\tau)$  is summable. Indeed, the inequality  $\|a+b\|^2 \leq 2(\|a\|^2 + \|b\|^2)$  gives:

$$\mathcal{E}(\tau) \leq 2\eta^2 \|\nabla \mathcal{L}(w(\tau))\|^2 + 2v(\tau)^2 \|\hat{w}\|^2$$

and we have assumed the gradients are  **$\ell^2$ -summable (successful run)**, and the second term satisfies  $v(\tau)^2 = O(1/\tau^2)$ . We now study the drift  $\mathcal{D}(\tau) = \langle -\eta \nabla \mathcal{L}(w(\tau)) - v(\tau)\hat{w}, r(\tau) \rangle$ .

### E.1 Drift decomposition

Since the gradient can be expressed as  $-\nabla \mathcal{L} = \sum_{(i,t) \in \mathcal{I}_{\text{SV}} \cup (\mathcal{I}_{\text{SV}})^c} \pi_{i,t}^{\text{MSE}}(w(\tau)) \tilde{x}_{i,t}$  (Theorem F.1), and KKT conditions give  $\hat{w} = \sum_{(i,t) \in \mathcal{I}_{\text{SV}}} \alpha_{i,t} \tilde{x}_{i,t}$ , we can decompose the drift as a sum of a contribution from support vectors and a contribution from non-support vectors:

$$\begin{aligned} \mathcal{D}(\tau) &= \underbrace{\sum_{(i,t) \in \mathcal{I}_{\text{SV}}} (\eta \pi_{i,t}^{\text{MSE}}(w(\tau)) - v(\tau) \alpha_{i,t}) \langle \tilde{x}_{i,t}, r(\tau) \rangle}_{\mathcal{D}_{\text{SV}}(\tau)} \\ &+ \underbrace{\sum_{(i,t) \notin \mathcal{I}_{\text{SV}}} \eta \pi_{i,t}^{\text{MSE}}(w(\tau)) \langle \tilde{x}_{i,t}, r(\tau) \rangle}_{\mathcal{D}_{\text{non-SV}}(\tau)}. \end{aligned} \quad (23)$$

### E.2 Analysis of the support drift

We analyze

$$\mathcal{D}_{\text{SV}}(\tau) := \sum_{(i,t) \in \mathcal{I}_{\text{SV}}} (\eta \pi_{i,t}^{\text{MSE}}(w(\tau)) - v(\tau) \alpha_{i,t}) u_{i,t}(\tau), \quad u_{i,t}(\tau) := \langle r(\tau), \tilde{x}_{i,t} \rangle.$$

To understand how to analyze this term, we begin with an informal explanation leading to the definition of the correction vector  $\tilde{w}$  in Theorem E.1 below.

**Why the target scale  $f(\tau) = \frac{1}{2} \log \tau$  and the correction  $\tilde{w}$  are forced if  $r(\tau)$  is bounded.** We start building intuition by assuming what we want to show, i.e., that  $r(\tau)$  remains bounded as  $\tau \rightarrow \infty$ . In particular,  $u_{i,t}(\tau) = \langle r(\tau), \tilde{x}_{i,t} \rangle$  remains bounded as  $\tau \rightarrow \infty$ . We rely on informal asymptotics<sup>5</sup> and the reader can confidently skip the details here if desired and resume at the definition of  $\tilde{w}$  in Theorem E.1 below.

<sup>5</sup>A rigorous version of these asymptotics can be derived under bounded  $r(\tau)$  using arguments similar to Theorem F.3, we omit the details here as they are not needed for the rest of the proof.

In the  $r(\tau)$  bounded regime, it can be seen that the leading contribution to the MSE gradient coefficients with  $(i, t) \in \mathcal{I}_{\text{SV}}$  is

$$\eta\pi_{i,t}^{\text{MSE}}(w(\tau)) \approx \eta h_{i,t} e^{-2f(\tau)} e^{-\tilde{w}^\top \tilde{x}_{i,t}} \sum_{s \in \mathcal{I}_{\text{SV}}(i)} e^{-\tilde{w}^\top \tilde{x}_{i,s}},$$

where  $\mathcal{I}_{\text{SV}}(i) := \{s : (i, s) \in \mathcal{I}_{\text{SV}}\}$  is the set of support vectors for sample  $i$ , and where  $h_{i,t} := \lim_{\tau \rightarrow \infty} h_{i,t}(w(\tau)) \in (0, \infty)$  automatically exists for bounded  $r(\tau)$ . These coefficients decay at rate  $e^{-2f(\tau)}$ . By contrast, non-support vector contributions can be shown to decay faster. So the gradient is supported asymptotically on the support vectors only:  $-\nabla \mathcal{L}(w(\tau)) \approx \sum_{(i,t) \in \mathcal{I}_{\text{SV}}} \pi_{i,t}^{\text{MSE}}(w(\tau)) \tilde{x}_{i,t}$  as  $\tau \rightarrow \infty$ , with a decay rate of order  $e^{-2f(\tau)}$  for the coefficients.

Meanwhile the target trajectory has an increment  $v(\tau)\hat{w}$  with  $v(\tau) = f(\tau+1) - f(\tau)$ , and if the target trajectory remains close to the GD iterates, their respective increments must match asymptotically:

$$-\eta \nabla \mathcal{L}(w(\tau)) \approx v(\tau)\hat{w}.$$

Since  $\nabla \mathcal{L}(w(\tau))$  is asymptotically supported on the support vectors only, and  $\hat{w} = \sum_{(i,t) \in \mathcal{I}_{\text{SV}}} \alpha_{i,t} \tilde{x}_{i,t}$ , with linearly independent  $\tilde{x}_{i,t}$ 's by the **rank (data geometry)** assumption, we must have, for each  $(i, t) \in \mathcal{I}_{\text{SV}}$ ,

$$\eta\pi_{i,t}^{\text{MSE}}(w(\tau)) \approx v(\tau)\alpha_{i,t}.$$

Based on the above asymptotics for  $\eta\pi_{i,t}^{\text{MSE}}(w(\tau))$ , this can be rewritten as

$$\eta h_{i,t} e^{-2f(\tau)} e^{-\tilde{w}^\top \tilde{x}_{i,t}} \sum_{s \in \mathcal{I}_{\text{SV}}(i)} e^{-\tilde{w}^\top \tilde{x}_{i,s}} \approx v(\tau)\alpha_{i,t}.$$

This forces  $v(\tau) \approx f'(\tau) \asymp e^{-2f(\tau)}$  which implies  $f(\tau) = \frac{1}{2} \log \tau + O(1)$ . We hence fix  $f(\tau) = \frac{1}{2} \log \tau$ . Then  $e^{2f(\tau)}v(\tau) \rightarrow \frac{1}{2}$ , so  $\tilde{w}$  must be a solution of:

$$\eta h_{i,t} e^{-\tilde{w}^\top \tilde{x}_{i,t}} \sum_{s \in \mathcal{I}_{\text{SV}}(i)} e^{-\tilde{w}^\top \tilde{x}_{i,s}} = \frac{1}{2} \alpha_{i,t}, \quad \forall (i, t) \in \mathcal{I}_{\text{SV}}. \quad (24)$$

**Definition E.1** (Correction vector  $\tilde{w}$ ). We define  $\tilde{w}$  as the unique solution of the system (24) in the linear span of the support vectors  $\text{span}(\mathcal{I}_{\text{SV}}) := \text{span}\{\tilde{x}_{i,t} : (i, t) \in \mathcal{I}_{\text{SV}}\}$ .

Existence and uniqueness follow from the following argument. Define  $c_{i,t} := \frac{\alpha_{i,t}}{2\eta h_{i,t}} > 0$  and consider  $z_{i,t} := c_{i,t} / \sqrt{\sum_{s \in \mathcal{I}_{\text{SV}}(i)} c_{i,s}}$ , which is well defined since  $c_{i,t} > 0$  for all  $(i, t) \in \mathcal{I}_{\text{SV}}$ . By **linear independence of the support vectors (data geometry)**  $\{\tilde{x}_{i,t} : (i, t) \in \mathcal{I}_{\text{SV}}\}$ , there exists a unique  $\tilde{w} \in \text{span}(\mathcal{I}_{\text{SV}})$  such that  $\tilde{w}^\top \tilde{x}_{i,t} = -\log(z_{i,t})$  for all  $(i, t) \in \mathcal{I}_{\text{SV}}$ . This  $\tilde{w}$  is a solution of (24) (and the only one in  $\text{span}(\mathcal{I}_{\text{SV}})$ ). We fix this  $\tilde{w}$  from now on and resume the proof of Theorem D.2.

**Softmax tail split and deterministic remainders.** Split the softmax tail

$$S_i(w) := \sum_{s \neq y_i} e^{-w^\top \tilde{x}_{i,s}}$$

into support and non-support parts:

$$S_i(w) = S_i^{\mathcal{I}_{\text{SV}}}(w) + S_i^{\mathcal{I}_{\text{nonSV}}}(w), \quad S_i^{\mathcal{I}_{\text{SV}}}(w) := \sum_{s \in \mathcal{I}_{\text{SV}}(i)} e^{-w^\top \tilde{x}_{i,s}}, \quad S_i^{\mathcal{I}_{\text{nonSV}}}(w) := \sum_{s \notin \mathcal{I}_{\text{SV}}(i)} e^{-w^\top \tilde{x}_{i,s}}.$$

For each  $(i, t) \in \mathcal{I}_{\text{SV}}$  define the remainders

$$\begin{aligned} \text{rest}_{i,t}^\pi(w) &:= \eta\pi_{i,t}^{\text{MSE}}(w) - \eta h_{i,t} e^{-w^\top \tilde{x}_{i,t}} S_i^{\mathcal{I}_{\text{SV}}}(w), \\ \text{rest}_{i,t}^v(\tau) &:= v(\tau)\alpha_{i,t} - \frac{1}{2\tau} \alpha_{i,t}, \end{aligned} \quad (25)$$

where  $h_{i,t} = \lim_{\tau \rightarrow \infty} h_{i,t}(w(\tau))$  is the limit given by the **convergence of pre-factors (stable trajectory)** assumption.

With this notation,

$$\eta\pi_{i,t}^{\text{MSE}}(w(\tau)) - v(\tau)\alpha_{i,t} = \left( \eta h_{i,t} e^{-w(\tau)^\top \tilde{x}_{i,t}} S_i^{\mathcal{I}_{\text{SV}}}(w(\tau)) - \frac{1}{2\tau} \alpha_{i,t} \right) + \text{rest}_{i,t}^\pi(w(\tau)) - \text{rest}_{i,t}^v(\tau), \quad (26)$$

and hence we split the support drift into a *restoring* term plus a *remainder* term:

$$\mathcal{D}_{\text{SV}}(\tau) = \mathcal{D}_{\text{SV}}^{\text{restore}}(\tau) + \mathcal{D}_{\text{SV}}^{\text{rest}}(\tau), \quad (27)$$

where

$$\begin{aligned} \mathcal{D}_{\text{SV}}^{\text{restore}}(\tau) &:= \sum_{(i,t) \in \mathcal{I}_{\text{SV}}} \left( \eta h_{i,t} e^{-w(\tau)^\top \tilde{x}_{i,t}} S_i^{\mathcal{I}_{\text{SV}}}(w(\tau)) - \frac{1}{2\tau} \alpha_{i,t} \right) u_{i,t}(\tau), \\ \mathcal{D}_{\text{SV}}^{\text{rest}}(\tau) &:= \sum_{(i,t) \in \mathcal{I}_{\text{SV}}} \left( \text{rest}_{i,t}^\pi(w(\tau)) - \text{rest}_{i,t}^v(\tau) \right) u_{i,t}(\tau). \end{aligned} \quad (28)$$

**Step 1:  $\mathcal{D}_{\text{SV}}^{\text{restore}}$  is restoring.** Introduce the notation

$$p_{i,t} := e^{-\tilde{w}^\top \tilde{x}_{i,t}} > 0.$$

Note that by definition of  $\tilde{w}$  in (24), it holds for all  $(i,t) \in \mathcal{I}_{\text{SV}}$ :

$$\eta h_{i,t} p_{i,t} \sum_{s \in \mathcal{I}_{\text{SV}}(i)} p_{i,s} = \frac{1}{2} \alpha_{i,t}. \quad (29)$$

We now plug  $w(\tau) = f(\tau)\hat{w} + \tilde{w} + r(\tau)$  with  $f(\tau) = \frac{1}{2} \log \tau$  into  $\mathcal{D}_{\text{SV}}^{\text{restore}}(\tau)$ . For  $(i,t) \in \mathcal{I}_{\text{SV}}$ ,

$$e^{-w(\tau)^\top \tilde{x}_{i,t}} = \tau^{-1/2} p_{i,t} e^{-u_{i,t}(\tau)}, \quad S_i^{\mathcal{I}_{\text{SV}}}(w(\tau)) = \tau^{-1/2} \sum_{s \in \mathcal{I}_{\text{SV}}(i)} p_{i,s} e^{-u_{i,s}(\tau)}.$$

Therefore,

$$\mathcal{D}_{\text{SV}}^{\text{restore}}(\tau) = \eta \tau^{-1} \sum_i \sum_{t \in \mathcal{I}_{\text{SV}}(i)} h_{i,t} p_{i,t} u_{i,t}(\tau) \left( e^{-u_{i,t}(\tau)} \sum_{s \in \mathcal{I}_{\text{SV}}(i)} p_{i,s} e^{-u_{i,s}(\tau)} - \sum_{s \in \mathcal{I}_{\text{SV}}(i)} p_{i,s} \right) \quad (30)$$

$$= \eta \tau^{-1} \sum_i \sum_{t,s \in \mathcal{I}_{\text{SV}}(i)} h_{i,t} p_{i,t} p_{i,s} u_{i,t}(\tau) (e^{-u_{i,t}(\tau) - u_{i,s}(\tau)} - 1). \quad (31)$$

Symmetrizing (31) in  $(s,t)$  yields (we add the same sum with  $s$  and  $t$  swapped and divide by 2):

$$\mathcal{D}_{\text{SV}}^{\text{restore}}(\tau) = \frac{\eta}{2} \tau^{-1} \sum_i \sum_{s,t \in \mathcal{I}_{\text{SV}}(i)} p_{i,t} p_{i,s} H_{i,t,s}(\tau) (e^{-U_{i,t,s}(\tau)} - 1), \quad (32)$$

with

$$H_{i,t,s}(\tau) := h_{i,t} u_{i,t}(\tau) + h_{i,s} u_{i,s}(\tau), \quad U_{i,t,s}(\tau) := u_{i,t}(\tau) + u_{i,s}(\tau).$$

For off-diagonal terms  $s \neq t$ , since  $U(e^{-U} - 1) \leq 0$  for all  $U \in \mathbb{R}$ , there might be positive contributions to the drift when  $H$  and  $U$  have opposite signs. However, after numerical inspections on Gaussian match-and-copy data, we find that eventually most off-diagonal contributions in (32) remain negative, i.e., most  $s \neq t$  pairs satisfy  $\text{sign}(H_{i,t,s}(\tau)) = \text{sign}(U_{i,t,s}(\tau))$ . To formalize this, we make the following assumption.

**Assumption E.2 (Alignment Assumption (A8) in Theorem D.2 (stable trajectory)).** There exists  $\varepsilon \in (0, 1/2)$  such that, for all sufficiently large  $\tau$ , the total off-diagonal contribution in (32) coming from pairs  $(s,t) \in \mathcal{I}_{\text{SV}}(i)^2$  with  $s \neq t$  and  $\text{sign}(H_{i,t,s}(\tau)) \neq \text{sign}(U_{i,t,s}(\tau))$  is at most an  $\varepsilon$ -fraction (in absolute value) of the total off-diagonal mass:

$$\sum_{\substack{s,t \in \mathcal{I}_{\text{SV}}(i), \\ s \neq t, \\ \text{sign}(H_{i,t,s}(\tau)) \neq \text{sign}(U_{i,t,s}(\tau))}} p_{i,t} p_{i,s} |H_{i,t,s}(\tau)| |e^{-U_{i,t,s}(\tau)} - 1| \leq \varepsilon \sum_{\substack{s,t \in \mathcal{I}_{\text{SV}}(i), \\ s \neq t}} p_{i,t} p_{i,s} |H_{i,t,s}(\tau)| |e^{-U_{i,t,s}(\tau)} - 1|. \quad (33)$$

Under this assumption, the off-diagonal terms have a non-positive contribution. Indeed, writing for brevity  $H_{t,s} = H_{i,t,s}(\tau)$  and  $U_{t,s} = U_{i,t,s}(\tau)$ , and all sums being restricted to  $s, t \in \mathcal{I}_{\text{SV}}(i)$  with  $s \neq t$  (off-diagonal terms):

$$\begin{aligned}
\sum p_{i,t} p_{i,s} H_{t,s} (e^{-U_{t,s}} - 1) &= \sum p_{i,t} p_{i,s} |H_{t,s}| |e^{-U_{t,s}} - 1| \underbrace{\text{sign}(H_{t,s}) \text{sign}(e^{-U_{t,s}} - 1)}_{= -\text{sign}(H_{t,s} U_{t,s})} \\
&= - \sum p_{i,t} p_{i,s} |H_{t,s}| |e^{-U_{t,s}} - 1| \text{sign}(H_{t,s} U_{t,s}) \\
&= \sum p_{i,t} p_{i,s} |H_{t,s}| |e^{-U_{t,s}} - 1| \delta_{HU < 0} - \sum p_{i,t} p_{i,s} |H_{t,s}| |e^{-U_{t,s}} - 1| \delta_{HU > 0} \\
&= 2 \sum p_{i,t} p_{i,s} |H_{t,s}| |e^{-U_{t,s}} - 1| \delta_{HU < 0} - \sum p_{i,t} p_{i,s} |H_{t,s}| |e^{-U_{t,s}} - 1| \\
&\leq -(1 - 2\epsilon) \sum p_{i,t} p_{i,s} |H_{t,s}| |e^{-U_{t,s}} - 1| \leq 0
\end{aligned} \tag{34}$$

which is negative since  $\epsilon \in (0, 1/2)$ . We deduce the following lemma, which shows that  $\mathcal{D}_{\text{SV}}^{\text{restore}}$  is a restoring force: it helps push the trajectory back towards the target trajectory when  $u_{i,t}(\tau)$  is large.

**Lemma E.3** (Restoring force from support-tail of support drift). *Fix any  $R > 0$  large enough. Under **Assumption (A8) of alignment (stable trajectory)**, formalized in Theorem E.2, there exist constants  $c > 0$  and  $\tau_1$  such that for all  $\tau \geq \tau_1$ ,*

$$\mathcal{D}_{\text{SV}}^{\text{restore}}(\tau) \leq -\frac{c}{\tau} \sum_{(i,t) \in \mathcal{I}_{\text{SV}}} \Phi(u_{i,t}(\tau)), \tag{35}$$

where

$$\Phi(u) := |u| \left( e^{2|u|} \delta_{\{u \leq -R\}} + \delta_{\{u \geq R\}} \right).$$

*Proof.* Consider first diagonal terms  $s = t$  in (32). They equal

$$p_{i,t}^2 (2h_{i,t} u_{i,t}(\tau)) (e^{-2u_{i,t}(\tau)} - 1) \leq 0.$$

Since  $u(e^{-2u} - 1) \sim -|u|e^{2|u|}$  for  $u \rightarrow -\infty$  and  $u(e^{-2u} - 1) \sim -u$  for  $u \rightarrow \infty$ , this diagonal term is close to  $-2p_{i,t}^2 h_{i,t} \Phi(u_{i,t}(\tau))$  provided that  $|u_{i,t}(\tau)|$  is large enough. In particular, there exists a constant  $c > 0$  (depending on  $R$  and on  $\min_{(i,t) \in \mathcal{I}_{\text{SV}}} p_{i,t}^2 h_{i,t} > 0$ ) such that the diagonal part is bounded above by  $-(c/\tau) \sum_{(i,t) \in \mathcal{I}_{\text{SV}}} \Phi(u_{i,t}(\tau))$ .

Since off-diagonal terms  $s \neq t$  remains non-positive (34), we get the upper bound in (35).  $\square$

**Step 2:  $\mathcal{D}_{\text{SV}}^{\text{rest}}$  is compensated by the restoring force  $\mathcal{D}_{\text{SV}}^{\text{restore}}$ .** We bound the remainder drift

$$\mathcal{D}_{\text{SV}}^{\text{rest}}(\tau) = \sum_{(i,t) \in \mathcal{I}_{\text{SV}}} \left( \text{rest}_{i,t}^{\pi}(w(\tau)) - \text{rest}_{i,t}^v(\tau) \right) u_{i,t}(\tau).$$

**The time-discretization remainder  $\text{rest}^v$ .** Since  $f(\tau) = \frac{1}{2} \log \tau$ , we have

$$v(\tau) = f(\tau + 1) - f(\tau) = \frac{1}{2} \log \left( 1 + \frac{1}{\tau} \right) = \frac{1}{2\tau} + O(\tau^{-2})$$

hence there exists  $c > 0$  such that for all  $\tau \geq 1$  and all  $(i,t) \in \mathcal{I}_{\text{SV}}$ ,

$$|\text{rest}_{i,t}^v(\tau)| = \left| v(\tau) - \frac{1}{2\tau} \right| \alpha_{i,t} \leq c \tau^{-2}. \tag{36}$$

Therefore,

$$\sum_{(i,t) \in \mathcal{I}_{\text{SV}}} |\text{rest}_{i,t}^v(\tau)| |u_{i,t}(\tau)| \leq c \tau^{-2} \sum_{(i,t) \in \mathcal{I}_{\text{SV}}} |u_{i,t}(\tau)| \leq c' \tau^{-2} \left( R + \sum_{(i,t) \in \mathcal{I}_{\text{SV}}} \Phi(u_{i,t}(\tau)) \right), \tag{37}$$

where we used  $u \leq R + \Phi(u)$  for all  $u \in \mathbb{R}$  in the last inequality. The first term  $c' R \tau^{-2}$  is summable in  $\tau$ , while the second term can be absorbed by the restoring force (35) for  $\tau$  large enough ( $c' \tau^{-2} \Phi(u) \leq \frac{1}{100} c \tau^{-1} \Phi(u)$  for  $\tau$  large enough so we still get a restoring force with modified constant  $0.99c$ , say).

**The gradient coefficient remainder**  $\text{rest}^\pi$ . Theorem F.1 in the appendix gives the exact expression for the MSE gradient coefficients:

$$\pi_{i,t}^{\text{MSE}}(w) = a_{t+1}^{(i)}(w) \left( (1 - a_{y_i+1}^{(i)}(w)) h_{i,t}(w) - \|r^{(i)}(w)\|_2^2 \right), \quad \forall(i, t), w.$$

Then,

$$\begin{aligned} \text{rest}_{i,t}^\pi(w(\tau)) u_{i,t}(\tau) &= \eta h_{i,t}(w(\tau)) u_{i,t}(\tau) \left[ a_{t+1}^{(i)}(w(\tau)) (1 - a_{y_i+1}^{(i)}(w(\tau))) - e^{-w(\tau)^\top \tilde{x}_{i,t}} S_i(w(\tau)) \right] \\ &\quad + \eta e^{-w(\tau)^\top \tilde{x}_{i,t}} S_i(w(\tau)) u_{i,t}(\tau) \left[ h_{i,t}(w(\tau)) - h_{i,t} \right] \\ &\quad + \eta h_{i,t} e^{-w(\tau)^\top \tilde{x}_{i,t}} u_{i,t}(\tau) \left[ S_i(w(\tau)) - S_i^{\mathcal{I}_{\text{SV}}}(w(\tau)) \right] \\ &\quad - \eta a_{t+1}^{(i)}(w(\tau)) \|r^{(i)}(w(\tau))\|_2^2 u_{i,t}(\tau). \end{aligned}$$

We treat each of these four terms separately. We will use repeatedly that for  $(i, t) \in \mathcal{I}_{\text{SV}}$ , expanding  $w(\tau) = f(\tau)\tilde{w} + \tilde{w} + r(\tau)$  with  $f(\tau) = \frac{1}{2} \log \tau$  and  $u_{i,t}(\tau) = \langle r(\tau), \tilde{x}_{i,t} \rangle$  gives

$$e^{-w(\tau)^\top \tilde{x}_{i,t}} = \tau^{-1/2} p_{i,t} e^{-u_{i,t}(\tau)},$$

with  $p_{i,t} = e^{-\tilde{w}^\top \tilde{x}_{i,t}} > 0$  a constant independent of  $\tau$  (only depending on the data through  $\tilde{w}$  and  $\tilde{x}_{i,t}$ ), and gives  $(i, s) \notin \mathcal{I}_{\text{SV}}$ ,

$$e^{-w(\tau)^\top \tilde{x}_{i,s}} = \tau^{-1/2 - \theta_{i,t}/2} p_{i,s} e^{-u_{i,s}(\tau)}.$$

1. Since  $a_{t+1}^{(i)}(w)(1 - a_{y_i+1}^{(i)}(w)) = e^{-w^\top \tilde{x}_{i,t}} S_i(w)/(1 + S_i(w))^2$  for all  $w$ , the first term equals

$$\eta h_{i,t}(w(\tau)) u_{i,t}(\tau) e^{-w(\tau)^\top \tilde{x}_{i,t}} S_i(w(\tau)) \underbrace{\left( \frac{1}{(1 + S_i(w(\tau)))^2} - 1 \right)}_{\leq 0}.$$

If  $u_{i,t}(\tau) \geq 0$ , this term is non-positive and keeps the sum bounded by something summable in  $\tau$ . If  $u_{i,t}(\tau) < 0$ , it is positive and using that  $S_i(w(\tau)) = S_i^{\mathcal{I}_{\text{SV}}}(w(\tau)) + S_i^{\mathcal{I}_{\text{nonSV}}}(w(\tau)) \leq (1 + g(\tau)) S_i^{\mathcal{I}_{\text{SV}}}(w(\tau)) \leq c\tau^{-1/2} e^{|u_{\min(\mathcal{I}_{\text{SV}})}(\tau)|}$  by the **softmax domination (stable trajectory)** assumption, we can bound it as

$$\begin{aligned} &\underbrace{c\eta h_{i,t}(w(\tau)) p_{i,t}}_{0 < c\eta h_{\max} p_{\max}} \tau^{-1/2} \underbrace{|u_{i,t}(\tau)| e^{|u_{i,t}(\tau)|}}_{\leq |u_{\min(\mathcal{I}_{\text{SV}})}(\tau)| e^{|u_{\min(\mathcal{I}_{\text{SV}})}(\tau)|}} \tau^{-1/2} p_{\max} e^{|u_{\min(\mathcal{I}_{\text{SV}})}(\tau)|} \underbrace{\left( 1 - \frac{1}{(1 + S_i(w(\tau)))^2} \right)}_{= \frac{S_i(2+S_i)}{(1+S_i)^2} \leq 2S_i} \\ &\leq c' \tau^{-1} |u_{\min(\mathcal{I}_{\text{SV}})}(\tau)| e^{2|u_{\min(\mathcal{I}_{\text{SV}})}(\tau)|} S_i(w(\tau)). \end{aligned}$$

Either  $u_{\min(\mathcal{I}_{\text{SV}})}(\tau) \geq -R$ , in which case the term is bounded by  $c' \tau^{-1} S_i(w(\tau))$ , and using again that  $S_i(w(\tau)) \leq c\tau^{-1/2} e^{|u_{\min(\mathcal{I}_{\text{SV}})}(\tau)|}$  by the **softmax domination (stable trajectory)** assumption, this is bounded by  $c'' \tau^{-3/2}$  which is summable in  $\tau$ ; or  $u_{\min(\mathcal{I}_{\text{SV}})}(\tau) \leq -R$ , in which case  $|u_{\min(\mathcal{I}_{\text{SV}})}(\tau)| e^{2|u_{\min(\mathcal{I}_{\text{SV}})}(\tau)|} = \Phi(u_{\min(\mathcal{I}_{\text{SV}})}(\tau))$  and since  $S_i(w(\tau)) \rightarrow 0$  as  $\tau \rightarrow \infty$  by divergence of the margins (Theorem G.3), this becomes negligible compared to the restoring force (35) for  $\tau$  large enough. In both cases, the first term is controlled.

2. For the second term

$$\eta e^{-w(\tau)^\top \tilde{x}_{i,t}} S_i(w(\tau)) u_{i,t}(\tau) (h_{i,t}(w(\tau)) - h_{i,t})$$

we bound it in absolute value using that  $S_i(w(\tau)) \leq c\tau^{-1/2} e^{|u_{\min(\mathcal{I}_{\text{SV}})}(\tau)|}$  by the **softmax domination (stable trajectory)** assumption, yielding the bound

$$c\tau^{-1} e^{-u_{i,t}(\tau)} |u_{i,t}(\tau)| e^{-u_{\min(\mathcal{I}_{\text{SV}})}(\tau)} |h_{i,t}(w(\tau)) - h_{i,t}|.$$

If  $u_{\min(\mathcal{I}_{\text{SV}})}(\tau) \geq -R$ , then this is bounded by  $c' \tau^{-1} e^{-u_{i,t}(\tau)} |u_{i,t}(\tau)| |h_{i,t}(w(\tau)) - h_{i,t}|$ . Either  $u_{i,t}(\tau) \geq 0$ , in which case  $|u_{i,t}(\tau)| e^{-u_{i,t}(\tau)} \leq 1$ , or  $-R \leq u_{i,t}(\tau) \leq 0$ , and in both cases the term is bounded by

$$c'' \tau^{-1} |h_{i,t}(w(\tau)) - h_{i,t}|,$$

which is summable in  $\tau$  by the **pre-factor convergence rate (stable trajectory)** assumption. If  $u_{\min(\mathcal{I}_{\text{SV}})}(\tau) \leq -R$ , then again if  $u_{i,t}(\tau) \geq 0$ , we have  $|u_{i,t}(\tau)|e^{-u_{i,t}(\tau)} \leq 1$ , and the term is bounded by

$$c\tau^{-1}\Phi(u_{\min(\mathcal{I}_{\text{SV}})}(\tau))|h_{i,t}(w(\tau)) - h_{i,t}|.$$

Or if  $u_{i,t}(\tau) \leq 0$ , then  $|u_{i,t}(\tau)|e^{-u_{i,t}(\tau)} \leq |u_{\min(\mathcal{I}_{\text{SV}})}(\tau)|e^{|u_{\min(\mathcal{I}_{\text{SV}})}(\tau)|}$  and the term can again be bounded by

$$c\tau^{-1}|u_{\min(\mathcal{I}_{\text{SV}})}(\tau)|e^{2|u_{\min(\mathcal{I}_{\text{SV}})}(\tau)|}|h_{i,t}(w(\tau)) - h_{i,t}| = c\tau^{-1}\Phi(u_{\min(\mathcal{I}_{\text{SV}})}(\tau))|h_{i,t}(w(\tau)) - h_{i,t}|.$$

In both cases, we have the same bound that can be absorbed by the restoring force (35) since  $|h_{i,t}(w(\tau)) - h_{i,t}| \rightarrow 0$  as  $\tau \rightarrow \infty$  by the **convergence of pre-factors (stable trajectory)** assumption.

3. For the third term

$$\eta h_{i,t} e^{-w(\tau)^\top \tilde{x}_{i,t}} u_{i,t}(\tau) (S_i(w(\tau)) - S_i^{\mathcal{I}_{\text{SV}}}(w(\tau))),$$

we note that  $S_i(w(\tau)) - S_i^{\mathcal{I}_{\text{SV}}}(w(\tau)) = S_i^{\mathcal{I}_{\text{nonSV}}}(w(\tau)) \geq 0$ . For  $u_{i,t}(\tau) \leq 0$ , this term is non-positive and keeps the sum bounded by something summable in  $\tau$ . For  $u_{i,t}(\tau) \geq 0$ , we use that  $S_i^{\mathcal{I}_{\text{nonSV}}}(w(\tau)) \leq g(\tau)S_i^{\mathcal{I}_{\text{SV}}}(w(\tau)) \leq cg(\tau)\tau^{-1/2}e^{|u_{\min(\mathcal{I}_{\text{SV}})}(\tau)|}$  by the **softmax domination (stable trajectory)** assumption, hence the term is bounded by

$$c'\tau^{-1}\underbrace{e^{-u_{i,t}(\tau)}|u_{i,t}(\tau)|}_{\leq 1}g(\tau)e^{|u_{\min(\mathcal{I}_{\text{SV}})}(\tau)|}.$$

If  $u_{\min(\mathcal{I}_{\text{SV}})}(\tau) \geq -R$ , this is bounded by  $c''\tau^{-1}g(\tau)$ , which is summable in  $\tau$  by the **softmax domination rate (stable trajectory)** assumption. If  $u_{\min(\mathcal{I}_{\text{SV}})}(\tau) \leq -R$ , this is bounded by

$$c'\tau^{-1}g(\tau)\Phi(u_{\min(\mathcal{I}_{\text{SV}})}(\tau)),$$

which can be absorbed by the restoring force (35) since  $g(\tau) \rightarrow 0$  as  $\tau \rightarrow \infty$  by the **softmax domination (stable trajectory)** assumption.

4. For the fourth term

$$-\eta a_{t+1}^{(i)}(w(\tau))\|r^{(i)}(w(\tau))\|_2^2 u_{i,t}(\tau),$$

it is non-positive when  $u_{i,t}(\tau) \geq 0$  and keeps the sum bounded by something summable in  $\tau$ . For  $u_{i,t}(\tau) \leq 0$ , we have  $e^{-u_{i,t}(\tau)}|u_{i,t}(\tau)| \leq |u_{\min(\mathcal{I}_{\text{SV}})}(\tau)|e^{|u_{\min(\mathcal{I}_{\text{SV}})}(\tau)|}$ . We also have that  $\|r^{(i)}(w(\tau))\|_2^2 \leq CS_i(w(\tau))^2$  by Theorem G.3 (no assumption needed here). So it is bounded in absolute value by

$$c\tau^{-1/2}|u_{\min(\mathcal{I}_{\text{SV}})}(\tau)|e^{|u_{\min(\mathcal{I}_{\text{SV}})}(\tau)|}S_i(w(\tau))^2.$$

Recall that  $S_i(w(\tau)) = c\tau^{-1/2}e^{|u_{\min(\mathcal{I}_{\text{SV}})}(\tau)|}$  by the **softmax domination (stable trajectory)** assumption. If  $u_{\min(\mathcal{I}_{\text{SV}})}(\tau) \geq -R$ , then  $S_i(w(\tau))^2 \leq c'\tau^{-1}$  and the term is bounded by  $c''\tau^{-3/2}$  which is summable in  $\tau$ . If  $u_{\min(\mathcal{I}_{\text{SV}})}(\tau) \leq -R$ , then we bound one  $S_i(w(\tau))$  by  $c\tau^{-1/2}e^{|u_{\min(\mathcal{I}_{\text{SV}})}(\tau)|}$  and keep the other, so the term is bounded by

$$c\tau^{-1}|u_{\min(\mathcal{I}_{\text{SV}})}(\tau)|e^{2|u_{\min(\mathcal{I}_{\text{SV}})}(\tau)|}S_i(w(\tau)) = c\tau^{-1}\Phi(u_{\min(\mathcal{I}_{\text{SV}})}(\tau))S_i(w(\tau)),$$

which can be absorbed by the restoring force (35) since  $S_i(w(\tau)) \rightarrow 0$  as  $\tau \rightarrow \infty$  by divergence of the margins (Theorem G.3).

### E.3 Analysis of non-support drift

We now bound

$$\mathcal{D}_{\text{non-SV}}(\tau) = \sum_{(i,t) \notin \mathcal{I}_{\text{SV}}} \eta \pi_{i,t}^{\text{MSE}}(w(\tau)) u_{i,t}(\tau).$$

Recall the gradient coefficients given by Theorem F.1:

$$\pi_{i,t}^{\text{MSE}}(w) = a_{t+1}^{(i)}(w) \left( (1 - a_{y_i+1}^{(i)}(w)) h_{i,t}(w) - \|r^{(i)}(w)\|_2^2 \right), \quad \forall (i,t), w.$$

We treat separately the two terms in the parenthesis.

1. For the first part of the drift given by

$$\sum_{(i,t) \notin \mathcal{I}_{\text{SV}}} \eta a_{t+1}^{(i)}(w(\tau)) (1 - a_{y_i+1}^{(i)}(w(\tau))) h_{i,t}(w(\tau)) u_{i,t}(\tau),$$

we note that if  $u_{i,t}(\tau) \leq 0$ , this term is non-positive and keeps the sum bounded by something summable in  $\tau$ . For  $u_{i,t}(\tau) \geq 0$ , we use that

$$a_{t+1}^{(i)}(w(\tau)) (1 - a_{y_i+1}^{(i)}(w(\tau))) = \frac{e^{-w(\tau)^\top \tilde{x}_{i,t}} S_i(w(\tau))}{(1 + S_i(w(\tau)))^2} \leq e^{-w(\tau)^\top \tilde{x}_{i,t}} S_i(w(\tau)).$$

Therefore the term is bounded by

$$c e^{-w(\tau)^\top \tilde{x}_{i,t}} S_i(w(\tau)) u_{i,t}(\tau).$$

Since  $(i, t) \notin \mathcal{I}_{\text{SV}}$ , we have

$$e^{-w(\tau)^\top \tilde{x}_{i,t}} = \tau^{-(1+\theta_{i,t})/2} p_{i,t} e^{-u_{i,t}(\tau)}.$$

Moreover, by the **softmax domination (stable trajectory)** assumption, we have  $S_i(w(\tau)) \leq c\tau^{-1/2} e^{|u_{\min}(\mathcal{I}_{\text{SV}})(\tau)|}$ . Therefore the term is bounded by

$$c' \tau^{-1-\theta_{i,t}/2} \underbrace{u_{i,t}(\tau) e^{-u_{i,t}(\tau)}}_{\leq 1} e^{|u_{\min}(\mathcal{I}_{\text{SV}})(\tau)|}.$$

If  $u_{\min}(\mathcal{I}_{\text{SV}})(\tau) \geq -R$ , this is bounded by  $c''\tau^{-1-\theta_{i,t}/2}$  which is summable in  $\tau$ . If  $u_{\min}(\mathcal{I}_{\text{SV}})(\tau) \leq -R$ , then it is bounded by  $c' \tau^{-1-\theta_{i,t}/2} \Phi(u_{\min}(\mathcal{I}_{\text{SV}})(\tau))$ , which can be absorbed by the restoring force (35) since  $\tau^{-\theta_{i,t}/2} \rightarrow 0$ .

2. For the second part of the drift given by

$$- \sum_{(i,t) \notin \mathcal{I}_{\text{SV}}} \eta a_{t+1}^{(i)}(w(\tau)) \|r^{(i)}(w(\tau))\|_2^2 u_{i,t}(\tau),$$

we note that if  $u_{i,t}(\tau) \geq 0$ , this term is non-positive and keeps the sum bounded by something summable in  $\tau$ . For  $u_{i,t}(\tau) \leq 0$ , the derivations are similar to those of the fourth term we have treated in the previous section for the support drift, but it decays even faster here since  $(i, t) \notin \mathcal{I}_{\text{SV}}$ . We have

$$|u_{i,t}(\tau)| e^{-u_{i,t}(\tau)} \leq |u_{\min}(\mathcal{I}_{\text{SV}})(\tau)| e^{|u_{\min}(\mathcal{I}_{\text{SV}})(\tau)|}.$$

We also have that  $\|r^{(i)}(w(\tau))\|_2^2 \leq C S_i(w(\tau))^2$  by Theorem G.3 (no assumption needed here). So the term is bounded in absolute value by

$$c \tau^{-(1+\theta_{i,t})/2} |u_{\min}(\mathcal{I}_{\text{SV}})(\tau)| e^{|u_{\min}(\mathcal{I}_{\text{SV}})(\tau)|} S_i(w(\tau))^2.$$

Recall that  $S_i(w(\tau)) \leq c\tau^{-1/2} e^{|u_{\min}(\mathcal{I}_{\text{SV}})(\tau)|}$  by the **softmax domination (stable trajectory)** assumption. If  $u_{\min}(\mathcal{I}_{\text{SV}})(\tau) \geq -R$ , then  $S_i(w(\tau))^2 \leq c'\tau^{-1}$  and the term is bounded by  $c''\tau^{-3/2-\theta_{i,t}/2}$  which is summable in  $\tau$ . If  $u_{\min}(\mathcal{I}_{\text{SV}})(\tau) \leq -R$ , then we bound one  $S_i(w(\tau))$  by  $c\tau^{-1/2} e^{|u_{\min}(\mathcal{I}_{\text{SV}})(\tau)|}$  and keep the other, so the term is bounded by

$$c \tau^{-1-\theta_{i,t}/2} |u_{\min}(\mathcal{I}_{\text{SV}})(\tau)| e^{2|u_{\min}(\mathcal{I}_{\text{SV}})(\tau)|} S_i(w(\tau)) = c \tau^{-1-\theta_{i,t}/2} \Phi(u_{\min}(\mathcal{I}_{\text{SV}})(\tau)) S_i(w(\tau)),$$

which can be absorbed by the restoring force (35) since  $\tau^{-\theta_{i,t}/2} S_i(w(\tau)) \rightarrow 0$  as  $\tau \rightarrow \infty$  by divergence of the margins (Theorem G.3).

This concludes the proof.  $\square$

## F Proof Details for Theorem D.2

This section contains:

- Section F.1: Gradient computations for MSE and CE losses, with a discussion about their differences.
- Section F.2: Proof that the MSE loss is non-convex in the merged key-query parameters, while CE is convex.

## F.1 Gradient coefficients

**Lemma F.1** (Per-sample gradients, feature-space form). *Fix one sample  $(\mathbf{E}, \mathbf{e}, t_0)$  with  $T_0 = t_0 + 1 \in \{2, \dots, T\}$ . Recall the model output  $\hat{y}(\mathbf{W}_{\text{KQ}}) = \mathbf{E} \mathbf{a}(z(\mathbf{W}_{\text{KQ}}))$  with linear logits and shifted softmax:*

$$z(\mathbf{W}_{\text{KQ}}) := \lambda \mathbf{E}^\top \mathbf{W}_{\text{KQ}} \mathbf{e} \in \mathbb{R}^T, \quad \mathbf{a}(z) := \begin{pmatrix} 0 \\ \text{softmax}(z_{1:T-1}) \end{pmatrix} \in \mathbb{R}^T.$$

Consider the losses

$$\text{MSE}(\mathbf{W}_{\text{KQ}}) = \frac{1}{2} \|\mathbf{E} \mathbf{a}(z(\mathbf{W}_{\text{KQ}})) - \mathbf{e}_{T_0}\|^2, \quad \text{CE}(\mathbf{W}_{\text{KQ}}) = -\log(\mathbf{a}_{T_0}(z(\mathbf{W}_{\text{KQ}}))).$$

Let  $\delta_{T_0} \in \mathbb{R}^T$  be the canonical basis vector and

$$\mathbf{S} = \begin{pmatrix} 0_{1 \times (T-1)} & 0 \\ I_{T-1} & 0_{(T-1) \times 1} \end{pmatrix}, \quad J(\mathbf{a}) = \text{diag}(\mathbf{a}) - \mathbf{a} \mathbf{a}^\top.$$

Then

$$\nabla_{\mathbf{W}_{\text{KQ}}} \text{MSE}(\mathbf{W}_{\text{KQ}}) = \lambda \mathbf{E} \mathbf{S}^\top J(\mathbf{a}) \mathbf{E}^\top \mathbf{E} (\mathbf{a} - \delta_{T_0}) \mathbf{e}^\top, \quad \nabla_{\mathbf{W}_{\text{KQ}}} \text{CE}(\mathbf{W}_{\text{KQ}}) = \lambda \mathbf{E} \mathbf{S}^\top (\mathbf{a} - \delta_{T_0}) \mathbf{e}^\top.$$

Equivalently, in the flattened feature notation of Theorem D.2, recall the notation  $w = \text{flatten}(\mathbf{W}_{\text{KQ}})$  and for  $t = 1, \dots, T-1$ ,

$$x_t := \lambda \text{flatten}(\mathbf{e}_t \mathbf{e}^\top) \in \mathbb{R}^{d_{\text{in}}^2}, \quad y := t_0 = T_0 - 1 \in \{1, \dots, T-1\}, \quad \tilde{x}_t := x_y - x_t \quad (t \neq y).$$

Then  $\nabla \mathcal{L}(w) = -\sum_{t \neq y} \pi_t(w) \tilde{x}_t$  for  $\mathcal{L} \in \{\text{CE}, \text{MSE}\}$ , with coefficients given by

$$\pi_t^{\text{MSE}}(w) = \lambda a_{t+1}(w) (v_{t+1}(w) - \bar{v}(w)), \quad (38)$$

$$\pi_t^{\text{CE}}(w) = a_{t+1}(w) \quad (39)$$

where  $v(w) = \mathbf{E}^\top \mathbf{E}(\mathbf{a}(w) - \delta_{T_0}) \in \mathbb{R}^T$ ,  $\bar{v}(w) := \sum_{s=1}^T \mathbf{a}_s(w) v_s = \mathbf{a}^\top v$ . An equivalent expression for the MSE coefficient, useful to analyze its sign under small residual  $r(w) := \mathbf{E} \mathbf{a}(w) - \mathbf{e}_{T_0}$ , is given next. Let  $d_t := \mathbf{e}_{t+1} - \mathbf{e}_{T_0}$  and  $h_t(w) := \sum_{s \neq y} \frac{a_{s+1}(w)}{1 - a_{y+1}(w)} \langle d_t, d_s \rangle$ ; we have

$$v_{t+1}(w) - \bar{v}(w) = \langle d_t, r(w) \rangle - \|r(w)\|_2^2 = (1 - a_{y+1}(w)) h_t(w) - \|r(w)\|_2^2. \quad (40)$$

*Proof.* Write the model output as  $\hat{y}(\mathbf{W}_{\text{KQ}}) := \mathbf{E} \mathbf{a}(z(\mathbf{W}_{\text{KQ}}))$ . For any direction  $\Delta$ ,

$$Dz(\mathbf{W}_{\text{KQ}})[\Delta] = \lambda \mathbf{E}^\top \Delta \mathbf{e}.$$

We first work out the Jacobian of the *shifted* softmax map  $\mathbf{a}(\cdot)$ . For  $t \geq 2$  and  $s \leq T-1$ ,

$$\frac{\partial \mathbf{a}_t}{\partial z_s} = \frac{\partial}{\partial z_s} \frac{\exp(z_{t-1})}{\sum_{r=1}^{T-1} \exp(z_r)} = \frac{\exp(z_{t-1})}{\sum_{r=1}^{T-1} \exp(z_r)} \delta_{s=t-1} - \frac{\exp(z_{t-1}) \exp(z_s)}{(\sum_{r=1}^{T-1} \exp(z_r))^2} = \mathbf{a}_t \delta_{s=t-1} - \mathbf{a}_t \mathbf{a}_{s+1}. \quad (41)$$

and all other partials are zero. This is exactly the matrix identity  $D\mathbf{a}(z) = J(\mathbf{a}(z)) \mathbf{S}$  since

$$\begin{aligned} J(\mathbf{a}) \mathbf{S} &= \begin{pmatrix} 0 & 0_{1 \times T-1} \\ 0_{T-1 \times 1} & \text{diag}(\mathbf{a}_{2:T}) - \mathbf{a}_{2:T} \mathbf{a}_{2:T}^\top \end{pmatrix} \begin{pmatrix} 0_{1 \times T-1} & 0 \\ I_{T-1} & 0_{T-1 \times 1} \end{pmatrix} \\ &= \begin{pmatrix} 0_{1 \times T-1} & 0 \\ \text{diag}(\mathbf{a}_{2:T}) - \mathbf{a}_{2:T} \mathbf{a}_{2:T}^\top & 0_{T-1 \times 1} \end{pmatrix} = D\mathbf{a}(z). \end{aligned} \quad (42)$$

Hence, by the chain rule,

$$D(\mathbf{a} \circ z)(\mathbf{W}_{\text{KQ}})[\Delta] = D\mathbf{a}(z(\mathbf{W}_{\text{KQ}}))[Dz(\mathbf{W}_{\text{KQ}})[\Delta]] = \lambda J(\mathbf{a}(z(\mathbf{W}_{\text{KQ}}))) \mathbf{S} \mathbf{E}^\top \Delta \mathbf{e}.$$

**MSE.** Let  $r(\mathbf{W}_{\text{KQ}}) := \hat{y}(\mathbf{W}_{\text{KQ}}) - \mathbf{e}_{T_0}$ , so  $\text{MSE}(\mathbf{W}_{\text{KQ}}) = \frac{1}{2} \|r(\mathbf{W}_{\text{KQ}})\|^2$  and

$$\text{DMSE}(\mathbf{W}_{\text{KQ}})[\Delta] = \langle r(\mathbf{W}_{\text{KQ}}), D r(\mathbf{W}_{\text{KQ}})[\Delta] \rangle = \langle r(\mathbf{W}_{\text{KQ}}), \mathbf{E} D(\mathbf{a} \circ z)(\mathbf{W}_{\text{KQ}})[\Delta] \rangle.$$

Plugging in the expression from above yields

$$\text{DMSE}(\mathbf{W}_{\text{KQ}})[\Delta] = \lambda \langle r, \mathbf{E} J(\mathbf{a}) \mathbf{S} \mathbf{E}^\top \Delta \mathbf{e} \rangle = \langle \lambda \mathbf{E} \mathbf{S}^\top J(\mathbf{a}) \mathbf{E}^\top r \mathbf{e}^\top, \Delta \rangle_F.$$

Finally note  $r = \mathbf{E}\mathbf{a} - \mathbf{e}_{T_0} = \mathbf{E}(\mathbf{a} - \delta_{T_0})$ , giving the claimed formula:

$$\nabla_{\mathbf{W}_{\text{KQ}}} \text{MSE}(\mathbf{W}_{\text{KQ}}) = \lambda \mathbf{E} \mathbf{S}^\top J(\mathbf{a}) \mathbf{E}^\top \mathbf{E}(\mathbf{a} - \delta_{T_0}) \mathbf{e}^\top.$$

In the flattened feature notation, we use that for any  $c \in \mathbb{R}^T$ , we have  $\mathbf{E}c = \sum_{t=1}^T c_t \mathbf{e}_t$ , hence  $\mathbf{E}c \mathbf{e}^\top = \sum_{t=1}^T c_t \mathbf{e}_t \mathbf{e}^\top$  and

$$\text{flatten}(\mathbf{E}c \mathbf{e}^\top) = \sum_{t=1}^T c_t \text{flatten}(\mathbf{e}_t \mathbf{e}^\top) = \sum_{t=1}^T c_t x_t. \quad (43)$$

Set  $v := \mathbf{E}^\top \mathbf{E}(\mathbf{a} - \delta_{T_0}) = \mathbf{E}^\top r \in \mathbb{R}^T$  and  $\bar{v} := \mathbf{a}^\top v$ . Using  $J(\mathbf{a})v = \text{diag}(\mathbf{a})v - \mathbf{a}(\mathbf{a}^\top v) = (\mathbf{a}_s(v_s - \bar{v}))_{s=1}^T$  and (43),

$$\begin{aligned} \nabla \text{MSE}(w) &= \text{flatten}(\nabla_{\mathbf{W}_{\text{KQ}}} \text{MSE}(\mathbf{W}_{\text{KQ}})) = \lambda \text{flatten}(\mathbf{E} \mathbf{S}^\top J(\mathbf{a}) v \mathbf{e}^\top) \\ &= \sum_{t=1}^{T-1} (J(\mathbf{a})v)_{t+1} x_t = \sum_{t=1}^{T-1} a_{t+1} (v_{t+1} - \bar{v}) x_t. \end{aligned}$$

Finally, since  $\sum_{t=1}^{T-1} a_{t+1} (v_{t+1} - \bar{v}) = \sum_{s=2}^T \mathbf{a}_s(v_s - \bar{v}) = \mathbf{a}^\top v - \bar{v} \sum_s \mathbf{a}_s = 0$ , we can subtract  $0 \cdot x_y = \sum_{t=1}^{T-1} a_{t+1} (v_{t+1} - \bar{v}) x_y$  and rewrite

$$\nabla \text{MSE}(w) = \sum_{t \neq y} a_{t+1} (v_{t+1} - \bar{v}) (x_t - x_y) = - \sum_{t \neq y} \pi_t^{\text{MSE}}(w) \tilde{x}_t.$$

Note that an equivalent expression for  $v$  is  $v = \mathbf{E}^\top r$ , so that  $v_{t+1} - \bar{v} = \mathbf{e}_{t+1}^\top r - a^\top \mathbf{E}^\top r = (\mathbf{e}_{t+1} - \mathbf{E}a)^\top r$ . Since  $\mathbf{e}_{t+1} - \mathbf{E}a = (\mathbf{e}_{t+1} - \mathbf{e}_{T_0}) - (\mathbf{E}a - \mathbf{e}_{T_0}) = d_t - r$  with  $d_t := \mathbf{e}_{t+1} - \mathbf{e}_{T_0}$ , we have the alternative expression

$$v_{t+1} - \bar{v} = \langle d_{t+1} - r, r \rangle = \langle d_t, r \rangle - \|r\|^2. \quad (44)$$

Moreover,  $r = \mathbf{E}a - \mathbf{e}_{T_0} = \sum_{s=1}^{T-1} a_{s+1} \mathbf{e}_{s+1} - (\sum_{s=1}^{T-1} a_{s+1}) \mathbf{e}_{T_0} = \sum_{s \neq y} a_{s+1} d_s$  so that  $\langle d_t, r \rangle = \sum_{s \neq y} a_{s+1} \langle d_t, d_s \rangle = (1 - a_{y+1}) h_t$ , which finishes the proof (40) and thus proves the lemma for MSE.

**CE.** We have  $\text{CE}(\mathbf{W}_{\text{KQ}}) = -\log(\mathbf{a}_{T_0}(z(\mathbf{W}_{\text{KQ}})))$ , hence

$$D\text{CE}(\mathbf{W}_{\text{KQ}})[\Delta] = -\frac{1}{\mathbf{a}_{T_0}} D\mathbf{a}_{T_0}(z(\mathbf{W}_{\text{KQ}}))[Dz(\mathbf{W}_{\text{KQ}})[\Delta]].$$

Using  $D\mathbf{a}(z) = J(\mathbf{a}(z))\mathbf{S}$  and  $Dz(\mathbf{W}_{\text{KQ}})[\Delta] = \lambda \mathbf{E}^\top \Delta \mathbf{e}$ ,

$$D\text{CE}(\mathbf{W}_{\text{KQ}})[\Delta] = -\frac{\lambda}{\mathbf{a}_{T_0}} (\delta_{T_0}^\top J(\mathbf{a}) \mathbf{S}) \mathbf{E}^\top \Delta \mathbf{e}.$$

Since  $\delta_{T_0}^\top J(\mathbf{a}) = \mathbf{a}_{T_0}(\delta_{T_0}^\top - \mathbf{a}^\top)$ , we have

$$-\frac{1}{\mathbf{a}_{T_0}} \delta_{T_0}^\top J(\mathbf{a}) = \mathbf{a}^\top - \delta_{T_0}^\top,$$

and thus

$$D\text{CE}(\mathbf{W}_{\text{KQ}})[\Delta] = \lambda (\mathbf{a} - \delta_{T_0})^\top \mathbf{S} \mathbf{E}^\top \Delta \mathbf{e} = \langle \lambda \mathbf{E} \mathbf{S}^\top (\mathbf{a} - \delta_{T_0}) \mathbf{e}^\top, \Delta \rangle_F,$$

which gives the gradient formula. In the flattened feature notation, this gives:

$$\nabla \text{CE}(w) = \text{flatten}(\nabla_{\mathbf{W}_{\text{KQ}}} \text{CE}(\mathbf{W}_{\text{KQ}})) = \lambda \text{flatten}(\mathbf{E} \mathbf{S}^\top (\mathbf{a} - \delta_{T_0}) \mathbf{e}^\top) = \sum_{t=1}^{T-1} ((\mathbf{S}^\top \mathbf{a})_t - \delta_{t=y}) x_t.$$

Since  $(\mathbf{S}^\top \mathbf{a})_t = \mathbf{a}_{t+1}$  and  $\sum_{t=1}^{T-1} a_{t+1} = 1$  so that  $x_y = x_y \sum_{t=1}^{T-1} a_{t+1}$ , we get

$$\nabla \text{CE}(w) = \sum_{t=1}^{T-1} a_{t+1}(w) x_t - x_y = - \sum_{t \neq y} a_t(w) (x_y - x_t) = - \sum_{t \neq y} \pi_t^{\text{CE}}(w) \tilde{x}_t,$$

as announced.  $\square$

*Remark F.2* (Sign of gradient coefficients for MSE vs CE). Theorem F.1 shows that both the MSE and CE loss have gradients that can be expressed as linear combinations of the same set of vectors  $\tilde{x}_{i,t} = x_{i,y_i} - x_{i,t}$  for  $t \neq y_i$ :

$$\nabla \mathcal{L}(w) = - \sum_{i=1}^n \sum_{t \neq y_i} \pi_{i,t}^{\mathcal{L}}(w) \tilde{x}_{i,t}. \quad (45)$$

A GD step thus moves the weights  $w$  in a direction given by a weighted combination of the  $\tilde{x}_{i,t}$ 's, with coefficients  $\pi_{i,t}^{\mathcal{L}}(w)$  depending on the loss  $\mathcal{L}$ .

- If  $\pi_t^{\mathcal{L}} > 0$ , we move *toward*  $\tilde{x}_t$  and increase the margin  $w^\top (x_y - x_t)$ , i.e., the inner product with the correct class  $y$  (the  $y$ 's logit) increases relative to class  $t$ .
- If  $\pi_t^{\mathcal{L}} < 0$ , we move *opposite* to  $\tilde{x}_t$  and raise class  $t$ 's score relative to the true class.

For CE, all coefficients are positive, so *every step monotonically increases the margins*. For MSE, coefficients can have either sign: sometimes (e.g., early on) increasing a wrong logit helps reduce squared error by pulling the mean  $\mathbf{E}a = \sum_t a_t \mathbf{e}_t$  toward  $\mathbf{e}_{T_0}$ . This comes from the fact that MSE also cares about the  $\ell^2$  geometry of the embeddings  $\mathbf{e}_t$ . Dropping the sample index  $i$  for readability, the CE coefficients are  $\pi_{i,t}^{\text{CE}} = a_{t+1}$  while  $\pi_{i,t}^{\text{MSE}} = a_{t+1}(v_{t+1} - \bar{v})$  has an additional factor  $v_{t+1} - \bar{v}$  which determines its sign. This term  $v_{t+1} - \bar{v}$  in  $\pi_{i,t}^{\text{MSE}}$  encodes how changing  $a_{t+1}$  affects the residual  $r = \mathbf{E}a - \mathbf{e}_{t_0+1}$ . If we infinitesimally shift attention toward  $t+1$  via  $a \mapsto a + \varepsilon(\delta_{t+1} - a)$ , then

$$\frac{d}{d\varepsilon} \Big|_{\varepsilon=0} \frac{1}{2} \|\mathbf{E}(a + \varepsilon(\delta_{t+1} - a)) - \mathbf{e}_{T_0}\|^2 = \langle \mathbf{e}_{t+1} - \mathbf{E}a, r \rangle = v_{t+1} - \bar{v}. \quad (46)$$

Hence  $v_{t+1} - \bar{v} > 0$  means pushing mass to  $t$  *increases* the error, while  $v_{t+1} - \bar{v} < 0$  *decreases* it. At least in aggregate,

$$\sum_{t \neq y} \pi_t^{\text{MSE}} = \sum_{t \neq y} a_{t+1}(v_{t+1} - \bar{v}) = a_{y+1}(v_{y+1} - \bar{v}) = a_{T_0} \|r\|^2 > 0, \quad (47)$$

so at least one non-target direction is decreased in favor of the true class.

The next lemma shows that along diverging-margin trajectories, the sign of  $\pi_{i,t}^{\text{MSE}}(w)$  is eventually determined by the first term:  $\text{sign}(\pi_{i,t}^{\text{MSE}}(w(\tau))) = \text{sign}(h_{i,t}(w(\tau)))$ . For Gaussian match-and-copy data, w.h.p.,  $\langle d_{i,t}, d_{i,s} \rangle > 0$  for all  $(i,t), (i,s)$ , so  $h_{i,t}(w) > 0$  for all  $w$  and  $(i,t)$ , and hence  $\pi_{i,t}^{\text{MSE}}(w(\tau)) > 0$  (eventually) along diverging-margin trajectories, thus ensuring margin monotone increase like for CE.

**Lemma F.3** (Asymptotics of MSE coefficients along diverging-margin trajectories). *If  $(w(\tau))_{\tau \geq 0}$  is a trajectory such that the margins diverge, i.e.,  $\min_i \min_{t \neq y_i} w(\tau)^\top \tilde{x}_{i,t} \rightarrow +\infty$  as  $\tau \rightarrow \infty$ , then eventually:*

$$\pi_{i,t}^{\text{MSE}}(w(\tau)) \sim h_{i,t}(w(\tau)) e^{-w(\tau)^\top \tilde{x}_{i,t}} S_i(w(\tau)), \quad (48)$$

where  $S_i(w) := \sum_{s \neq y_i} e^{-w^\top \tilde{x}_{i,s}}$  is the softmax tail.

*Proof.* Equation (38) gives the explicit expression

$$\pi_{i,t}^{\text{MSE}}(w) = a_{t+1}^{(i)}(w) \left( (1 - a_{y_i+1}^{(i)}(w)) h_{i,t}(w) - \|r^{(i)}(w)\|_2^2 \right).$$

Since the margins diverge, the loss goes to zero and hence the MSE residuals  $r^{(i)}(w(\tau)) \rightarrow 0$  for each  $i$ . By (40),

$$(1 - a_{y_i+1}^{(i)}(w)) h_{i,t}(w) = \langle d_{i,t}, r^{(i)}(w) \rangle$$

so the first term in  $\pi_{i,t}^{\text{MSE}}(w)$  is linear in  $r^{(i)}(w)$ , while the second term is quadratic in  $r^{(i)}(w)$ . As  $r^{(i)}(w(\tau)) \rightarrow 0$ , the quadratic term becomes negligible:

$$\pi_{i,t}^{\text{MSE}}(w(\tau)) \sim a_{t+1}^{(i)}(w(\tau)) (1 - a_{y_i+1}^{(i)}(w(\tau))) h_{i,t}(w(\tau)).$$

The final asymptotic equivalent is obtained by noting that since  $S_i(w(\tau)) \rightarrow 0$  (as margins diverge), we have

$$a_{t+1}^{(i)}(w) = \frac{e^{-w^\top \tilde{x}_{i,t}}}{1 + S_i(w)} \sim e^{-w^\top \tilde{x}_{i,t}}, \quad 1 - a_{y_i+1}^{(i)}(w) = \frac{S_i(w)}{1 + S_i(w)} \sim S_i(w).$$

□

## F.2 Convexity of CE and nonconvexity of MSE

Fix one sample  $(\mathbf{E}, \mathbf{e}, T_0)$  and denote  $z(\mathbf{W}_{\text{KQ}}) = \lambda \mathbf{E}^\top \mathbf{W}_{\text{KQ}} \mathbf{e}$  and  $\mathbf{a} = \mathbf{a}(z(\mathbf{W}_{\text{KQ}}))$ .

**(i) CE is convex in  $\mathbf{W}_{\text{KQ}}$ .** This is standard:  $\text{CE}(\mathbf{W}_{\text{KQ}}) = -\log(\mathbf{a}_{T_0}(z(\mathbf{W}_{\text{KQ}})))$  depends on  $\mathbf{W}_{\text{KQ}}$  only through the affine map  $\mathbf{W}_{\text{KQ}} \mapsto z_{1:T-1}(\mathbf{W}_{\text{KQ}})$ , and on these logits it equals the log-sum-exp form

$$\text{CE}(\mathbf{W}_{\text{KQ}}) = \log \left( \sum_{s=1}^{T-1} e^{z_s(\mathbf{W}_{\text{KQ}})} \right) - z_{T_0-1}(\mathbf{W}_{\text{KQ}}),$$

hence CE is convex as a composition of a convex function (log-sum-exp) with an affine one.

**(ii) MSE is not convex in  $\mathbf{W}_{\text{KQ}}$  in general.** Write the per-sample residual

$$r(\mathbf{W}_{\text{KQ}}) := \mathbf{E} a(z(\mathbf{W}_{\text{KQ}})) - \mathbf{e}_{T_0}, \quad \text{MSE}(\mathbf{W}_{\text{KQ}}) = \frac{1}{2} \|r(\mathbf{W}_{\text{KQ}})\|^2.$$

For any direction  $\Delta$ , the second derivative admits the generic ‘‘Gauss-Newton + curvature’’ decomposition by the product rule:

$$D^2 \text{MSE}(\mathbf{W}_{\text{KQ}})[\Delta, \Delta] = \underbrace{\|Dr(\mathbf{W}_{\text{KQ}})[\Delta]\|^2}_{\geq 0} + \underbrace{\langle r(\mathbf{W}_{\text{KQ}}), D^2 r(\mathbf{W}_{\text{KQ}})[\Delta, \Delta] \rangle}_{\text{can have either sign}}. \quad (49)$$

The first term is always positive semidefinite. The second term is *indefinite* in general, it can be written as  $\langle r, \mathbf{E} H(\mathbf{a})[\delta, \delta] \rangle$  where  $\delta := \lambda \mathbf{S} \mathbf{E}^\top \Delta \mathbf{e}$  and  $H(\mathbf{a})$  denotes the second differential of the shifted-softmax; since  $H(\mathbf{a})[\delta, \delta]$  changes sign with  $\delta$  while  $r$  can point in arbitrary directions, the inner product can be negative for suitable  $(\mathbf{W}_{\text{KQ}}, \Delta)$  whenever  $r \neq 0$ . This rules out global convexity of MSE in  $\mathbf{W}_{\text{KQ}}$  under our setup (in contrast with CE). In practice, negative curvature is easy to witness by minimizing the Rayleigh quotient  $\langle \Delta, \nabla^2 \text{MSE}(\mathbf{W}_{\text{KQ}})[\Delta] \rangle_F / \|\Delta\|_F^2$  over  $\Delta$  at a given  $\mathbf{W}_{\text{KQ}}$ .

## G Remarks on the Assumptions of Theorem D.2

*Remark G.1.* The assumptions used in Theorem D.2 play distinct roles.

1. Geometric assumptions are shown to hold with high probability for GMC data under appropriate dimensional scaling (Section G.1).
2. Identifiability is the only obstruction to margin divergence under vanishing MSE loss (Section G.2).
3. The remaining assumptions concern properties of the optimization trajectory and are illustrated empirically in Section G.3 for a representative run.

We emphasize that the present analysis characterizes one interpretable asymptotic regime of MSE training dynamics. It does not preclude the existence of other behavior outside the scope of the assumptions considered here, including convergence to locally optimal separating directions rather than the globally optimal max-margin solution, as observed in related settings [39].

### G.1 Geometric assumptions for Gaussian match-and-copy

We work under the GMC model of Theorem 1.1. For each sample  $i$ , write  $y_i := t_0^{(i)}$  for the hidden match index and define, for  $t \neq y_i$ ,

$$d_{i,t} := \mathbf{e}_{t+1}^{(i)} - \mathbf{e}_{y_i+1}^{(i)}, \quad \tilde{x}_{i,t} := \text{flatten}(d_{i,t} \mathbf{e}^{(i)\top}) \in \mathbb{R}^{d_{\text{in}}^2}.$$

Tokens are i.i.d.  $\mathbf{e}_t^{(i)} \sim \mathcal{N}(0, \frac{\sigma_{\text{token}}^2}{d_{\text{in}}} \mathbf{I}_{d_{\text{in}}})$ , and

$$\mathbf{e}^{(i)} = \mathbf{C} \mathbf{e}_{y_i}^{(i)} + \xi^{(i)}, \quad \xi^{(i)} \perp \{\mathbf{e}_t^{(i)}\}_{t=1}^{T+1}.$$

**Proposition G.2** (Validity of Geometric Assumptions). **1. Linear Independence (A2):** Let  $n_{\mathcal{I}_{\text{SV}}} = |\{i : \exists t, (i, t) \in \mathcal{I}_{\text{SV}}\}|$  be the number of samples containing support vectors, and  $T_{\mathcal{I}_{\text{SV}}} = \max_i |\{t : (i, t) \in \mathcal{I}_{\text{SV}}\}|$  be the maximum number of support vectors in a single sample. Then  $d_{\text{in}} \geq \max(n_{\mathcal{I}_{\text{SV}}}, T_{\mathcal{I}_{\text{SV}}}) \implies \text{a.s. the support vectors are linearly independent.}$

**2. Identifiability (A3):**  $d_{\text{in}} \geq T - 1 \implies \text{a.s. the target token is not in the convex hull of distractors.}$

**3. Half-space (A4):**  $d_{\text{in}} \gg \log(nT) \implies \text{w.h.p. all pairwise correlations } \langle d_{i,t}, d_{i,s} \rangle \text{ are positive.}$

In particular, these assumptions hold more easily as the input dimension  $d_{\text{in}}$  grows relative to  $T$  and  $n$ .

*Proof of Theorem G.2.* **1. Linear Independence:** We exploit the rank-one structure  $\tilde{x}_{i,t} = \text{flatten}(d_{i,t}\mathbf{e}^{(i)\top}) = \mathbf{e}^{(i)} \otimes d_{i,t}$ . Consider a linear dependence  $\sum_{(i,t) \in \mathcal{I}_{\text{SV}}} \alpha_{i,t} \tilde{x}_{i,t} = 0$ . Regrouping terms by sample index  $i$ , this can be written as  $\sum_i \mathbf{e}^{(i)} \otimes v_i = 0$ , where  $v_i = \sum_{t \in \mathcal{I}_{\text{SV}}(i)} \alpha_{i,t} d_{i,t}$ . If  $d_{\text{in}} \geq n_{\mathcal{I}_{\text{SV}}}$ , the query vectors  $\{\mathbf{e}^{(i)}\}$  associated with the active samples are linearly independent a.s. (as they are independent Gaussian vectors). This implies that  $v_i = 0$  for each sample  $i$ . Furthermore, if  $d_{\text{in}} \geq T_{\mathcal{I}_{\text{SV}}}$ , the difference vectors  $\{d_{i,t}\}_{t \in \mathcal{I}_{\text{SV}}(i)}$  within each sample are linearly independent a.s. (as they are Gaussian in  $\mathbb{R}^{d_{\text{in}}}$ ). The condition  $v_i = 0$  thus forces  $\alpha_{i,t} = 0$  for all coefficients.

**2. Identifiability:** Fix a sample  $i$ . The set of distractor tokens  $D_i = \{\mathbf{e}_{t+1}^{(i)} : t \neq y_i\}$  contains  $T - 1$  vectors. The convex hull  $\mathcal{K} = \text{Conv}(D_i)$  is contained in an affine subspace of dimension at most  $T - 2$ . Since  $d_{\text{in}} > T - 2$ , the Lebesgue measure of  $\mathcal{K}$  in  $\mathbb{R}^{d_{\text{in}}}$  is zero. The target token  $\mathbf{v} = \mathbf{e}_{y_i+1}^{(i)}$  is drawn from  $\mathcal{N}(0, \frac{\sigma_{\text{token}}^2}{d_{\text{in}}} I_{d_{\text{in}}})$  independently of  $D_i$ . Therefore,  $\mathbb{P}(\mathbf{v} \in \mathcal{K}) = \mathbb{E}[\mathbb{P}(\mathbf{v} \in \mathcal{K} | D_i)] = 0$ . Taking a union bound over  $n$  samples preserves the almost sure validity.

**3. Half-space condition:** We show that for some universal constants  $c_1, c_2 > 0$ ,

$$\mathbb{P}\left(\exists i, \exists s \neq t \neq y_i : \langle d_{i,s}, d_{i,t} \rangle \leq 0\right) \leq c_1 n T^2 e^{-c_2 d_{\text{in}}}.$$

The event is scale-invariant, so assume  $\mathbf{e}_t^{(i)} \sim \mathcal{N}(0, I_{d_{\text{in}}})$ . Fix a sample  $i$  and distinct  $s, t \neq y_i$ . Omit index  $i$  for brevity. Let  $d_s = \mathbf{e}_{s+1} - \mathbf{e}_{t_0+1}$  and  $d_t = \mathbf{e}_{t+1} - \mathbf{e}_{t_0+1}$ . Expanding the inner product:

$$\langle d_s, d_t \rangle = \mathbf{e}_{s+1}^\top \mathbf{e}_{t+1} - \mathbf{e}_{s+1}^\top \mathbf{e}_{t_0+1} - \mathbf{e}_{t+1}^\top \mathbf{e}_{t_0+1} + \|\mathbf{e}_{t_0+1}\|^2.$$

Expanding in coordinates, this is a sum of  $d_{\text{in}}$  i.i.d. random variables  $Z_k$  with the structure  $XY - XW - YW + W^2$  (where  $X, Y, W$  are standard normal). We calculate the moments:  $\mathbb{E}[Z_k] = \mathbb{E}[W^2] = 1$  and  $\mathbb{E}[Z_k^2] = \mathbb{E}[X^2Y^2] + \mathbb{E}[X^2W^2] + \mathbb{E}[Y^2W^2] + \mathbb{E}[W^4] = 1 + 1 + 1 + 3 = 6$  since terms in the square expansion with odd powers have zero expectation. Thus,  $\text{Var}[Z_k] = \mathbb{E}[Z_k^2] - \mathbb{E}[Z_k]^2 = 5$  and we deduce that

$$\mathbb{E}[\langle d_s, d_t \rangle] = d_{\text{in}}, \quad \text{Var}(\langle d_s, d_t \rangle) = 5d_{\text{in}}.$$

Thus  $\langle d_s, d_t \rangle$  is a sum of i.i.d. *sub-exponential* variables with mean  $d_{\text{in}}$  and variance of order  $d_{\text{in}}$ . By standard concentration inequalities for sub-exponential sums there exist universal constants  $c_1, c_2 > 0$  such that

$$\mathbb{P}(\langle d_s, d_t \rangle \leq 0) = \mathbb{P}(\langle d_s, d_t \rangle - d_{\text{in}} \leq -d_{\text{in}}) \leq c_1 e^{-c_2 d_{\text{in}}}.$$

There are at most  $n \binom{T-2}{2} \leq nT^2/2$  such pairs. By a union bound, the probability of any violation is at most  $c_1 n T^2 e^{-c_2 d_{\text{in}}}$ , which vanishes exponentially fast in  $d_{\text{in}} - \log(nT)$ .  $\square$

## G.2 On why identifiability is the only obstacle to margin divergence under vanishing MSE loss

The MSE loss can go to zero even when the margins do not diverge, unlike the CE loss studied in Soudry et al. [38]. A trivial example is when the target token  $\mathbf{e}_{T_0} = \sum_{t \neq T_0} \alpha_t \mathbf{e}_t$  is in the convex hull of the non-target tokens, with  $(\alpha_t)_t$  that can be realized as attention weights. In that case, setting the attention weights to  $(\alpha_t)_t$  yields zero MSE loss, but the margins remain bounded. The next lemma shows that this is the only obstacle to margin divergence.

**Lemma G.3** (Identifiability implies margin divergence under vanishing MSE loss). *For each sample  $i$ , let  $C_i := \text{conv}\{\mathbf{e}_t^{(i)} : t \in 2, \dots, T_i \setminus T_0^{(i)}\}$  be the convex hull of the non-target tokens and define its identifiability gap as*

$$\gamma_i := \text{dist}(\mathbf{e}_{T_0^{(i)}}^{(i)}, C_i).$$

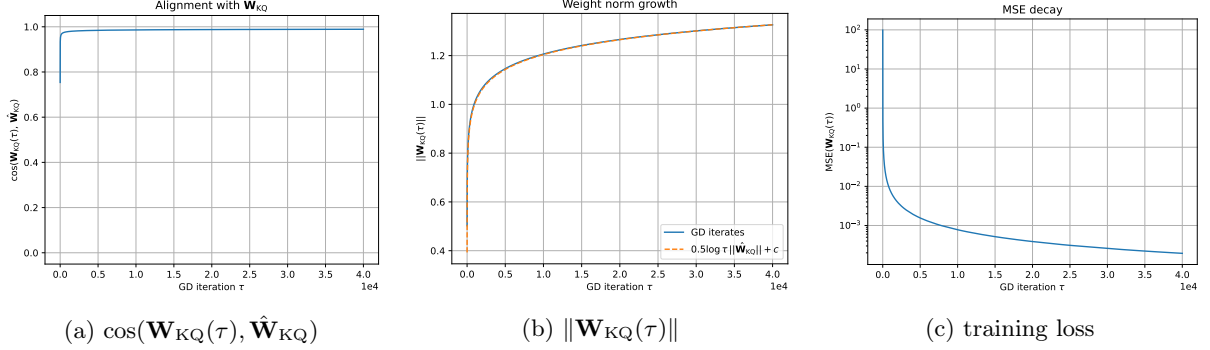


Figure 10: GD on MSE for shifted-key one-layer attention on GMC data with exact match and copy ( $d_{\text{in}}=16$ ,  $T=4$ ,  $n=8$ , step size  $10^{-3}$ , 40k iterations). We plot (left) cosine similarity between  $\mathbf{W}_{\text{KQ}}(\tau)$  and the max-margin solution  $\hat{\mathbf{W}}_{\text{KQ}}$ , (middle) the weight norm  $\|\mathbf{W}_{\text{KQ}}(\tau)\|$ , and (right) training loss. In (b), we verify that the norm diverges at speed  $\frac{1}{2} \log \tau \|\hat{\mathbf{W}}_{\text{KQ}}\|$  (dashed line), confirming the rate in Theorem D.2.

There exists a constant  $C_i > 0$  such that the MSE residual  $r^{(i)}(w) = \mathbf{E}^{(i)} a^{(i)}(w) - \mathbf{e}_{T_0^{(i)}}^{(i)}$  for sample  $i$  satisfies for all  $w$ :

$$(1 - a_{T_0^{(i)}}^{(i)}) C_i \geq \|r^{(i)}\| \geq (1 - a_{T_0^{(i)}}^{(i)}) \gamma_i.$$

In particular, when  $\gamma_i > 0$ , we have  $\text{MSE}_i \rightarrow 0$  iff  $a_{T_0^{(i)}}^{(i)} \rightarrow 1$ , and there is no finite-norm minimizer of the MSE loss under identifiability.

*Proof.* We drop the index  $i$ . By definition of shifted attention,  $a_1 = 0$ , hence

$$\mathbf{E}a = a_{T_0} \mathbf{e}_{T_0} + (1 - a_{T_0}) \underbrace{\sum_{t \neq T_0, t \geq 2} \frac{a_t}{1 - a_{T_0}} \mathbf{e}_t}_{=:u}$$

where  $u$  lies in the convex hull  $C$ . Therefore,  $r = \mathbf{E}a - \mathbf{e}_{T_0} = (1 - a_{T_0})(u - \mathbf{e}_{T_0})$  and taking the norms yields the claim.  $\square$

### G.3 A representative run where the assumptions hold

We provide an empirical sanity check that the technical assumptions used in our analysis can hold in practice on Gaussian match-and-copy (GMC) data in a regime where gradient descent exhibits clear directional alignment with the max-margin solution within a finite iteration budget. This section is intentionally illustrative: it documents one representative configuration where all proxy diagnostics behave consistently with the assumptions of Theorem D.2.

**Setup.** We consider GMC samples with exact copy ( $\mathbf{v} = \mathbf{e}_{t_0+1}$ ) and exact match ( $\mathbf{e} = \mathbf{e}_{t_0}$ ), and we optimize the MSE objective by (full-batch) gradient descent. Unless stated otherwise, we run for 40k iterations with step size  $10^{-3}$  and log relevant quantities at each iteration. In particular, partial sums indexed by time iteration are computed with all terms.

**Directional alignment and loss decay.** Figure 10 reports the training loss decay and the cosine similarity between the iterate  $\mathbf{W}_{\text{KQ}}(\tau)$  and the max-margin predictor  $\hat{\mathbf{W}}_{\text{KQ}}$ . In this run, the loss converges to a small value and the direction of  $\mathbf{W}_{\text{KQ}}(\tau)$  rapidly aligns with  $\hat{\mathbf{W}}_{\text{KQ}}$ . Empirically, we observe that such strong alignment within a fixed budget occurs in some regimes but not uniformly across all configurations depending on the interplay of  $(d_{\text{in}}, T, n)$  and step size. Since our theoretical statement concerns the asymptotic max-margin regime, we focus here on runs that clearly align within the iteration budget, and seek to verify whether the assumptions used to guarantee the alignment occur or not, and hence explain or not the observed behavior.

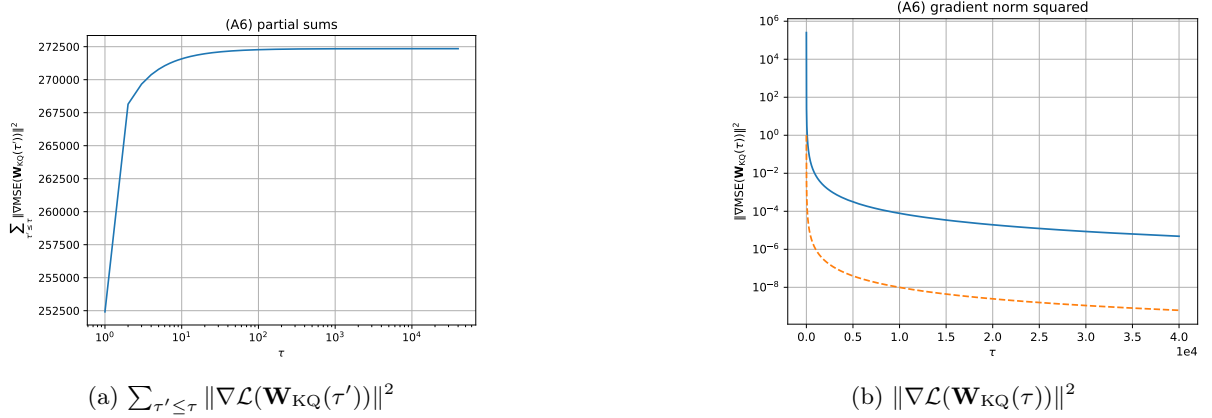


Figure 11: Empirical proxies for (A6). The orange dashed line in (b) corresponds to a power-law decay  $\tau^{-2}$  fitted on the last 10k iterations.

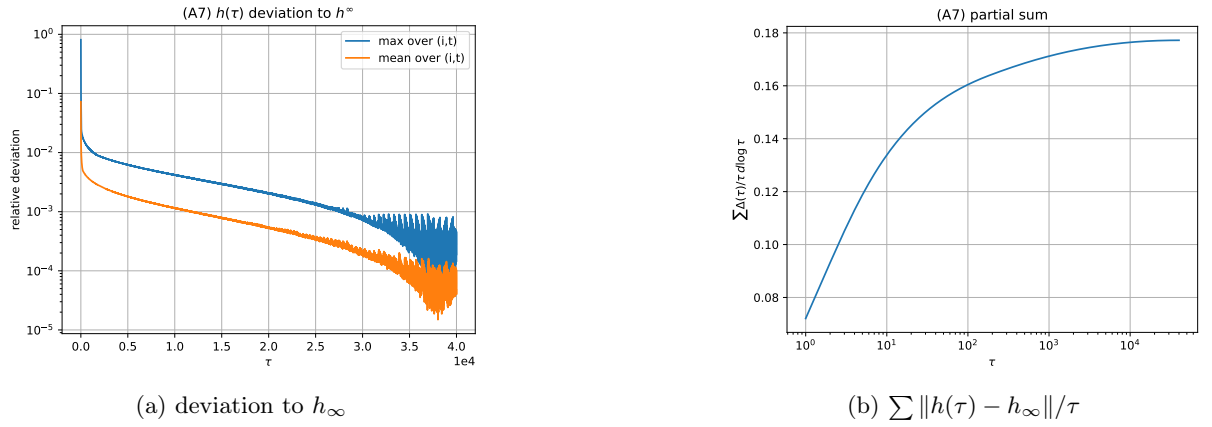


Figure 12: Empirical proxies for (A7) based on estimation of  $h^\infty$  from tail averages.

**Geometric conditions (A1–A4).** We verify a hard-margin feasibility condition (minimum margin  $\geq 1$ ), linear independence of support vectors (numerical rank), strict separation from convex hull of distractors, and positivity of relevant dot-products within the support set. These are direct finite-dimensional checks on the synthetic data, which are satisfied in this configuration.

**Training loss (A5).** Figure 10 shows that the loss decreases monotonically across iterations, and has reached a low-loss regime at the end of the run.

**Gradient-square summability proxy (A6).** Figure 11 shows that the cumulative sum of squared gradient norms appears to stabilize, tail increments decrease, and  $\|\nabla \mathcal{L}(\mathbf{W}_{\text{KQ}}(\tau))\|^2$  exhibits an approximate power-law decay on log-log axes  $\tau^{-2}$ . Together these observations are consistent with the summability condition required in (A6).

**Pre-factor convergence proxy (A7).** Figure 12 reports empirical proxies for convergence of the auxiliary quantities  $h_{i,t}(\mathbf{W}_{\text{KQ}}(\tau))$  and for the weighted series that appears in (A7). We estimate  $h^\infty$  by a tail average over the last percent of checkpoints, and report the maximum relative deviation  $\max_{i,t} |h_{i,t}(\tau) - h_{i,t}^\infty| / \sum_{i,t} |h_{i,t}^\infty|$  and the mean of these relative deviations across  $i, t$  as a function of iteration  $\tau$ . We observe stabilization of  $h_{i,t}(\mathbf{W}_{\text{KQ}}(\tau))$  and a saturating behavior of the partial sums. Precisely estimating asymptotic summability rates from finite horizons is delicate, but these plots are consistent with the qualitative behavior required by (A7).

**Alignment-ratio proxy (A8).** We estimate the ratio between the off-diagonal contributions in (33) with disagreeing signs and the total off-diagonal contributions. The estimation is based on the estimate of  $h^\infty$  from tail averages, and subsequent estimates of  $\tilde{w}_{i,t}(\tau)$ ,  $U_{i,t,s}(\tau)$ ,  $H_{i,t,s}(\tau)$ . We find that this ratio

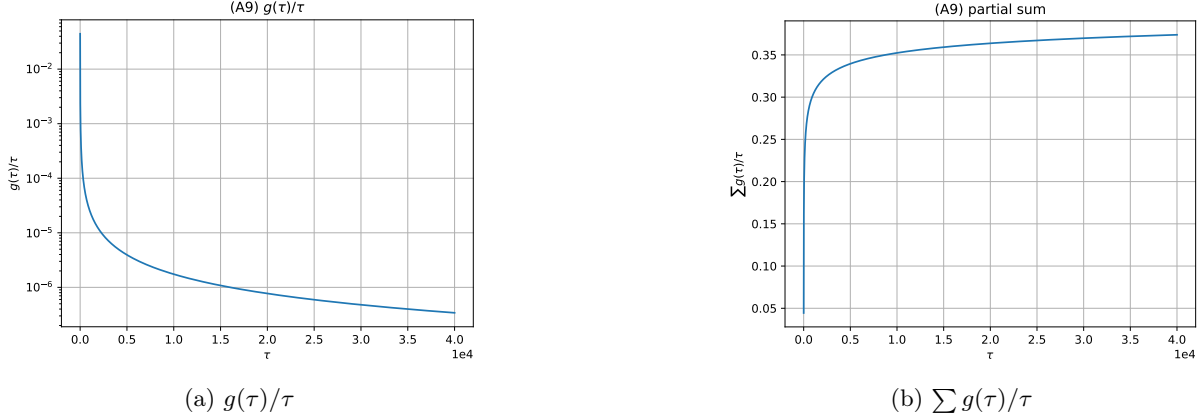


Figure 13: (A9) Softmax tail domination.

remains close to zero across iterations. Since (A8) only requires that misaligned off-diagonal contributions remain a strict minority of the total off-diagonal mass, this behavior is compatible with the condition in this configuration.

**Softmax tail domination proxy (A9).** Figure 13 reports proxies for the softmax tail domination condition (A9). The tail-mass proxy  $g(\tau)$  decreases, and the corresponding partial sum appears to stabilize, which is consistent with the behavior required by (A9).

## H Notes on Benchmark Classification and Design Choices

Table 4 summarizes several benchmarks from the literature that study match-and-copy or in-context learning tasks. This table is not intended to be exhaustive (and is surely not, given the size of the literature). Instead, it is intended to highlight how the design choices vary across works and how GMC fits within this landscape.

Overall, Table 4 should be read as a navigational aid rather than a definitive taxonomy. Its purpose is to highlight which benchmarks simultaneously (i) make match-and-copy structure explicit, (ii) give rise to empirically observable and robust PTH→IH behavior, (iii) exhibit architectural sensitivity favoring Transformers, and (iv) is amenable to the theoretical analysis of the optimization dynamics.

Obviously, each column compresses a wide range of modeling and experimental choices across works, so the annotations should be interpreted with care.

**Classification of Marion et al. [24].** The task of single-location regression studied in Marion et al. [24] can be reformulated as a special case of Gaussian match-and-copy (GMC) with a deterministic, fixed query across samples. We therefore include Marion et al. [24] in the GMC family, with the annotation “fixed query” to emphasize this restriction.

**Why some entries are marked as “not discussed” or “unlikely”.** In several works, the presence or robustness of PTH→IH mechanisms is not examined, and we therefore mark the corresponding entries as “not discussed”. In a small number of cases, although this aspect is not studied explicitly, we label the entry as “unlikely”, as the reported results indirectly suggest that PTH→IH mechanisms do not emerge or are not robust.

For instance, in Marion et al. [24], a solution based on detecting a mean shift can solve the task without requiring a PTH→IH circuit. Likewise, in Lee et al. [22], metrics associated with PTH→IH behavior vary across data distributions, suggesting limited robustness of such mechanisms.

Table 4: Comparison of synthetic and empirical benchmarks for match-and-copy / ICL. **Task:** NTP = next-token prediction; NLP = natural language processing; NLP Class. ICL = NLP classification in-context learning as in (2), like sentiment analysis, topic classification, etc.; (G)MC = (Gaussian) match-and-copy; AR = recent variants of associative recall, which differ from the original discrete version of Graves et al. [17] as discussed in Section 2; MQAR = multi-query associative recall; n-gram ICL = in-context learning of n-gram models; LinReg ICL = in-context learning of linear regression ( $f$  in (2) is a linear function); Class. ICL = classification in-context learning ( $f$  in (2) is a classifier), typically Omniglot or Gaussian clusters. **Match signal:** = for exact equality (the query is equal to the context token it should match); C1 for injected mean-shift (first-order marker); C2 for injected second-order correlation;  $\emptyset$  for no explicit match signal provided (typically the case for ICL tasks as in (2), where the query  $x$  is independent of the examples  $x_i$ ); same marg. for query and match having the same marginal distribution. **Arch. sens.:** qualitative architectural sensitivity of the benchmark: pre-T for pre-Transformer architecture comparisons (e.g., RNNs, LSTMs, Fast Weights);  $T >$  when Transformers outperform alternatives;  $\approx$  when ranking depends on setup and no clear winner; Alt when a new architecture is proposed to close a gap; left blank when no comparison with non-Transformer architectures. **PTH→IH:** *Obs.* = observed in trained models; *Rob.* = robust across setups. ✓ when observed/robust; ✗ when not emerging or not robust; ✗ when not discussed but indirect evidence against; left blank when not studied. **Theory:** → for works establishing results about the optimization dynamics;  $\nabla$  for ones exhibiting that among critical points, some are (close to) PTH→IH solutions;  $\exists$  for ones establishing representational/existence statements only (e.g., the model can be instantiated to implement a PTH→IH circuit, but it is not known whether it is learned by optimization), left blank when no such results are provided.

Paper	Task	Match	Arch. sens.	PTH→IH		Theory
				Obs.	Rob.	
[14, 28]	NLP NTP	$\emptyset$		✓	✓	
[25]	NLP ICL	$\emptyset$				
[12]	NLP Class. ICL	$\emptyset$				
[11]	NLP Class. ICL	$\emptyset$	$T >$	✓	✓	
[17]	discrete MC (orig. AR)	=	pre-T			$\exists$
[24]	GMC with fixed query	C1		✗		→
<b>This work (GMC)</b>	GMC	C2	$T >$	✓	✓	→
[4]	AR	=	pre-T			
[3]	MQAR	=	$T >$			$\exists$
[15, 31]	AR	=	Alt			
[6]	n-gram ICL	=		✓	✗	$\exists$
[2]	n-gram ICL	$\emptyset$	$T >$	✓		
[27]	n-gram ICL	$\emptyset$		✓		→
[9]	n-gram ICL	$\emptyset$		✓		→
[23]	n-gram ICL	$\emptyset$		✓		$\exists$
[13]	n-gram ICL	$\emptyset$		✓		$\exists$
[33]	n-gram ICL	$\emptyset$		✓		$\exists$
[42]	n-gram ICL	$\emptyset$		✓		$\nabla$
[1]	LinReg ICL	=				$\exists$
[44]	LinReg ICL	$\emptyset$				
[16]	LinRe / Reg. Tree / 2-layer NN ICL	$\emptyset$				
[8, 36]	Class. ICL	mix	$T >$	✓	✗	
[37]	Class. ICL	=		✓		
[34]	Class. ICL	same marg.		✓	✗	
[5]	Boolean ICL	$\emptyset$	$\approx$	$\approx$		
[45]	mix 4-gram and IH	$\emptyset$		✓		→
[22]	AR / ICL	$\emptyset$	$\approx$		✗	